Formation and composition of organic aerosols from the uptake of glyoxal on natural mineral dust aerosols: a laboratory study

Francesco Battaglia[1,a§], Paola Formenti[1], Chiara Giorio[2], Mathieu Cazaunau[3], Edouard Pangui[3], Antonin Bergé[3], Aline Gratien[1], Diana L. Pereira[1,b#], Thomas Bertin[3], Joel F. de Brito[4], Manolis N. Romanias[4], Vincent Michoud[1], Clarissa Baldo[1,3], Servanne Chevaillier[3], Gael Noyalet[3], Philippe Decorse[5], Bénédicte Picquet-Varrault[3], and Jean-François Doussin[3]

[1] Université Paris Cité and Univ Paris Est Créteil, CNRS, LISA, F-75013 Paris, France
[2] Yusuf Hamied Department of Chemistry, University of Cambridge, Lensfield Road, Cambridge, CB2 1EW, UK
[3] Univ Paris Est Créteil and Université Paris Cité, CNRS, LISA, F-94010 Créteil, France
[4] IMT Nord Europe, Institut Mines-Télécom, Université de Lille, Centre for Energy and Environment, 59000, Lille, France
[5] Université Paris Cité, CNRS, Itodys, F-75013 Paris, France
[a§] now at Dipartimento di Scienze Chimiche, Università degli Studi di Padova, Padova, Italy
[b#] now at institute for Atmospheric and Earth System Research, University of Helsinki, Finland

For submission to Atmos. Chem. Phys.

Corresponding author: P. Formenti (paola.formenti@lisa.ipsl.fr)

Mis en forme : Interligne : simple
Mis en forme : Espace Après : 0 pt
Mis en forme : Police :10 pt, Italien (Italie)
Mis en forme : Police :10 pt, Anglais (États-Unis)
Mis en forme : Anglais (États-Unis)
Code de champ modifié

Abstract

The uptake of glyoxal on realistic submicron mineral dust aerosol particles from a natural soil (Gobi Desert) is investigated during experiments in a large simulation chamber, under variable experimental conditions of relative humidity (RH), irradiation, and ozone concentrations. The uptake of glyoxal on the dust particles starts as soon as the glyoxal is injected in the chamber. At 80% RH, the measured uptake coefficient of glyoxal on mineral dust is $\gamma = (9 \pm 5) \times 10^{-3}$. The totality of the mass of reacting glyoxal is transformed in organic matter on the surface of the dust particles. The uptake of glyoxal is accompanied by the appearance of marker peaks in the organic mass spectra and a persistent growth in the volume concentration of the dust particles. While the mass of the organic matter on the dust rapidly reverts to values prior to uptake, the organic composition of the dust is modified irreversibly. Glycolic and other organic acids but also oligomers are detected on the dust. At 80% RH, compounds ranging from C_4 to C_{10} are observed as oligomerization products of glyoxal mono- and di-hydrate forms. The study suggests that dust aerosols could play a very substantial role in the formation of organic aerosols at high RH~~relative humidity~~, but also that the

reaction could have potential important implications for the dust optical and hygroscopic properties, including their pH.

1. Introduction

Mineral dust originates naturally from the wind erosion of arid or semi-arid soils, resulting in the suspension of particles with diameters from fractions to hundreds of microns, which can be transported over thousands of kilometres whilst in the atmosphere (Adebiyi et al., 2023; Mahowald et al., 2014). The total global mass of mineral dust particles emitted annually in the atmosphere is of the order of 4600 Tg yr^{-1}, accounting for approximately 40% of the total annual aerosol emissions (Knippertz and Stuut, 2014; Kok et al., 2021). Major natural source areas of mineral dust are North Africa (~50% of the global annual dust emissions), Asia (~40%), North America, and the Southern Hemisphere (~10%; Kok et al., 2023). Anthropogenic emissions are associated with soil erosion for agriculture, pasture, and deforestation (Tegen and Fung, 1995; Webb and Pierre, 2018), but their contribution to the total annual dust mass loading is uncertain, ranging from 5 to 60% (Chen et al., 2023). Mineral dust significantly impacts the Earth's energy balance by absorbing and scattering radiation in the solar and terrestrial spectra (Di Biagio et al., 2019; Kok et al., 2023) and by influencing the lifetime and optical properties of mixed-phase and ice clouds (e.g., Atkinson et al., 2013; Harrison et al., 2001; Steinke et al., 2016). Current estimates of the effective radiative forcing (sum of direct and indirect) of natural mineral dust are in the range of -0.07 ± 0.18 W m^{-2} (Kok et al., 2023), owing to large uncertainties in the atmospheric mass loading and properties of dust at emission and during transport (Castellanos et al., 2024; Li et al., 2021).

Gas-particle interactions along the dust lifecycle contribute to these uncertainties. Numerous laboratory and field studies show that mineral dust is capable to adsorb various reactive gaseous compounds, which may modify its chemical composition, and in turn to alter optical properties, hygroscopicity and ice nucleation activity but also may affect the oxidative capacity of the atmosphere (Bauer et al., 2007; Chirizzi, 2017; Crowley et al., 2010; Joshi et al., 2017; Liu et al., 2013; Ooki and Uematsu, 2005; Romanias et al., 2012; Seisel et al., 2004; Tang et al., 2017; Turpin and Huntzicker, 1995; Usher et al., 2003; Wagner et al., 2008). Dust aerosol may promote photocatalytic reactions of inorganic gases such as SO_2 and NO_2, initiating nucleation events (Dupart et al., 2012; Nie et al., 2014).

The uptake of volatile organic compounds (VOCs) on mineral dust such as limonene, toluene (Romanías et al., 2016), isoprene (Zeineddine et al., 2017), phenol (Hettiarachchi and Grassian, 2024), and dicarboxylic acids (Ponczek et al., 2019), is also documented. These reactions may alter the VOC budget in the atmosphere and lead to the formation of secondary organic aerosols (SOA) (Li et al., 2019; Tang et al., 2017; Usher et al., 2003; Xu et al., 2023; Zeineddine et al., 2023), one of the key players of atmospheric chemistry (Shrivastava et al., 2017).

Glyoxal (CHOCHO) is one of the most abundant VOCs in the troposphere (Lewis et al., 2020). It ~~Atmospheric glyoxal~~ is produced through the oxidation of aromatic compounds like benzene, toluene, and p-xylene (Volkamer et al., 2001) as well as by the photochemical oxidation of isoprene (Chan et al., 2017). The global atmospheric concentrations of glyoxal have been evaluated in the range of 10 – 100 pptv by Fu et al. (2008). However, case studies show sometimes higher concentrations. During a field study in Shanghai in the summer of 2018, Guo et al. (2021) reported an average glyoxal concentration of 164 ± 73 pptv, due to daytime photochemistry. Local concentrations of up to 400 pptv have been documented in regions influenced by aromatic pollution (Li et al., 2022). Satellite measurements of glyoxal show that the highest concentrations in tropical and sub-tropical regions are found during warm, dry periods influenced by biogenic emissions and vegetation fires, but also anthropogenic pollution (Vrekoussis et al., 2009). Elevated glyoxal concentrations have been observed in aged biomass burning plumes and tropical ocean regions, revealing model under-predictions in high-emission areas due to missing complex organic compound sources (Kluge et al., 2023). Field measurements in the north-east Atlantic Ocean reveal that models generally underestimate glyoxal concentrations due to missing contributions from acetaldehyde and other chemical precursors, and a potential glyoxal source from the ocean surface organic microlayer, particularly significant at night (Walker et al., 2022).

Glyoxal is a very soluble molecule which readily oligomerises in water, leading to the formation of larger molecules (Kalberer et al., 2004; Shapiro et al., 2009). Several previous studies have revealed that glyoxal ~~It also~~ has the ability to uptake onto aerosol particles, potentially serving as a significant source of organic aerosols (e.g., Liggio et al., 2005b, Carlton et al., 2007; Ervens and Volkamer, 2010; Galloway et al., 2009; Knote et al., 2014). The uptake of glyoxal on ammonium sulphate particles can lead to

the formation of carbon-nitrogen compounds (such as imidazole derivatives), oligomers, and organic acids (Galloway et al., 2009), that has been observed to cause ~~their~~ browning (De Haan et al., 2020). The light-absorbing imidazole derivatives formed by glyoxal have been found to act as a photosensitizer, initiating radical chemistry under realistic irradiation conditions in the aerosol phase and initiating aerosol growth in the presence of limonene (Rossignol et al., 2014).

The study by

Shen et al. (2016) revealed that glyoxal can also uptake onto synthetic minerals proxies of natural mineral dust, forming oligomers, organo-sulphates, formic acid, and glycolic acid, henceforth suggesting a potential significant mechanism for organic aerosol formation and modification of the optical and hygroscopic properties of mineral dust. ~~More r~~Recently, Zogka et al. (2024) ~~have investigated the uptake of glyoxal on soils and soil surrogates (synthetic mineral) and~~ highlighted the dependence of the soil composition and size for the uptake of glyoxal on soils and soil surrogates (synthetic mineral).

Following up from ~~the pioneering study by Shen et al. (2016~~those studies~~)~~, in this paper we present ~~the~~ novel~~results of~~ laboratory experiments using a large-scale simulation chamber to investigate the formation of organic aerosol ~~OA~~ from the uptake of glyoxal on realistic airborne mineral dust particles, in atmospherically-relevant conditions.~~.~~ Dust aerosols are generated from a natural parent soil from the Gobi Desert, one of the most important sources of tropospheric dust and representative of an area where this interaction could take place (Wang et al., 2015).

This paper has two major objectives. First, it provides experimental observations of the uptake of glyoxal on mineral dust aerosol, leading to the formation of organic aerosol mass upon interaction and measuring glyoxal uptake coefficient of mineral dust. Secondly, it presents the chemical composition of the mixed organic-dust aerosols, in terms of its oxidation state, molecular composition and the evolution of SOA~~secondary organic aerosol~~ content from glyoxal.

2. Experiments and methods~~al~~

This study uses the ~~-~~CESAM atmospheric simulation chamber (CESAM – Chambre ~~d'Étude de~~s Simulation~~s~~ Atmosphérique~~s~~ ~~Multiphasées~~Multiphasique, which translates to Experimental Multiphasic Atmospheric Simulation Chamber in

Mis en forme : Police :12 pt

English)~~CESAM atmospheric simulation chamber~~, a 4.2 m^3 cylindrical stainless-steel reactor initially described by Wang et al. (2011). CESAM ~~is~~ was specifically designed to study multiphase processes involving aerosol particles, gas-phase compounds and water, both in the vapour and liquid phases (Brégonzio-Rozier et al., 2016; Denjean et al., 2014; Giorio et al., 2017). CESAM is equipped with three 6.5 kW high-pressure arc xenon lamps (model EX-170GM3-E, IREM SpA, Borgone, Italy) and 6 mm Pyrex plate filters to mimic the solar radiation. A 50 cm stainless-steel four-blade fan located at the bottom of the chamber ensures a mixing time of about 1 minute for the gas phase and the homogeneity of the internal composition.

~~The ageing experiments last up to five hours. Before each experiment, the chamber is evacuated down to 10^{-4} mbar. The chamber is then filled with a mixture of 80% N_2 (Messer, purity > 99.995%) and 20% O_2 (Linde, 5.0) to an internal pressure exceeding by about 5 to 10 mbar the local atmospheric pressure, to prevent accidental contamination during the experiments. For the experiments carried out in wet conditions, the injection of water vapour precedes the injection of dust. The injection of glyoxal (1 ppmv) was conducted at least after 30 minutes after the dust to ensure that the dust particles are homogenously distributed. Irradiation is started within one hour after the glyoxal uptake onto the particles. Ozone is used to verify the sensitivity of the reactions to the presence of an oxidant. For those experiments, ozone is injected before glyoxal.~~

2.1. ~~Experimental~~ Injection and cleaning protocols

Dust aerosols wea~~a~~re generated and injected into the chamber according to the protocol detailed in Battaglia et al. (2025~~4~~) using a ~~. The~~ natural soil sample ~~used in this study is~~ from the Gobi Desert (107.48°N; 36.49°E). Prior use, the soil was~~is~~ sieved at 1000 µm and dried at 100°C for less than ~~an~~ one hour to remove adsorbed water and contamination from volatile gases. A quantity ranging from 30 and 50 g ~~is~~ was placed in a 1 L Büchner flask and shaken at 100 Hz using a sieve shaker (Retsch® AS200) to simulate the saltation and sandblasting mechanisms through which wind erosion generates airborne dust in the real atmosphere (Di Biagio et al., 2017). An Aerodynamic Aerosol Classifier (AAC, Cambustion®) ~~is~~ was placed between the dust generator and the chamber to inject mono-modal dust centred between 300 and 400 nm in geometric diameter.

Glyoxal wais prepared by heating a mixture of equal amounts of its trimer hydrate (Fluka® Analytical) and P_2O_5 (Sigma – Aldrich ReagentPlus®, 99%) at 150°C (Horowitz et al., 2001). The trimer decomposition occurs inside a vial connected to a vacuum gas manifold. Glyoxal is was collected as yellow crystals in a second vial immersed in an ethanol – liquid nitrogen cold trap at around -90°C and then vaporised in a 2.1 L glass bulb to a controlled pressure. This vial is was connected to the simulation chamber to inject the glyoxal through a pure nitrogen flow.

Ozone wasis generated by a Corona discharge in pure O_2 using a commercial dielectric ozone generator (MBT 802N, Messtechnik GmbH, Stahnsdorf, Germany). Water vapour is was generated by heating ultrapure water (Milli-Q IQ 7000, Merk™) inside a pressurised stainless-steel vessel, previously rinsed at least three times. The total organic carbon (TOC) content of the ultrapure water wasis monitored in each experiment to evaluate the influence on the production of organic particles, which was found to be minor (see **Text S1** in the Supplementary Material). The relative humidity (RH) inside the chamber wais measured by a HMP234 Vaisala® humidity and temperature transmitter. Before each experiment, the chamber was evacuated down to 10^{-4} mbar and then filled with a mixture of 80% N_2 (Messer, purity > 99.995%) and 20% O_2 (Linde, 5.0, purity 99.999%) to an internal pressure exceeding by about 5 to 10 mbar the roomlocal atmospheric pressure, to prevent accidental contamination during the experiments.

2.2. Instrumentation

The CESAM chamber was is equipped with a suite of standard instrumentation for the detection of the aerosol and the gas-phase, whose details are reported in **Table S1**. The analytical and data treatments specific to this study are reported in

Gas-phase glyoxal was measured by a combination of Measurements and instrumentation*2.2.1 Gas-phase composition*

CESAM is equipped with an in-situ long-path Fourier Transform Infra-Red (FTIR) spectrometry (Bruker Tensor 37) in the 2720-2930 cm^{-1} absorption band corresponding to the C–H bonds, by a Cavity Attenuated Phase Shift (CAPS) NO_2 analyser (Model T500U, from Teledyne API) and a Proton Transfer Reaction-Time Of Flight-Mass Spectrometer (PTR-ToF-MS) (KORE Technology®, second generation) operated in H_3O^+ ionization mode for VOC detection. The FTIR spectrometer provided

also with the concentrations of formic acid (HCOOH), measured in the C-O bond vibration band centred at 1105 cm^{-1}; ozone (O_3) measured in the asymmetric stretching of the absorption band centred at about 1043 cm^{-1}; and carbon monoxide (CO), detected at about 2143 cm^{-1}. The standard infrared absorption spectra of the compounds used for quantification, along with the specific absorption bands integrated for their quantification, are shown in **Figure S1**. CO and carbon dioxide (CO_2) were additionally measured by an APEE ProCeas® analyser. Nitrogen oxides (NO_x) where monitored by APNA-370 analyser by Horiba®.

The aerosol total number concentration above 2.5 nm was measured by a Condensation Particle Counter (TSI® model 3075). The aerosol number size distribution in the submicron fraction was measured by a combination of a Scanning Mobility Particle Sizer (SMPS) consisting of a Differential Mobility Analyser (TSI®, model 3080) coupled with a Condensation Particle Counter (TSI® model 3072) and an Optical Particle Counter (sky-GRIMM® OPC model 1.109).

~~The procedure for combining the aerosol size distributions measured by the SMPS and the sky-GRIMM® OPC is based on the method by Baldo et al. (2023), as described in detail in Battaglia et al. (2024). The number size distributions, expressed in dN/dlogD (cm-3), are used to evaluate the total particle surface S (μm2 cm-3) and volume V (μm3 cm-3) by assuming spherical particles as~~

~~$$S = \int \pi D^2 \frac{dN}{d\log D} d\log D \quad (1)$$~~

~~$$V = \int \frac{\pi}{6} D^3 \frac{dN}{d\log D} d\log D \quad (2)$$~~

The aerosol chemical composition was measured by a combination of online and offline methods. A Time-of-flight Aerosol Chemical Speciation Monitor (ToF–ACSM, Aerodyne Research Inc.) equipped with a standard vaporiser provided quantitative unitary mass resolution spectra between 40 nm and 1 μm vacuum aerodynamic diameter (Fröhlich et al., 2013). The instrument was operated through a Nafion membrane dryer (model PD-50T-12).

The organic mass concentration (m$_{org}$) was obtained considering a unitary collection efficiency (CE = 1) and a relative ionization efficiency (REI) of 1.4 (Nault et al., 2023).

The glyoxal fragment CH_2O^+ at m/z 30 has an isobaric interference with the NO^+ fragment from nitrate. Following Galloway et al. (2009), ~~Given that the glyoxal fragment CH_2O^+ (m/z =30) has an isobaric interference with the NO^+ fragment from nitrate, the contribution of glyoxal to the organic signal at 30 m/z is estimated with a minor modification of the standard fragmentation table made following the method proposed by Galloway et al. (2009) in their study of glyoxal uptake on ammonium sulphate (AS) particles. Th~~the~~e~~ contribution of ~~to the total signal at 30 m/z from~~ nitrate to the total signal at m/z 30 was calculated as ~~is imposed to be~~ 1.7 times the intensity of the nitrate signal at m/z 46 ~~m/z~~, which corresponds to the 30/46 signal ratio measured during nitrate calibration. The contribution to m/z 30 of ~~the organic~~glyoxal was then calculated from the total signal by subtracting the ~~is then the total signal minus the~~ contribution of the nitrate and the contribution of air. The elemental ratios of the organic fraction O/C and H/C are calculated from the measured f_{44} and f_{43} respectively, following the parametrizations proposed by Aiken et al. (2008) and Ng et al. (2011), respectively.

~~**2.2.3.2. Filter sampling**~~

Filter samples were collected on PTFE filters (Zefluor, 47 mm diameter, 2 µm pore size, Pall Life Sciences) and quartz fiber~~fibre~~ membranes (Tissuquartz 2500 QATUP, 47 mm diameter, Pall Life Sciences) ~~are collected~~ using ~~a~~ a series of custom-made stainless-steel holder of ~~(~~6 ~~-~~mm diameter ~~to concentrate particles on a small surface)~~ operated at 10 L min^{-1}, ~~-~~and preceded by an ~~active charcoal~~ denuder filled with active charcoal paper to remove ozone and VOCs. The sampling time range~~s~~d from 30 minutes to 3 hours. The filter holders and PTFE filters were pre-cleaned with dichloromethane (99.8 %, HPLC grade) in an ultrasonic bath, while the quartz filters were pyrolyzed at 550°C for approximately 8 hours. After sampling, filters were folded and placed in an aluminium paper envelope previously pyrolyzed (same protocol than the filters), and stored in a refrigerator at -18°C. Chamber blanks were collected by sampling for about 20 min from the chamber only filled with N_2 and O_2. Analytical blanks were also collected.~~Particles are collected on PTFE filters (Zefluor, 47 mm diameter, 2 µm pore size, Pall Life Sciences), and quartz fibre filters (Tissuquartz 2500 QATUP, 47 mm diameter, Pall Life Sciences). Before sampling, the PTFE filters and filter holders are cleaned with dichloromethane (99.8 %, HPLC grade) in an ultrasonic~~

~~bath. Quartz filters are pyrolyzed at 550°C for approximately 8 hours. After sampling, filters are folded and placed in an aluminium paper envelope previously pyrolyzed (same protocol as for filters), and stored in a refrigerator at -18°C. For each experiment, one blank sample is collected by sampling for about 20 min from the chamber only filled with N_2 and O_2. Analytical blanks, corresponding to pyrolyzed filters that had not undergone any sampling, were also collected.~~

2.~~3~~2.~~3.~~3. Filter analysis

The analysis of the filter samples was conducted by a combination of three techniques to provide with a comprehensive view of the chemical composition of the organic fraction formed on the dust particles as the result of the processing by glyoxal. The full details of the analysers and analytical protocols are reported in as detailed in **Text S2** in the supplementary material. Those include ~~The techniques and their complementarity are~~

1/ the ~~SFE/GC-MS organic aerosol analysis~~

Supercritical fluid extraction coupled with gas chromatography mass spectrometry (SFE/GC-MS; ~~) is used to analyse the molecular composition of the aerosol organic fraction. It was originally developed by~~ Chiappini et al. (~~,~~2006)) ~~and was slightly modified by a Teledyne ISCO model 260D pump for the extraction and a GC (Clarus 680 PerkinElmer) –MS (Clarus MS SQ8C Perkin Elmer) for the analysis.~~

~~The analytical protocol of the SFE/GC-MS analysis begins by placing the quartz filters inside the extraction cell. Prior to the extraction, 5 µL of two different solutions are deposited on the filters using a precision syringe (CR700-20 1-20ul (22s/2"/3), Hamilton, USA): (a) an internal standard solution composed by 20 µg mL^{-1} of Tridecane (99%, Sigma-Aldrich) and o-Toluic acid (Sigma-Aldrich, purity >97 %) in dichloromethane (99.8 %, HPLC grade) and (b) a derivatizing agent solution composed by N,O-bis(trimethylsilyl)trifluoroacetamide (BSTFA) and 1% of trimethylchlorosilane as catalyst, provided by Sigma-Aldrich. The first step of the analysis is a static extraction, in which the cell is filled with supercritical CO_2 (LINDE, reference CO_2 High Purity)), that interacts with the filter at 300 bar and 60°C, for 40 min. During this step, the trimethylsilylation of hydroxy and carboxy functions by BSTFA also occurs (generating trimethylsilyl~~

Mis en forme : Police :
Mis en forme : Titre 3, Justifié
Mis en forme : Police :(Par défaut) Arial, 12 pt
Mis en forme : Espace Avant : 0 pt, Après : 8 pt
Mis en forme : Police :Gras
Mis en forme : Normal, Justifié
Mis en forme : Retrait : Gauche : 0 cm, Suspendu : 1.24 cm

~~(TMS) derivatives). The supercritical fluid containing the analytes is transferred to the GC injector through a deactivated silica transfer line. The injector is cooled at -20°C using liquid nitrogen flowing around the injector for 15 minutes, where the compounds are retained, and the gaseous CO_2 is removed. Once the extraction step was completed, the chemical analysis was continued with the injection of the condensed compounds by heat flash on the GC injector from -20°C to 280°C. The compounds are then eluted with helium flowing at 1 mL min^{-1} (Linde) and transferred to the GC (Clarus 680 PerkinElmer) for separation. The temperature gradient of the GC column (Rxi® 5Sil MS column (30 m, 0,25mmi.d., film thickness: 0.25 µm, Restek) goes from 60°C to 280°C at a rate of 5°C min^{-1} and held at 280°C for 10 min. Detection is achieved through electron impact (70 eV electron energy) ionisation followed by a quadrupole mass spectrometer (Clarus MS SQ8C Perkin Elmer) analysis that produces mass spectra from m/z 50 to m/z 300.~~

~~The data analysis is conducted using the proprietary software (TurboMass Version 6.1.0.1965 PerkinElmer®). The analysis is limited to the chromatographic peaks which elutes before the internal standards (around 42 minutes), as for higher retention times the signal to noise ratio is lower and not conclusive. The chromatograms of each filter sample are compared with those of the analytical and procedural blanks and a mass spectrum is extracted from each chromatographic peak that is not present in the blank. To account for the method variability in extraction efficiency concentrations are corrected using the internal standard o-Toluic acid TMS derivatives. The structural analysis of the molecule generating every chromatographic peak is then carried out using two methods. Each mass spectrum is compared with the reference spectra of the National Institute of Standards and Technology (NIST) Mass Spectral Library (Version 2.2), which assigns a structure to each spectrum with a relative probability. For spectra for which the automatic structural assignment fails (low assignment~~providing~~ probability), we searched for~~-~~ for target analysis of low-weight mass fragments derived from molecules linked to glyoxal reactivity (see **Table S2.1~~1~~** in the Supplementary Material)~~.~~ ~~in particular the m/z 73 m/z fragment corresponding to a TMS derivatization $[Si(CH_3)_3]^+$, the m/z 147 m/z fragment corresponding to two TMS derivatizations $[(CH_3)_2Si=OSi(CH_3)_3]^+$,~~ such

Mis en forme : Police :Gras

Mis en forme : Police :Gras

Commenté [DP1]: I am not sure those fragments are specific only for glyoxal as it can be any alcohol or acid function that contributes to those.

as the m/z 131 ~~m/z~~ fragment (Glyoxylic acid TMS derivatized – CH_3), and the m/z 205 ~~m/z~~ fragment (Glyoxal monohydrate – CH_3);

2/ ~~-~~

~~2.2.3.4. Electrospray ionization (ESI) high-resolution mass spectrometry~~

~~Molecular analysis of the organic fraction collected on the quartz filters is performed by e~~Electrospray ionization (ESI) high-resolution mass spectrometry (Kourtchev et al., 2015) was~~. A high resolution (mass resolution=100000 at *m/z* 400) LTQ Orbitrap Velos mass spectrometer (Thermo Fisher, Bremen, Germany) equipped with a TriVersa Nanomate robotic nanoflow chip based ESI source (Advion Biosciences, Ithaca NY, USA) is~~ used to obtain high-resolution mass spectra and formulae assignments for low-volatility compounds in the ranges ~~of the methanol extracts following an adaptation of the procedure described in Kourtchev et al. (2015). Filters are extracted one time in 1 mL of methanol (Optima TM grade, Fisher Scientific) and two times in 0.5 mL of methanol under ultrasonic agitation in slurry ice for 15 min. Extracts are combined and filtered sequentially through a 0.45 µm pore size and a 0.2 µm pore size Teflon filter (ISODiscTM Supelco), which are then reduced by volume to approximately 50–200 µL under a gentle stream of nitrogen. The resulting sample is injected by direct infusion. The negative ionization mass spectra are collected in three replicates at ranges~~ m/z 50–500 and m/z 150–1000 ~~and processed using Xcalibur 2.1 software (Thermo Scientific). In the settings of the data processing, the following atoms are included in the peak assignment~~(~~: C (from 1 to 100 atoms in the possible assigned molecular formula), H (1-200), O (0-50), N (0-5), S (0-2), ^{13}C (0-1) and ^{34}S (0-1). The allowed mass accuracy in the formula assignment is ± 4 ppm.~~

~~The peak assignment to a molecular formula is done according to~~ Zielinski et al.~~,~~ ~~(~~2018). These were processed to provide with ~~. The protocol includes internal calibration, noise removal, blank subtraction, and additional atomic constraints for formula filtering: elemental ratios were set as 0.3 ≤H/C≤ 2.5, O/C≤ 2, N/C≤ 0.5, S/C≤ 0.2, $^{13}C/^{12}C$≤ 0.011 and $^{34}S/^{32}S$≤ 0.045, and nitrogen rule. In the case of multiple assignments for the same peak, the formula with the lowest mass error was kept. This process allowed for the retrieval of~~ parameters describing the carbon oxidation, through ~~such as the~~ O/C and H/C bulk ratios, and the

Mis en forme : Police :(Par défaut) Arial

Mis en forme : Normal, Justifié, Retrait : Gauche : 0 cm, Suspendu : 1.24 cm

Mis en forme : Retrait : Gauche : 0 cm, Suspendu : 1.24 cm

Mis en forme : Police :(Par défaut) Arial

identification of molecular . ~~Consequently, each mass spectrum was analysed to construct a van Krevelen diagram, which is a graphical representation illustrating the sample composition in terms of carbon, oxygen, and hydrogen in the identified molecular formulas (Patriarca et al., 2018). Identified molecular formulas are categorised into the following~~ groups such as : CHO, CHON, CHOS, CHNS, and CHONS.

ESI-HR-MS was also used for a screening ~~the A targeted~~ analysis of ~~search for~~ molecules ~~ar formulas r~~resulting from the glyoxal transformation due to ~~reactivity is also done. In this search, we included formulas associated with glyoxal chemical transformations such as~~ hydration, oxidation, and oligomerization. These included ~~Starting from the glyoxal formula, $C_2H_2O_2$,~~ formulas for mono- and dihydration products ~~are~~ ($C_2H_4O_3$ and $C_2H_6O_4$, respectively), . ~~O~~oxidation products ~~included~~ (formic acid (CH_2O_2), glycolic acid ($C_2H_4O_3$), glyoxylic acid ($C_2H_2O_3$), and oxalic acid ($C_2H_2O_2$)), and oligomers . ~~Oligomers formed~~formed by the hydrolysis of hydrated glyoxal formulas ~~were also sought. In the process of hydrolysis-driven oligomerization, each successive molecular addition results in the loss of a water molecule. If the oligomer is a ring, an additional water molecule is lost due to the condensation of the linear oligomer terminations. Denoting n as the number of molecules of the monohydrated form ($C_2H_4O_3$) and m as the number of molecules of the dihydrated glyoxal form ($C_2H_6O_4$) participating in the formation of an oligomer, the generated~~ linear oligomers ~~will have the~~with generic stoichiometric formula $C_{2n+2m}H_{4n+6m-2(n+m-1)}O_{3n+4m-(n+m-1)}$, ~~where the terms 2(n+m-1) and (n+m-1) in the hydrogen and oxygen atom stoichiometry indicate water loss from the oligomerization process. For~~and ring oligomers with generic ~~,~~ formula~~es~~ ~~characterised by the stoichiometry $C_{2n+2m}H_{4n+6m-2(n+m)}O_{3n+4m-(n+m)}$)are searched~~. ~~Similarly, formulas resulting from the condensation of hydrated forms with the listed organic acids are calculated and researched.~~

~~2.2.3.5. X-ray photoelectron spectrometry (XPS)~~

3/ X-ray photoelectron spectrometry (XPS) was~~is~~ used following ~~as in~~ Denjean et al. (2015) to quantify the elemental O/C ratio of the particle surface (O/C_{surf}) to

Mis en forme : Normal, Justifié, Retrait : Gauche : 0 cm, Suspendu : 1.24 cm

Mis en forme : Retrait : Gauche : 0 cm, Suspendu : 1.24 cm

a depth less than 10 nm. The O/C_{surf} was calculated as ~~: Measurements are performed with a VG ES CALAB 250 instrument using monochromatic Al K_α radiation (1486.6 eV). The O/C ratio is quantified by integrating the areas of O_{1s} and C_{1s} peaks. This last is contributed by a number of functions, including CO_2, C–O, C–C/C–H as well as C–F from the Teflon substrate. The contribution of the latter can be evaluated from the F1s (approximately 690 eV) as described in Denjean et al., (2015). The contribution of SiO_2 from the mineralogical composition of the dust to O1s was evaluated by integrating the Si2p peak (107 eV) and applying the stoichiometric proportions between silicon and oxygen in the composition of quartz (O/Si = 2)~~, as explained in Text S2 in the Supplementary Material. The XPS measurement on a filter collected during one ageing experiment are shown as an example in **Figure S2.1** in the Supplementary Material.

2.4. Calculation of the aerosol size distribution

The procedure for combining the ~~aerosol size distributions~~measurements of the ~~measured by the~~ SMPS and the sky-GRIMM® OPC is based on ~~the method by~~ Baldo et al. (2023) and ~~, as~~ it is described in detail in Battaglia et al. (2024~~5~~). The number size distributions, expressed in d*N*/dlog*D* (cm^{-3}), are used to evaluate the total particle surface S ($\mu m^2\ cm^{-3}$) and volume *V* ($\mu m^3\ cm^{-3}$) by assuming spherical particles as

$$S = \int \pi D^2 \frac{\mathrm{d}N}{\mathrm{dlog}D}\ \mathrm{dlog}D \quad (2~~1~~)$$

$$V = \int \frac{\pi}{6} D^3 \frac{\mathrm{d}N}{\mathrm{dlog}D}\ \mathrm{dlog}D \quad (3~~2~~)$$

2.~~3~~5. Calculation of the glyoxal uptake coefficient and rate of particle formation

The uptake coefficient (γ) is defined as the probability of the gas to be taken up on the aerosol surface. It is a unit-less parameter expressed by the ratio between the number of molecules taken up on a surface and the total number of collisions of the gas on the surface as

$$\gamma = \frac{number\ of\ total\ molecules\ taken\ up}{total\ number\ of\ collisions} \quad (4)$$

The gas-phase uptake coefficient (γ) ~~can be calculated in two ways. First of all~~was, ~~it can be~~ estimated from the first-order heterogeneous loss rate of glyoxal (k_{het}, s^{-1}) as

$$\gamma = \frac{k_{het}}{\omega} \quad (5)$$

The rate of collisions (collision frequency, ~~where~~ ω) is ~~is~~ the ~~rate of collisions (collision frequency)~~ defined as

$$\omega = \frac{cA_S}{4} \quad (6)$$

where:

- $c = 146 \times \sqrt{\frac{T}{MW}}$ is the mean molecular speed (m s^{-1}), where T is the air temperature (here 298 K) and MW the molecular weight of the compound of interest (in the case of glyoxal MW = 58 g mol^{-1}).
- A_S is total aerosol surface concentration (m^2 m^{-3}).

The total aerosol surface concentration (A_S) is calculated from the aerosol size distribution recorded at the end of the dust injection.

The heterogeneous loss rate of glyoxal (k_{het}) due to its uptake on dust particles can be determined as the difference of the loss rate of glyoxal measured during the uptake experiments (k_{obs}) and the glyoxal loss rate on the chamber walls (k_{loss}) as

$$k_{het} = k_{obs} - k_{loss} \quad (7)$$

The glyoxal wall loss is represented by a partition equilibrium described by two first-order reactions: one for the adsorption of gas phase molecules onto the chamber walls, and one for the reverse process. The rate constants for both processes have been obtained experimentally through control experiments with only glyoxal in the chamber

Mis en forme : Espace Avant : 6 pt, Après : 0 pt

Mis en forme : Ajouter un espace entre les paragraphes de même style

Mis en forme : Espace Avant : 6 pt, Après : 0 pt, Ajouter un espace entre les paragraphes de même style

Mis en forme : Anglais (États-Unis)

and at ~~under~~ different relative humidity conditions, as detailed in **Text S3** in the ~~S~~supplementary material ~~Text S2~~. ~~The rate constants for both processes have been obtained experimentally through control experiments with only glyoxal in the chamber in different relative humidity conditions.~~

If the uptake reaction is of the first rate, k_{het} is henceforth calculated as

$$k_{het} = \frac{ln\left(\frac{[Gly]_0}{[Gly]_{obs}}\right) - ln\left(\frac{[Gly]_0}{[Gly]_{loss}}\right)}{t} \quad (8)$$

where $[Gly]_0$ is the initial concentration of glyoxal, $[Gly]_{obs}$ represents the observed evolution of glyoxal concentration in time, resulting from the sum of uptake and wall loss, and $[Gly]_{loss}$ represents the estimated glyoxal concentration resulting from the wall loss.

The rate of formation of the particulate organic matter (POM; ~~*In addition,* k_{F-POM}~~) ~~, the rate of formation of the particulate organic matter (POM) on pre-existing particles~~ due to the ~~following the~~ uptake of glyoxal on the dust can be calculated as

$$k_{F-POM} = \frac{ln\left(\frac{[POM]_t}{[POM]_0}\right)}{t} \quad (9)$$

where $[POM]_0$ represents the initial POM concentration in the particle phase, and $[POM]_t$ represents the concentration of the POM formed at a given time.

I~~n~~f the hypothesis that the POM formation is solely due to the uptake of glyoxal, γ can be also evaluated as

$$\gamma = \frac{k_{F-POM}}{\omega} \quad (10)$$

Mis en forme : Police :Gras

Mis en forme : Police :Italique

Mis en forme : Police :Italique

3. Results and discussion

3.1. ~~Timeline of experiments~~Overview of experiments

The ageing experiments of monodispersed mineral dust and glyoxal described in this paper are summarised in **Table 1**. All the aerosol data are corrected for dilution, wall loss, and particle loss through the tubing systems as detailed in **Text S4~~2~~** in the Supplementary Material. Gas phase concentrations are corrected for dilution only.

Table 1. Listing and initial conditions of the experiments considered in this study, including experiments with glyoxal only (experiment type GL), ammonium sulphate and glyoxal (AS + GL), dust only (D) and dust with glyoxal (D + GL). The glyoxal and ozone gas phase concentrations correspond to the maximum value measured by FTIR after the respective injections. V_{seed} indicates the maximum volume concentrations of seed particles (either dust or ammonium sulphate) measured after the particle injection. The notation "dark/light" indicates experiments when filter samples were collected both in the dark and with irradiation.

Experiment type	Reagents	Date	Experiment number	RH, %	Light	$[O_3]$, ppb_v	Temp, K	[GL], ppb_v	V_{seed}, $\mu m^3 cm^{-3}$
Control	GL	29/04/2021	G_1	< 5	dark	---	292	1130	---
		11/02/2022	G_2	77	light	1440	291	627	---
	AS+GL	21/02/2023	AS_1	38	dark	---	298	527	50.1
		23/02/2023a	AS_2	35	dark	---	298	516	48.3
		23/02/2023b	AS_3	32	light	---	298	445	64.8
		07/09/2023	AS_4	81	light	---	301	779	304.1
		08/09/2023	AS_5	83	light	---	300	430	161.2
	D	31/01/2022	D_1	< 5	$^{dark}/_{light}$	---	292	---	31.5
		03/02/2022	D_2	75%	$^{dark}/_{light}$	---	293	---	55.4
Uptake	D+GL	04/02/2022	D_3	< 5	$^{dark}/_{light}$	---	293	690	35.6
		08/02/2023	D_4	32	dark	---	294	940	21.5
		09/02/2023	D_5	31	light	---	295	1050	52.7
		10/02/2023	D_6	35	dark	---	294	809	37.4
		13/02/2023	D_7	34	light	---	296	850	51.3
		30/04/2021	D_8	76	light	---	289	759	28.3
		03/05/2021	D_9	79	light	---	290	607	38.7
		04/05/2021	D_{10}	81	light	---	290	371	31.5
		05/05/2021	D_{11}	78	dark	---	291	805	30.1
		06/05/2021	D_{12}	82	dark	---	292	432	21.1
		08/02/2022	D_{13}	81	$^{dark}/_{light}$	1270	293	555	64.0
		09/02/2022	D_{14}	78	$^{dark}/_{light}$	1450	293	756	79.8
		10/02/2022	D_{15}	75	$^{dark}/_{light}$	---	295	600	68.4
		14/02/2023	D_{16}	83	dark	---	296	661	35.8
		15/02/2023	D_{17}	75	light	---	298	444	41.0

Table 1 also lists the few control experiments using ammonium sulphate as seed particles, described in detail in **Text S5~~3~~** in the Supplementary Material. No POM

Mis en forme : Police :Gras
Mis en forme : Police :Gras
Mis en forme : Police :Gras
Mis en forme : Police :Gras
Mis en forme : Espace Avant : 6 pt, Après : 0 pt
Mis en forme : Police :Gras
Mis en forme : Police :Gras

formation was~~is~~ observed during control experiments with dust or glyoxal only, both dry and humid conditions and with and without irradiation.

3.1.1. Timeline of particle concentration and composition

The ageing experiments lasted up to five hours. For the experiments carried out in wet conditions, the injection of water vapour preceded the injection of dust. The injection of glyoxal (nominal concentration of 1 ppmv) was conducted at least after 30 minutes after the dust to ensure that the dust particles were homogenously distributed in the reactor. Irradiation was started within one hour after the glyoxal uptake onto the particles. On a few experiments, ozone was injected before glyoxal to verify the sensitivity of the reactions to the presence of an oxidant.

The typical timelines of the particle concentrations (number and volume) and the non-refractory composition measured in dry conditions and at 30% and 80% relative humidity are shown in **Figure 1**.

Mis en forme : Police :Non Italique

Mis en forme : Titre 4, Gauche, Espace Avant : 6 pt

Mis en forme : Espace Avant : 6 pt, Après : 0 pt

Mis en forme : Police :Gras

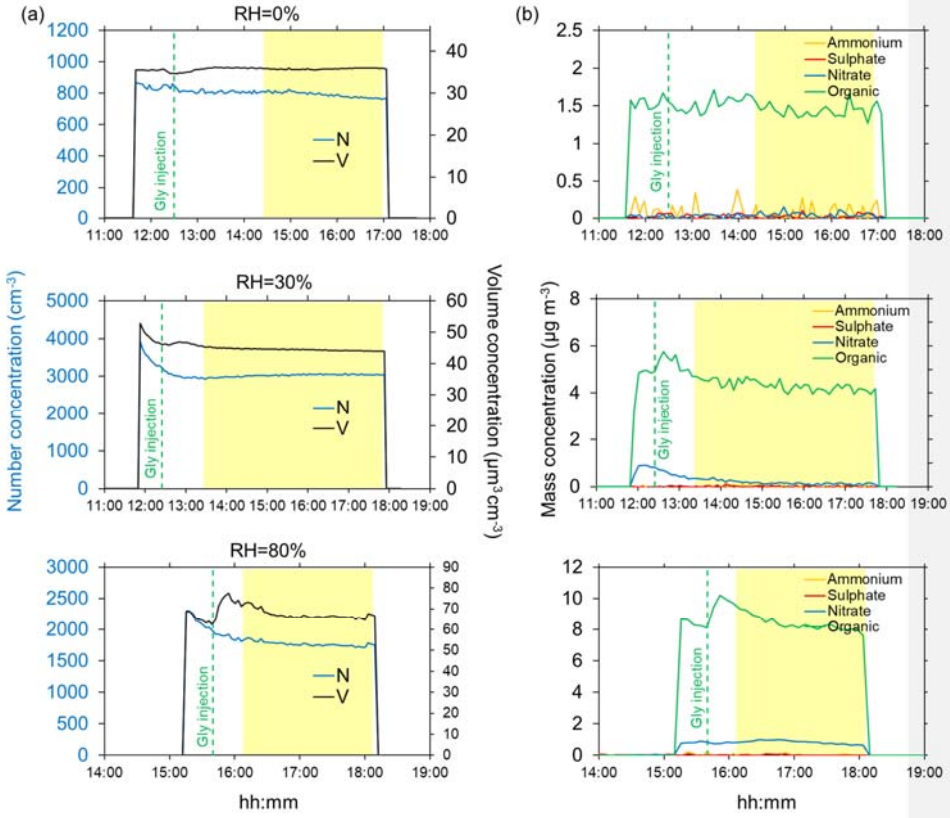

509

510 **Figure 1.** Timeline of ageing experiments of submicron dust with gas-phase glyoxal in dry conditions
511 (top, experiment D_3), 30% (middle, experiment D_7), and 80% RH (bottom, experiment D_{15}). Left (a):
512 aerosol total number (N) and volume (V) concentrations (blue and black lines, respectively) calculated
513 from the measured dust size distributions. Right (b): mass concentrations of ammonium, sulphate,
514 nitrate and organic (yellow, red, blue and green lines, respectively) measured by the ACSM. The yellow-
515 highlighted portion of the graph indicates the interval where irradiation takes place, while the green
516 vertical dashed lines indicate the injection glyoxal in the chamber. The dust injection corresponds to the
517 time of the initial increase of the number and volume concentrations. Aerosol time series are corrected
518 for dilution, wall loss and particle loss through the tubings.

519

520 **Figure 1** shows that in dry conditions, there is no significant variation of either the
521 aerosol number or the volume concentrations, nor the chemical composition (including
522 organics) following the glyoxal injection.

523 At 30% RH, a small increase in the total volume concentration (approximately 5 μm^3
524 cm^{-3}) is observed for about 30 minutes after the injection of glyoxal. This corresponds
525 to an increase of the POM of about 1 $\mu g\ m^{-3}$, approximately 20% more with respect to

the value measured before the uptake. On the other hand, the particle number concentration shows an apparent decrease at the beginning of the experiments, possibly because the particle loss correction model of Lai and Nazaroff (2000) does not fully apply to dust particles and humid conditions (see discussion in Battaglia et al. (20254). After that, and through the duration of the experiment, however, it remains constant, indicating that the increase in the particle volume occurs on the dust particles and not because of new particle formation.

At 80% RH, the increase in both the total volume and the POM concentrations is more pronounced, approximately 10-15 $\mu m^3\ cm^{-3}$ and 2 $\mu g\ m^{-3}$, respectively. As for 30% RH, both total particle volume and the POM concentrations return to values observed prior the injection of glyoxal, within approximately 30 minutes from their maximum values, likely due to evaporation. A similar behaviour is observed in the presence of ozone (**Figure S2** in the Supplementary Material~~not shown~~). As for 30% RH, the particle number concentration slightly decreases in time at the beginning of the experiment, but then remains constant, again excluding the formation of new particles but rather confirming the formation of organic matter on pre-existing particles. This is also supported by the fact that the rate of increase of POM and particle volume is the same (slope $3.2 \times 10^{-4}\ s^{-1}$ and $3.2 \times 10^{-4}\ s^{-1}$, respectively for POM and total volume), as shown by **Figure S32** in the Supplementary Material.

~~On the other hand, the ratio between the observed increase of the POM (2 $\mu g\ m^{-3}$) and that of the particle volume concentration (20 $\mu m^3\ cm^{-3}$) corresponds to an estimated mass density of the order of 0.1 $g\ cm^{-3}$, that is, about 10 times lower than the value of 1 $g\ cm^{-3}$ expected for glyoxal. This would suggest that part of the organic matter formed on dust is not detected by the ACSM, as will be further demonstrated in Ssection 3.3. On the other hand, **Figure S42** shows that, after reaching its maximum value, the volume concentration decreases at a lower rate than the POM (slope $3.9 \cdot 10^{-5}\ s^{-1}$ and $6.1 \cdot 10^{-5}\ s^{-1}$, respectively). This suggests that an additional process could contribute the particle volume concentration partially compensating the loss of organic matter on the dust particles.~~

~~This is confirmed by **Figure 2** comparing the variation in time of the particle volume distributions, normalised to the total volume, at four different times of the experiments~~

Mis en forme : Exposant
Mis en forme : Police :Gras
Mis en forme : Police :Gras
Mis en forme : Surlignage
Mis en forme : Police :Gras, Surlignage
Mis en forme : Surlignage
Mis en forme : Police :Gras, Surlignage
Mis en forme : Surlignage
Mis en forme : Police :Gras, Surlignage
Mis en forme : Surlignage

~~at 30% and the one at 80%: prior and when the glyoxal is injected, when the POM reaches its peak value, and at the end of the experiment.~~

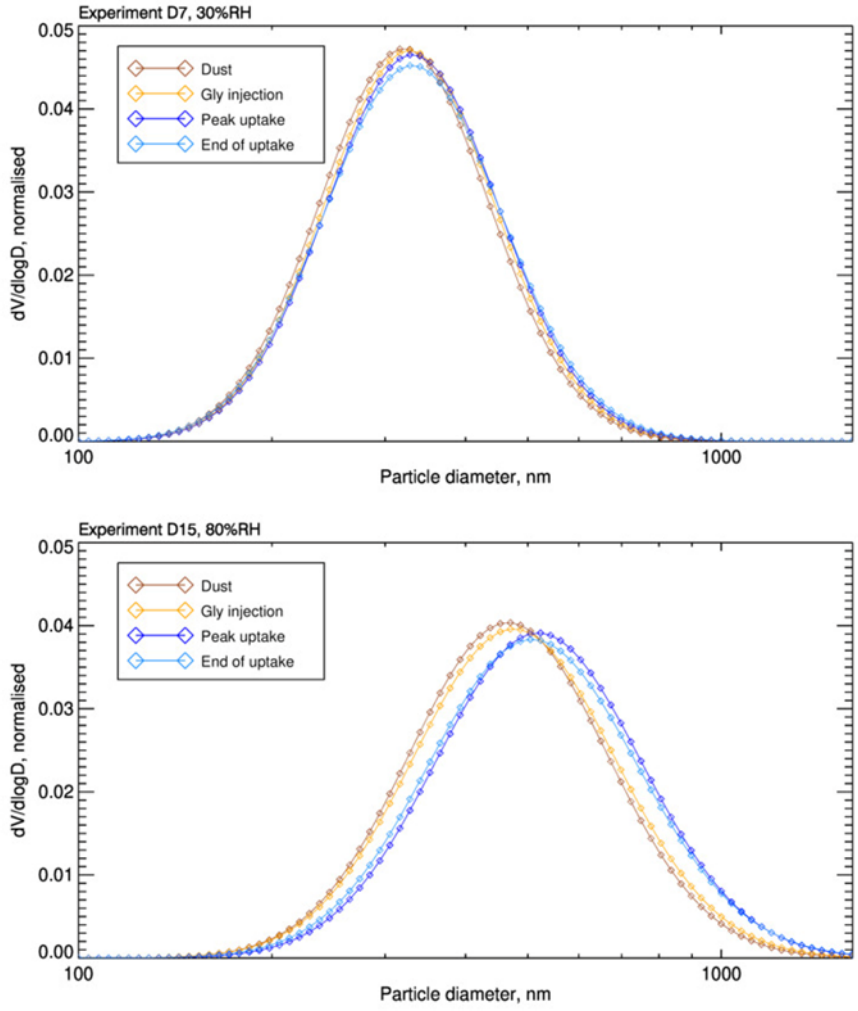

~~**Figure 2.** Evolution of volume-size distributions for two glyoxal uptake experiments in different relative humidity conditions. The images illustrate the progression of volume-size distributions recorded at four key moments during the experiments. The first distribution (orange) is recorded after the dust is injected into the simulation chamber. The second distribution (yellow) is recorded at the moment of glyoxal injection. The third distribution (blue) corresponds to the peak uptake of glyoxal on the aerosol, and the~~

Mis en forme : Espace Avant : 6 pt

Mis en forme : Anglais (États-Unis)

Mis en forme : Espace Avant : 6 pt, Interligne : 1.5 ligne

~~fourth (light blue) is recorded at the end of glyoxal uptake process. The left image depicts the evolution for the experiment D7 conducted at 30% RH, while the image on the right shows the distributions for the experiment D15 conducted at 80% RH. The results highlight that the distributions grow more significantly at 80% RH, indicating a higher glyoxal uptake and organic formation at elevated humidity levels.~~

~~All distributions have a single mode. However, after the injection of glyoxal, the geometric mean volume diameter, measured at the maximum POM concentration, increases by up to 10% (from 310 to 340 nm) at 30% RH, and up to 20% (from 450 to 540 nm) at 80% RH. Interestingly, even at the end of the experiment, when the POM concentration returns to its initial value, the increase in geometric mean diameter of the aerosol is irreversible. This effect could be explained by the hypothesis that the uptake of glyoxal enhances the dust hygroscopicity. After glyoxal uptake, the particle becomes more hygroscopic and the difference in total volume between the beginning and end of the experiment is due to water uptake which adds up to the formed organic aerosol mass.~~

3.1.2. Timeline of gas-phase concentration

~~Finally,~~ **Figure 1** shows also that, while sulphate and ammonium are never detected, a background concentration of nitrate up to 1 µg m^{-3} is measured by the ACSM as soon as the dust particles are injected in the presence of water. We attribute it to the heterogeneous interaction between NO_2 and the dust particles (Goodman et al., 1999) as indeed, a background concentration of a few ppb of NO_2 is present in the chamber as a result of the procedure used to reduce the TOC content in the injected water (see **Figure S~~43~~** in the Supplementary Material). However, since the contribution of nitrate represents at maximum 1% of the injected dust mass and whether decreases or remains constant throughout the experiment, its contribution to the particle growth and overall ageing of the mineral dust should be negligible.

Figure ~~3~~ 2 shows the time series of the gas-phase compounds detected during the same experiment (D_{15}) at 80% RH.

Mis en forme : Espace Avant : 6 pt

Mis en forme : Normal, Justifié

Mis en forme : Police :Non Italique

Mis en forme : Titre 4

Mis en forme : Police :Gras

Mis en forme : Police :Gras

Mis en forme : Police :Gras

Mis en forme : Police :Gras

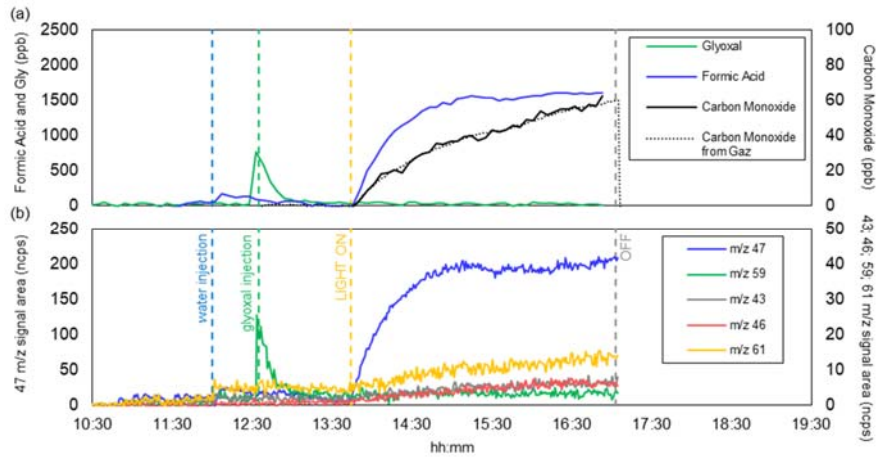

Figure 3~~a~~2a. Time series of the gas-phase composition observed during experiment D_{15}: (a) concentrations of carbon monoxide, glyoxal and formic acid measured by FTIR (for CO the measured of the online analyser are also shown); (b) various VOC ions (m/z 47, 59, 43, 46 and 61) measured by the PTR-MS. Ion signals measured by PTR-MS are normalized by signals of reagent ions (i.e. H_3O^+ and $H_3O^+(H_2O)$) and therefore expressed in normalized counts (ncps). The blue vertical dashed lines indicate the injection of water in the chamber; the green vertical dashed lines indicate the injection of glyoxal in the chamber, the yellow dashed lines indicate the beginning of irradiation and the grey dashed lines indicate the end of irradiation.

The measured glyoxal concentration after the injection (**Figure 3~~a~~2a**) is lower than the nominal concentration of 1 ppm and goes to zero within minutes due to the rapid interactions with the walls of the chamber, water vapour, and the dust particles. Upon irradiation, formic acid and carbon monoxide are formed, as expected by the photolysis of glyoxal (De Haan et al., 2020). Fragments m/z = 46 and 47 are observed during water injection and photolysis, which ~~and~~ could originate from the deprotonated and protonated form of formic acid, respectively. This suggests that a minor fraction of the formic acid could result from the desorption of compounds (including glyoxal) from the chamber walls. Fragments m/z = 43 and m/z = 61, and occasionally m/z = 45 (not seen during experiment D_{15} and therefore not shown in **Figure 2b**), are observed at a normalised intensity two orders of magnitude lower than that of formic acid, but not attributed. The quantification with both PTR-MS and FTIR in our experimental RH conditions is ~~complicated by the presence of water~~complex due to water presence, which reduces the sensitivity of PTR-MS and can interfere with the absorption of various organic compounds, making their quantification less accurate.

Mis en forme : Police :Gras

Mis en forme : Police :Gras

Mis en forme : Police :Gras

3.~~2~~2. Evaluation of g~~G~~lyoxal uptake coefficient and rate of formation of organic aerosols

~~For experiment D_{15} at 80% RH,~~ **Figure 3** shows an example of the temporal evolution of the natural logarithm of the glyoxal concentration measured by the FTIR, compared to that measured during a typical blank experiment without dust particles (top panel) and . ~~**Figure 4** additionally shows~~ the variation of the aerosol organic fraction measured by the ToF-ACSM during the same time period (lower panel).

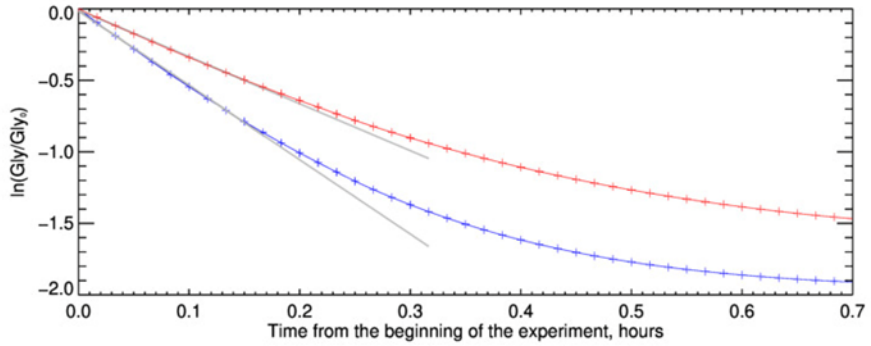

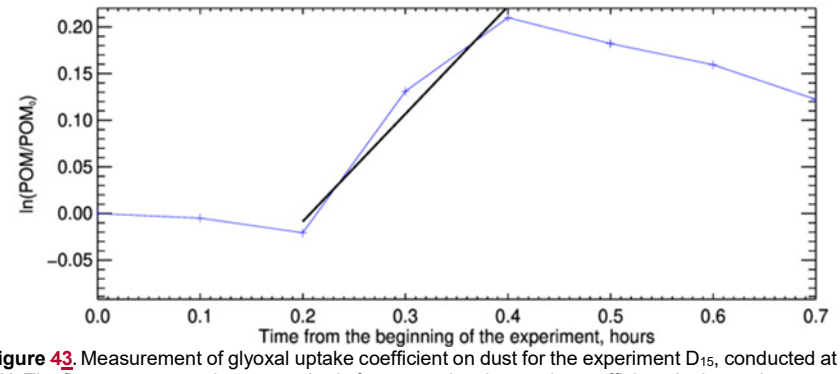

Figure ~~4~~3. Measurement of glyoxal uptake coefficient on dust for the experiment D_{15}, conducted at 80% RH. The figure compares the two methods for measuring the uptake coefficient. In the top image, results are shown for the method based on monitoring the decay of gas-phase glyoxal. The red and blue curves represent the logarithm of the ratio between the calculated decay of gas-phase glyoxal in the absence and presence of dust aerosols, respectively. The black lines represent the linear fit whose slope provides the heterogeneous kinetic constants of the two processes. The image at the bottom displays the result of the uptake coefficient measurement for the same experiment, obtained from the organic formation on the dust aerosol monitored by the ToF-ACSM. The blue time series shows the logarithm of the ratio between the measured organic concentration divided by the initial organic on dust aerosol, while the black line is the linear fit representing the kinetics of organic formation.

Mis en forme : Justifié

Mis en forme : Police :Gras

Mis en forme : Police :Gras

Within the first 10 minutes after the injection of glyoxal, the decrease of the natural logarithm concentrations ratio with time in the presence of dust is linear (that is, the rate is constant). After that, the loss slightly deviates from linearity. The difference from linearity is more evident for the blank experiment, when it occurs earlier than when the dust is present. These observations indicate that, within the first 10 minutes, the uptake of glyoxal on the dust particles can be considered to follow a first-order kinetic and its rate represents an initial uptake coefficient. In the following 20 minutes approximately, the uptake slows down, possibly because all the sites available on the particle surface become occupied, but also because that desorption from the particle surface could reinject glyoxal in the reactive mixture. On the particle phase, the natural logarithm of the organic concentration, normalised by its initial value increases rapidly and linearly, almost on the same time scale of that of the loss of glyoxal, but then decreases to return to its initial value within approximately one hour. These observations confirm that the uptake of glyoxal results in a formation of OA on the dust particles, but that this process is reversible.

The uptake coefficients calculated as the linear fit of the glyoxal and particle organic concentration are presented in **Table 2**.

Mis en forme : Police :Gras

Table 2. Uptake coefficients for glyoxal on mineral dust and ammonium sulphate calculated from the loss of gas-phase glyoxal and the rate of OA formation for the experiments conducted at 80% RH. The initial glyoxal concentration is reported. The aerosol surface concentration (A_s) corresponds to the value preceding the glyoxal injection. Ozone concentration is the maximum concentration measured by FTIR spectroscopy after the injection. For ammonium sulphate, only the γ values calculated from the loss of gas phase glyoxal are presented, as the ACSM collection efficiency (CE) for ammonium sulphate varies significantly during OA formation (Matthew et al., 2008).

Tableau mis en forme

Date	Experiment ID	RH%	$[GL]_0$, ppb_v	Ozone (ppb)	A_S ($m^2\ m^{-3}$)	ω (s^{-1})	γ_{gas}	$\gamma_{OA\ glyxoal}$
30/04/2021	D_8	76	759	---	4.8×10^{-4}	3.9×10^{-2}	6.0×10^{-3}	1.0×10^{-3}
03/05/2021	D_9	79	607	---	6.1×10^{-4}	5.0×10^{-2}	1.5×10^{-2}	1.5×10^{-2}
04/05/2021	D_{10}	81	371	---	5.1×10^{-4}	4.2×10^{-2}	1.7×10^{-2}	9.0×10^{-3}
05/05/2021	D_{11}	78	805	---	4.6×10^{-4}	3.8×10^{-2}	8.0×10^{-3}	5.0×10^{-3}
06/05/2021	D_{12}	82	432	---	3.5×10^{-4}	2.9×10^{-2}	1.2×10^{-2}	2.3×10^{-2}
08/02/2022	D_{13}	81	555	1270	7.1×10^{-4}	5.8×10^{-2}	4.0×10^{-3}	4.0×10^{-3}
09/02/2022	D_{14}	78	756	1450	8.5×10^{-4}	7.0×10^{-2}	4.0×10^{-3}	5.0×10^{-3}
10/02/2022	D_{15}	75	600	---	8.4×10^{-4}	6.9×10^{-2}	1.0×10^{-2}	5.0×10^{-3}
14/02/2023	D_{16}	83	661	---	6.0×10^{-4}	4.9×10^{-2}	4.0×10^{-3}	1.5×10^{-2}
07/09/2023	AS_4	81	779	---	6.3×10^{-3}	5.2×10^{-1}	9.8×10^{-4}	---
08/09/2023	AS_5	83	430	---	2.0×10^{-3}	1.7×10^{-1}	1.2×10^{-3}	---
Average dust							$9 (\pm 5) \times 10^{-3}$	$9 (\pm 7) \times 10^{-3}$

Average AS	1.1 (± 0.2) ×10^{-4}

The average uptake coefficients for glyoxal on the Gobi mineral dust calculated at 80% RH from the gas-phase uptake and the particle formation are $\gamma_{Gly\text{-}Dust\text{-}gas}$ = 9 × 10^{-3} (standard deviation ± 5) and $\gamma_{Gly\text{-}Dust\text{-}OA}$ = 9 × 10^{-3} (standard deviation ± 7), respectively. The two average values agree. This suggests that every glyoxal molecule in the gas phase is taken up by the airborne dust particles. This suggests also that the uptake occurs on airborne particles only, as expected as the dust particles are selected in the submicron range and that minimal deposition of dust particles is observed in the first 30 minutes after injection. The primary mechanism of particle loss during this period is dilution, which does not interfere with uptake. The standard deviations of the mean values are large, being attributed to the fact that the state of the chamber walls and the dust size distribution vary from one experiment to the other, and that the aerosol/chamber walls surface ratio is very low (0.08-1.5 × 10^{-3}). The presence of ozone appears uninfluential.

~~The results of the current study can be compared with the literature. Shen et al. (2016) investigated the uptake of glyoxal on mineral proxies, i.e. SiO_2, and $CaCO_3$ and α-Al_2O_3 under various levels of relative humidity. These authors determined the uptake coefficients after a long exposition of the surface to glyoxal (steady state uptakes) and found that the uptake coefficients are reduced with increasing the gas phase concentration of glyoxal. At 1 ppb concentration and a relative humidity of 60% the uptake coefficients determined on suspended particles of calcite ($CaCO_3$, γ = (1.4 ± 0.1) × 10^{-4}) and alumina (α-$Al_2O_3$$AlO_3$, γ = (5.5 ± 0.1) × 10^{-5}). Our values are measured in a shorter time frame and correspond to an initial uptake of glyoxal. They are approximately one order of magnitude higher than those obtained by Shen et al. (2016). These authors scaled the uptake coefficient to the specific surface area of the dust, which henceforth could correspond to a lower limit. On the contrary, in our case, we use a geometric surface area (assuming spherical particles) which could lead to an overestimation of the uptake coefficient.~~

~~Zogka et al. (2024) used a Knudsen cell to evaluate the initial and steady state glyoxal uptake coefficient bulk soil samples of various origins. At low relative humidity, these authors found that for Gobi soil sieved to less than 63 μm in diameter the initial uptake~~

Mis en forme : Anglais (États-Unis)

Mis en forme : Anglais (États-Unis), Indice

Mis en forme : Anglais (États-Unis)

Mis en forme : Anglais (États-Unis), Indice

~~coefficient using the geometric surface area was 0.18 (corresponding to an upper limit of the uptake) independent of glyoxal concentration. However, the steady state uptake coefficients determined after a long processing of surface were found to decrease with increasing glyoxal concentration, due to aging of the surface.~~

~~Various reasons can explain these apparently different results. First of all, in CESAM we measure the initial uptake coefficient at humid conditions, which is independent of concentration. On the other hand, Shen et al. (2016) measured steady-state uptake coefficient at lower glyoxal concentrations (< 1 ppb) than we did (>400 ppb). As shown by both Shen et al. (2016) and Zogka et al. (2024), the steady state uptake coefficient decreases with the concentration of glyoxal, regardless of the relative humidity.~~

~~Secondly, the uptake coefficient is inversely proportional to the available particle surface, which in our case is smaller than Zogka et al. (2024) who used soils sieved to 63 µm. Shen et al (2016) used standard mineral particles of various sizes from 35 nm to 5 µm, while our particle size distribution peaked between 300 and 400 nm. Shen et al. (2016) used single minerals, while Zogka et al. (2024) and our study share the same soil sample from Gobi. While the uptake coefficient should depend on the dust mineralogy, this is difficult to ascertain in the present study.~~

~~**Overall, although the experiments performed in literature with those of the current study were performed under different conditions, results indicate that natural Gobi dust is an effective sink of glyoxal, with initial uptake coefficient independent of glyoxal concentration, pointing to a first order removal process. However, the long term ageing of particles leads to lower uptake coefficients that strongly depend on glyoxal concentration due to the depletion of surface sites.**~~

3.3. Evidence of irreversible particle growth

Figure 1 shows that, even in the more favourable conditions (RH=80%), the ratio between the observed increase of the POM (2 µg m^{-3}) and that of the particle volume concentration (20 μm^3 cm^{-3}) corresponds to an estimated mass density of the order of 0.1 g cm^{-3}, which is about 10 times lower than the value of 1 g cm^{-3} expected for glyoxal. This is partially attributed to the fact that only part of the organic matter formed on dust is detected by the ACSM~~, as will be discussed in **Section 3.5**~~. On the other hand, **Figure S34** shows that, after reaching its maximum value, the volume concentration

Mis en forme : Police :Gras

Mis en forme : Police :Gras

decreases at a lower rate than the POM (slope 3.9 × 10^{-5} s^{-1} and 6.1 × 10^{-5} s^{-1}, respectively). This suggests that an additional process could contribute the particle volume concentration partially compensating the loss of organic matter on the dust particles.

Mis en forme : Police :Gras

This is confirmed by **Figure 4,** which shows the variation in time of the normalised particle volume distributions, at four steps of the experiments performed at 30% RH and 80% RH. Those include prior and glyoxal injection, POM maximum peak value, and the end of the experiment.

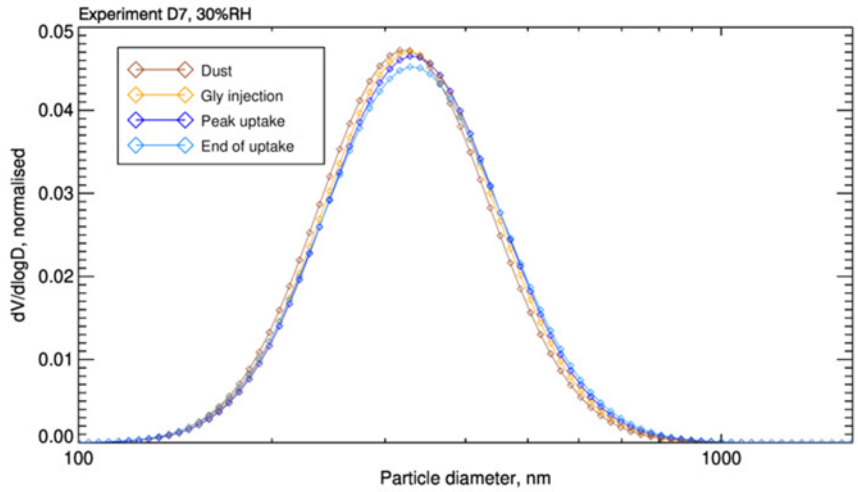

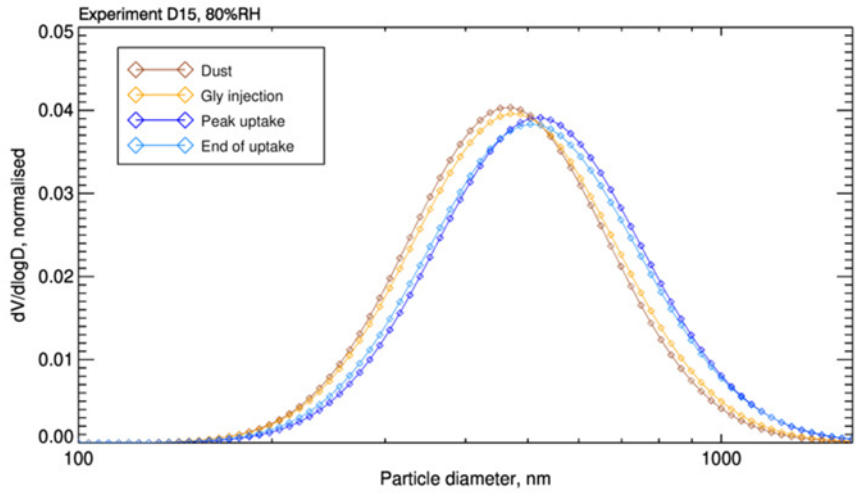

Figure 4. Evolution of volume-size distributions for two glyoxal uptake experiments in different relative humidity conditions. The images illustrate the progression of volume-size distributions recorded at four key moments during the experiments. The first distribution (orange) is recorded after the dust is injected into the simulation chamber. The second distribution (yellow) is recorded at the moment of glyoxal injection. The third distribution (blue) corresponds to the peak uptake of glyoxal on the aerosol, and the fourth (light blue) is recorded at the end of glyoxal uptake process. The left image depicts the evolution for the experiment D7 conducted at 30% RH, while the image on the right shows the distributions for the experiment D15 conducted at 80% RH. The results highlight that the distributions grow more significantly at 80% RH, indicating a higher glyoxal uptake and organic formation at elevated humidity levels.

All distributions have a single mode. However, after the injection of glyoxal, the geometric mean volume diameter, measured at the maximum POM concentration,

increases by up to 10% (from 310 to 340 nm) at 30% RH, and up to 20% (from 450 to 540 nm) at 80% RH. Interestingly, even at the end of the experiment, when the POM concentration returns to its initial value, the increase in geometric mean diameter of the aerosol is irreversible. ~~This effect could be explained by the hypothesis~~We hypothesize that the uptake of glyoxal enhances the dust hygroscopicity~~.~~ Therefore ~~After glyoxal uptake, the particle becomes more hygroscopic and the~~ the difference in total volume between the beginning and end of the experiment is due to ~~to water uptake which adds up to the~~ formed organic aerosol mass, resulting from water uptate.

3.~~3~~4~~5~~. Chemical composition of the particulate o~~O~~rganic matter~~c composition~~

This section discusses the chemical composition of the particulate organic matter formed on the mineral dust following the interaction with glyoxal. The list and conditions of the filter samples analysed by SFE/GC-MS and ESI-Orbitrap are reported in **Table S2~~3~~** in the Supplementary Material. Details of~~n~~ the organic composition of the native dust are provided in **Text S6** ~~in the supplementary material~~.

3.~~4~~5.1. Timeline of chemical evolution

Figure 5 shows the time evolution of the intensity of the organic fragments detected by the ToF-ACSM at 80% RH (experiment D_{15}) at four moments of the experiment: 1) before the injection of glyoxal ~~(dust only)~~; 2) during the uptake and the ~~POM~~ formation of the organic matter; 3) after the organic matter has reached its maximum concentration; and 4) at the end of the experiment, when ~~it~~the organic matter returned to its initial ~~value~~concentration.

Mis en forme : Police :12 pt
Mis en forme : Police :12 pt
Mis en forme : Police :12 pt
Mis en forme : Police :12 pt
Mis en forme : Niveau 4, Espacement automatique entre les caractères asiatiques et latins, Espacement automatique entre les caractères asiatiques et les chiffres
Mis en forme : Police :12 pt
Mis en forme : Police :12 pt
Mis en forme : Police :12 pt
Mis en forme : Police :12 pt
Mis en forme : Police :12 pt
Mis en forme : Police :12 pt
Mis en forme : Police :Non Italique
Mis en forme : Titre 4
Mis en forme : Police :12 pt
Mis en forme : Gauche, Niveau 4, Espacement automatique entre les caractères asiatiques et latins, Espacement automatique entre les caractères asiatiques et les chiffres
Mis en forme : Niveau 4, Espacement automatique entre les caractères asiatiques et latins, Espacement automatique entre les caractères asiatiques et les chiffres
Mis en forme : Police :12 pt
Mis en forme : Police :12 pt
Mis en forme : Police :12 pt
Mis en forme : Police :12 pt
Mis en forme : Police :12 pt
Mis en forme : Police :12 pt
Mis en forme : Police :12 pt
Mis en forme : Police :12 pt
Mis en forme : Police :12 pt
Mis en forme : Police :12 pt
Mis en forme : Police :12 pt
Mis en forme : Police :12 pt

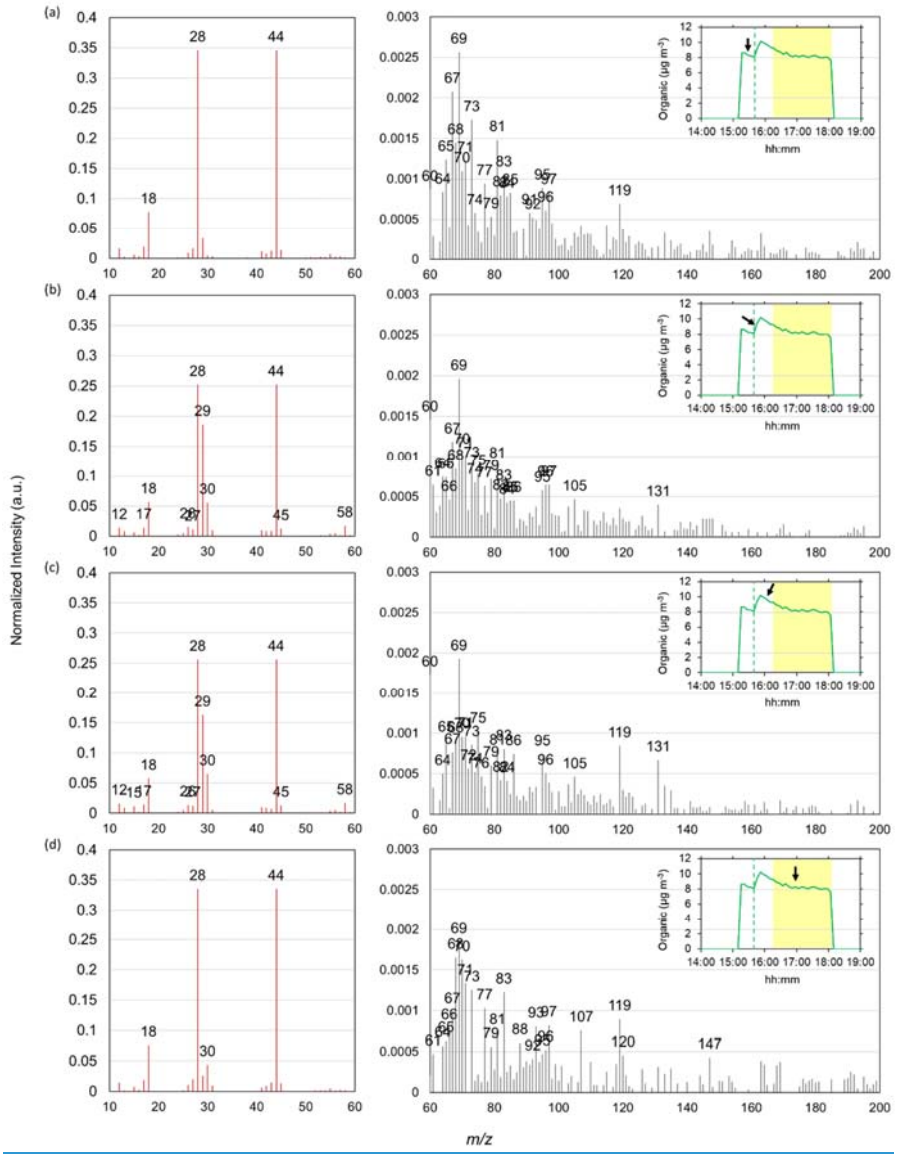

Figure 2. ACSM organic mass spectra (intensities normalized to the total organic concentration) recorded during the experiment D_{15}: (a) before glyoxal uptake (dust organic fraction composition), (b) during glyoxal uptake, (c) after reaching the maximum uptake on the particles and (d) 1h later under irradiation. Panels on the left show the mass spectra ranging from m/z 10 to 60, while the panels on the right represent fragments from m/z 60 to 200 (their intensity is approximately one hundred times lower). The inserts display the time series of organic concentrations measured by the ToF-ACSM. A black arrow indicates the time corresponding to the mass spectrum shown. The yellow-highlighted shaded area indicates the interval where irradiation takes place, while the green vertical dashed lines indicate the moment of glyoxal injection in the chamber.

Mis en forme : Police :9 pt

Mis en forme : Police :9 pt

Mis en forme : Police :9 pt

Mis en forme : Police :9 pt

Mis en forme : Police :11 pt

Mis en forme : Police :(Par défaut) Arial, 12 pt

~~The chemical composition of organic matter~~**Figure 5** reveals that the organic matter formed as a result of the interaction between~~ on m~~ mineral dust ~~following~~and glyoxal ~~interaction reveals that organic aerosol formation~~ is composed of oxidized organic fragments, organic acids, oligomers.

Oxidized organic fragments such as CO^+ (m/z 28) and CO_2^+ (m/z 44)~~, indicators of oxidized organics, were~~are ~~consistently~~ observed through all phases of experiments~~, reflecting the dynamic glyoxal uptake and subsequent chemical transformations~~. ~~Additional~~F~~ fr~~ragments such ~~, including~~as CHO^+ (m/z 29), CH_2O^+ (m/z 30), and $C_2H_2O_2^+$ (m/z 58), ~~prominently emerged~~appear during the uptake of glyoxal~~,~~ but diminish ~~uptake, diminishing~~ over time, ~~potentially~~ due to oligomerization or further oxidation processes. The most intense fragment above m/z 60 is~~,~~ m/z 69, which appears unrelated to glyoxal reactivity but could be ~~and has been~~ attributed to nitrogen-containing organic~~s~~ species such as $C_3H_3NO^+$, ~~potentially~~ originating from glyoxal–ammonia reactions (Galloway et al., 2009) or plant and soil residues (Sun et al., 2010; Nieder et al., 2018). Fragments at m/z 105 and 131, observed consistently during the uptake and the photolysis, ~~are~~could be attributed to condensed glyoxal hydrates (Liggio et al., 2005; Carlton et al., 2007). Fragments at m/z 119 and 120, associated with oxidized products from isoprene-derived aerosols (Safi Shalamzari et al., 2013), increased after glyoxal uptake and under irradiation, suggesting formation of oxidized oligomers. Upon irradiation, the appearance of m/z 147 and 165 – ~~—~~products of aqueous glyoxal oxidation and oligomer condensation (Lim et al., 2010) – ~~—~~suggests photo-chemically enhanced transformation, though their presence in native dust also points to reversible adsorption processes.

3.~~4~~5.2. Molecular identification

The list and conditions of the samples analysed by SFE/GC-MS and ESI-Orbitrap are reported in **Text S7~~X~~** in the Supplementary Material, which also provides with examples of analysis. The summary of the organic molecules detected by those analysis is presented in **Table 3.**

Table 3. Summary of observed compounds identified by SFE/GC-MS analysis and glyoxal-related formulas observed with ESI-Orbitrap, along with the suggested structures under the different experimental conditions tested.

Molecular formula	Name	Tentative Structure	Technique	Experimental conditions

Mis en forme : Police :12 pt
Mis en forme : Police :(Par défaut) Arial, 12 pt, Gras
Mis en forme : Police :(Par défaut) Arial, 12 pt
Mis en forme : Police :12 pt
Mis en forme : Police :12 pt
Mis en forme : Police :12 pt
Mis en forme : Police :12 pt
Mis en forme : Police :12 pt
Mis en forme : Police :12 pt, Surlignage
Mis en forme : Police :12 pt
Mis en forme : Police :12 pt
Mis en forme : Police :12 pt
Mis en forme : Police :12 pt
Mis en forme : Police :12 pt
Mis en forme : Police :12 pt
Mis en forme : Police :12 pt
Mis en forme : Police :12 pt
Mis en forme : Police :12 pt
Mis en forme : Police :12 pt
Mis en forme : Police :12 pt
Mis en forme : Police :12 pt
Mis en forme : Police :12 pt
Mis en forme : Police :12 pt
Mis en forme : Police :12 pt
Mis en forme : Police :12 pt
Mis en forme : Police :12 pt
Mis en forme : Police :12 pt
Mis en forme : Police :12 pt
Mis en forme : Titre 4, Espace Avant : 0 pt, Interligne : simple
Mis en forme : Police :Gras
Mis en forme : Non Surlignage
Mis en forme : Police :Gras

$C_2H_2O_3$	Glyoxylic acid		ESI-Orbitrap	Dust+Gly, 80%, Dark, O_3
$C_2H_4O_3$	Glycolic acid		ESI-Orbitrap SFE/GC-MS	Dust+Gly, 30%, Dark Dust+Gly, 30%, Light Dust+Gly, 80%, Light Dust+Gly, 80%, Light, O_3
$C_2H_2O_4$	Oxalic acid	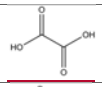	ESI-Orbitrap	Dust+Gly, 80%, Light
$C_2H_4O_4$	Glyoxylic acid monohydrate		ESI-Orbitrap SFE/GC-MS	Dust+Gly, 80%, Light
$C_4H_4O_4$	Glycolic acid dimer		ESI-Orbitrap	Dust+Gly, 80%, Light
$C_5H_6O_5$	Glyoxal oligomer	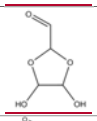	ESI-Orbitrap	Dust+Gly, 80%, Light
$C_6H_6O_6$	Glyoxal oligomer	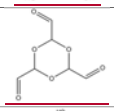	ESI-Orbitrap	Dust+Gly, 80%, Light
$C_8H_{16}O_{12}$	Glyoxal oligomer	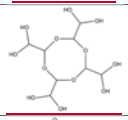	ESI-Orbitrap	Dust+Gly, 80%, Light
$C_{10}H_{12}O_{11}$	Glyoxal oligomer	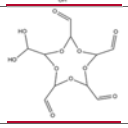	ESI-Orbitrap	Dust+Gly, 80%, Dark

Oxidized organic compounds such as glycolic acid ($C_2H_4O_3$), oxalic acid ($C_2H_2O_4$), and a possible dimer of glycolic acid ($C_4H_4O_4$) were mainly observed under irradiated conditions, while their hydrated forms also appeared in dark conditions. Glyoxylic acid was detected in dark conditions in the presence of ozone. Glycolic and glyoxylic acids consistently form under humid conditions, indicating that their pathways may be less sensitive to water competition or that their precursors interact more strongly with dust surfaces. Light but also ozone tends to favor the formation of glycolic acid from glyoxal at high RH (**Figure S7.1**), suggesting two possible oxidative ~~7-1~~pathways. Glycolic acid is also detected at 30% RH (not showed), with and without irradiation~~light~~, in agreement with the experiments on dust by Shen et al. (2016), but differently than reported by Galloway et al. (2009) on ammonium sulphate. Monohydrated glyoxylic acid is found in one sample at 80% RH under irradiated conditions, likely due to the known pattern of oxidation of glyoxal and glycolic acid with OH radicals (Buxton et al.,

Mis en forme : Non Surlignage

1997). Unlike previous studies (Galloway et al., 2009; Rubasinghege et al., 2013; Shen et al., 2016), formic acid was not detected, possibly due to high RH suppressing its formation by limiting access to reactive surface sites, as suggested by Shen et al. (2016).

Figure 7 illustrates the mass spectrum and the assigned formula for experiment D_{10}.

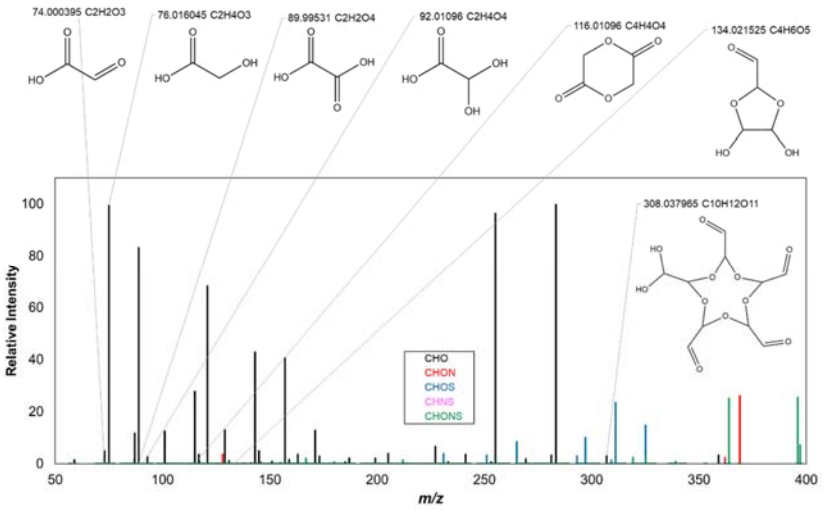

Figure 7: ESI Orbitrap MS from the filter D_{10}: uptake of glyoxal on mineral dust at 80% RH and under irradiation. In the mass spectra, the peaks referring to *formulas for which is possible to suggest a structure from glyoxal reactivity are labelled.*

Compounds from C_4 to C_{10}, oOligomerization products (compounds from C4 to C10) of the glyoxal mono- and di-hydrate forms, are observed only at 80% RH. These are: $C_4H_6O_5$ (1 monohydrated glyoxal + 1 dehydrated glyoxal forming a 5-atom ring), $C_8H_{16}O_{12}$ (4 dehydrated glyoxal molecules forming an 8-membered ring), and $C_{10}H_{12}O_{11}$ (4 monohydrated glyoxal molecules + 1 dehydrated glyoxal molecule forming a ring structure). The oligomer $C_6H_6O_6$ (3 molecules of monohydrated glyoxal forming a 6-membered ring) is detected only under dark conditions. $C_8H_{16}O_{12}$, can correspond to an oligomer previously observed by Shen et al. (2016) on mineral dust.

Mis en forme : Police :Non Gras

Mis en forme : Espace Avant : 6 pt, Après : 0 pt

Mis en forme : Police :Non Gras

The persistence of low-volatility, heavy compounds, such as oligomers at the surface of mineral dust has implications for its oxidation state, which is modified in an irreversible way its surface composition, as already shown by previous studies on ammonium sulphate seeds (Kroll et al., 2005; Galloway et al., 2009; De Haan et al., 2020; Hu et al., 2022). This is illustrated by the van Krevelen diagrams obtained from the ESI-Orbitrap analysis in ~~Figure~~ 69.

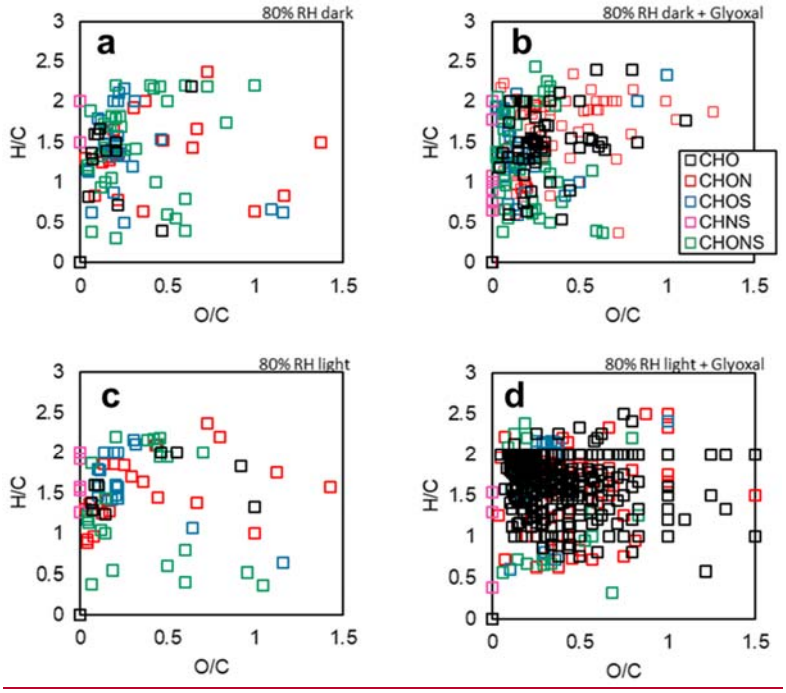

Figure 69. Van Krevelen diagrams recorded at 80% RH for: in the top line experiments in the dark for mineral dust only (control experiment D_2, left) and one ageing experiment of dust with glyoxal (experiment D10); bottom line: same with irradiation. Samples are equivalent in terms of load of particulate organic matter. These are 0.9 µg (sample a), 0.8 µg (sample b), 1.7 µg (sample c) and 0.6 µg (sample d). Despite an equivalent loading of particulate organic mass, the number of signals detected is significantly higher when the dust is exposed to glyoxal (86 and 102 peaks detected for dust only against 398 and 310 with glyoxal, and with and without light, respectively).

The processing by the glyoxal clearly has an effect on the oxidation state of the dust, particularly when lights are on, resulting in the appearance of signals with O/C ratio higher than 1, attributed to photo-oxidation. The predominant family in this case is that

Mis en forme : Police :Gras

Mis en forme : Non Surlignage

of CHO molecules, while the appearance of molecules for families CHON and CHONS is also observed.

~~The list and conditions of the filter samples analysed by SFE/GC-MS and ESI-Orbitrap are reported in **Table S3** in the Supplementary Material. The summary of the organic molecules detected by those analysis is presented in **Table 3** and discussed in the next paragraphs.~~

~~**Table .** Summary of frequently observed compounds identified by SFE/GC-MS analysis and glyoxal-related formulas observed with ESI-Orbitrap, along with the suggested structures under the different experimental conditions tested.~~

Molecular formula	Name	Tentative Structure	Technique	Experimental conditions
$C_2H_2O_3$	Glyoxylic acid		ESI-Orbitrap	Dust+Gly, 80%, Dark, O_3
$C_2H_4O_3$	Glycolic acid	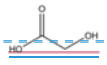	ESI-Orbitrap SFE/GC-MS	Dust+Gly, 30%, Dark Dust+Gly, 30%, Light Dust+Gly, 80%, Light Dust+Gly, 80%, Light, O_3
$C_2H_2O_4$	Oxalic acid	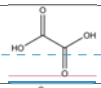	ESI-Orbitrap	Dust+Gly, 80%, Light
$C_2H_4O_4$	Glyoxylic acid monohydrate	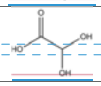	ESI-Orbitrap SFE/GC-MS	Dust+Gly, 80%, Light
$C_3H_6O_3$	Lactic acid	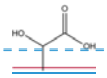	SFE/GC-MS	Dust, 80%, Light Dust+Gly, Dry, Dark Dust+Gly, 30%, Dark Dust+Gly, 30%, Light Dust+Gly, 80%, Light Dust+Gly, 80%, Dark, O_3 Dust+Gly, 80%, Light, O_3
$C_5H_8O_3$	Levulinic acid	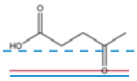	SFE/GC-MS	Dust, Dry, Dark Dust, 80%, Dark Dust, Dry, Light Dust+Gly, 30%, Dark Dust+Gly, 30%, Light Dust+Gly, 80%, Dark, O_3 Dust+Gly, 80%, Light, O_3
C_7H_8O	Benzyl alcohol		SFE/GC-MS	Dust, 80%, Dark Dust+Gly, 30%, Dark Dust+Gly, Dry, Light Dust+Gly, 30%, Light Dust+Gly, 80%, Light
$C_9H_{16}O$	Cyclohexanone, 3,3,5-trimethyl	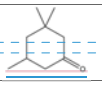	SFE/GC-MS	Dust, 80%, Dark Dust+Gly, 30%, Dark Dust+Gly, 30%, Light Dust+Gly, 80%, Light, O_3
$C_4H_6O_4$	Glycolic acid dimer		ESI-Orbitrap	Dust+Gly, 80%, Light
$C_6H_8O_6$	Glyoxal oligomer	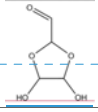	ESI-Orbitrap	Dust+Gly, 80%, Light

Mis en forme : Police :12 pt

Mis en forme : Anglais (États-Unis)

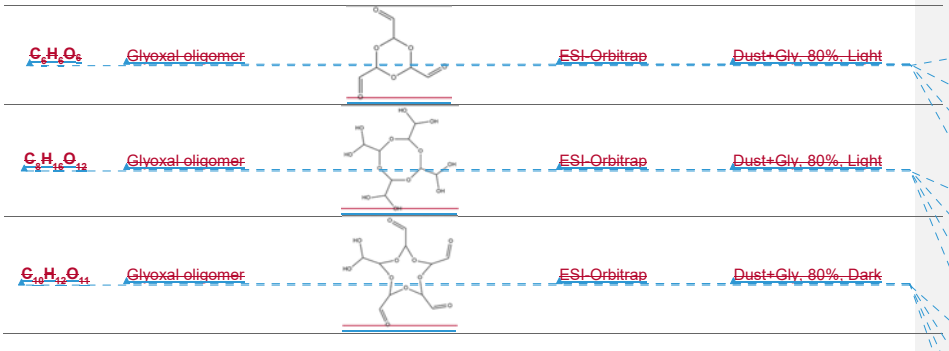

Oxidized organic compounds such as glycolic acid ($C_2H_4O_3$), oxalic acid ($C_2H_2O_4$), and a possible dimer of glycolic acid ($C_4H_4O_4$) are mainly observed under irradiated conditions, while their hydrated forms also appear in the dark. Glyoxylic acid emerges in dark conditions in the presence of ozone. Unlike previous studies (Galloway et al., 2009; Rubasinghege et al., 2013; Shen et al., 2016), formic acid is not detected, possibly due to high RH suppressing its formation by limiting access to reactive surface sites, as suggested by Shen et al. (2016). In contrast, glycolic and glyoxylic acids consistently form under humid conditions, indicating that their pathways may be less sensitive to water competition or that their precursors interact more strongly with dust surfaces. Light and the presence of ozone favor its formation. Indeed, the fourth panel in **Figure 6** suggests that ozone might substitute light in promoting the formation of glycolic acid from glyoxal at high RH, suggesting an alternative oxidative pathway. Glycolic acid is also detected at 30% RH (not showed), both with and without light, in agreement with the experiments on dust by Shen et al. (2016), but differently than reported by Galloway et al. (2009) on ammonium sulphate. Monohydrated glyoxylic acid is found in one sample at 80% RH under irradiated conditions, likely due to the known pattern of oxidation of glyoxal and glycolic acid with OH radicals (Buxton et al., 1997).

The observation of organic acid formation following glyoxal uptake could have important implications for aerosol properties. In the study from (Ortiz-Montalvo et al., 2014), even mildly acidic conditions significantly enhanced glyoxal oligomerization and favoured the formation of low volatility compounds, contributing to SOA mass through gas-particle partitioning. An organic acid produced from glyoxal oxidation, such as oxalic acid, was observed to facilitate the dissolution of transition metals like iron and

Mis en forme : Anglais (États-Unis)
Mis en forme : Anglais (États-Unis)
Mis en forme : Anglais (États-Unis)
Mis en forme : Anglais (États-Unis)
Mis en forme : Anglais (États-Unis)
Mis en forme : Anglais (États-Unis)
Mis en forme : Anglais (États-Unis)
Mis en forme : Anglais (États-Unis)
Mis en forme : Anglais (États-Unis)
Mis en forme : Anglais (États-Unis)
Mis en forme : Anglais (États-Unis)
Mis en forme : Anglais (États-Unis)
Mis en forme : Police :12 pt, Anglais (États-Unis)
Mis en forme : Police :12 pt
Mis en forme : Police :12 pt, Surlignage
Mis en forme : Police :12 pt

copper, thereby altering their speciation and enhancing their bioavailability in aqueous aerosol environments (Giorio et al., 2022).

Furthermore, the acidification of aerosols increased their hygroscopicity, especially under high RH conditions, affecting particle growth dynamics, phase behaviour, and cloud condensation nuclei (CCN) potential (Song and Ocada, 2021). Collectively, these processes highlight how aerosol acidity modulates not only chemical transformations but also key physical properties and atmospheric lifetimes of dust-glyoxal systems.

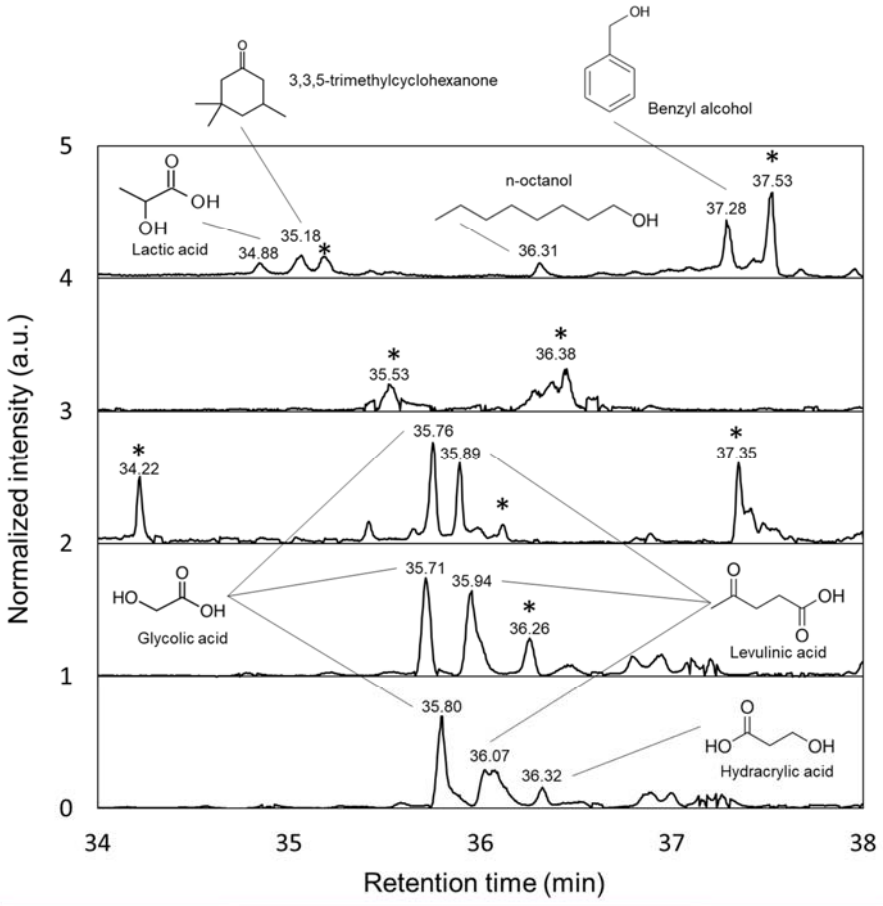

Figure 6. SFE/GC-MS chromatograms recorded from filters collected during one dust control experiment and four glyoxal uptake experiments under four different conditions. From up to bottom: the first chromatogram is from Experiment D_2, dust control experiment under 80% RH and irradiation. The second is from Experiment D_{16} with dust and glyoxal at 80% RH under dark conditions. The third is from

Mis en forme : Anglais (États-Unis)

Experiment D_{15} with dust and glyoxal at 80% RH under irradiated conditions. The fourth and fifth chromatograms are from Experiment D_{13} with dust and glyoxal at 80% RH in the presence of ozone under dark and irradiated conditions, respectively. The two peaks of higher intensity appearing after 41 minutes are from the internal standards added to the solution: tridecane around 41 minutes and ortho-toluic acid at about 41.8 minutes. The intensity is normalized to peak of the internal standard ortho-toluic acid. The chromatograms start at 32 minutes as 15 minutes are required for the removal of CO_2 from the extraction fluid, and approximately another 15 minutes represent the delay required for the solvent to pass through the column and reach the electron ionization (EI) MS detection. For *the second and third spectra, is noticeable that under irradiated conditions the number of peaks increases significantly compared to dark conditions, likely due to enhanced chemical reactions driven by light. This effect appears to be less pronounced in the presence of ozone.*

On the 15 samples analysed by ESI Orbitrap (**Table S3** in the Supplementary Material), signals attributable to products of the oxidation, hydration, or oligomerization of glyoxal are found only for experiments at high relative humidity (80%), both in the dark but mostly in irradiated conditions. **Figure 7** illustrates the mass spectrum and the assigned formula for experiment D_{10}.

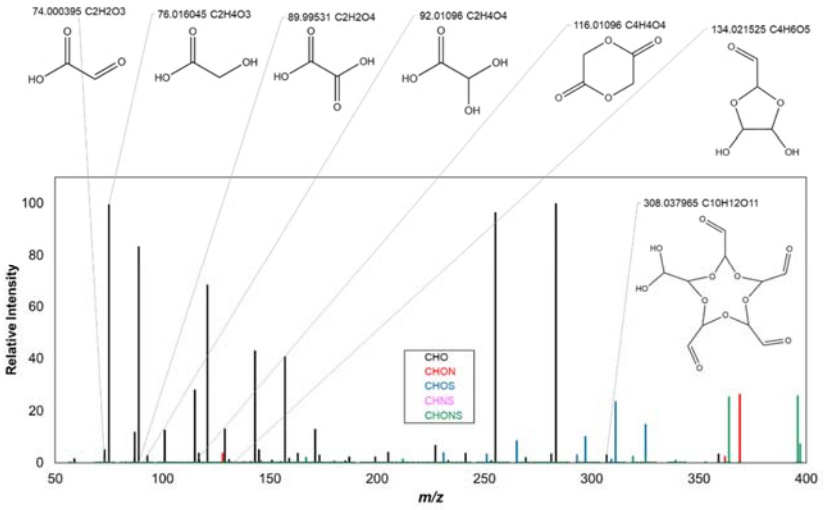

Figure 7. ESI Orbitrap MS from the filter D_{10}: uptake of glyoxal on mineral dust at 80% RH and under irradiation. In the mass spectra, the peaks referring to formulas for which is possible to suggest a structure from glyoxal reactivity are labelled.

Compounds from C_4 to C_{10}, oligomerization products of the glyoxal mono and di hydrate forms, are observed only at 80% RH. The following peaks are detected and attributed: $C_4H_6O_6$ (1 monohydrated glyoxal + 1 dehydrated glyoxal forming a 5-atom ring), $C_8H_{10}O_{12}$ (4 dehydrated glyoxal molecules forming an 8 membered ring), and $C_{10}H_{12}O_{11}$ (4 monohydrated glyoxal molecules + 1 dehydrated glyoxal molecule

Mis en forme : Police :12 pt

Mis en forme : Anglais (États-Unis)

Mis en forme : Police :12 pt

forming a ring structure). The oligomer $C_6H_6O_6$ (3 molecules of monohydrated glyoxal forming a 6-membered ring) is detected only under dark conditions. $C_6H_{16}O_6$ corresponds to an oligomer previously observed by Shen et al. (2016) on mineral dust.

Based on the observations above, **Figure 8** shows the suggested chemical mechanism.

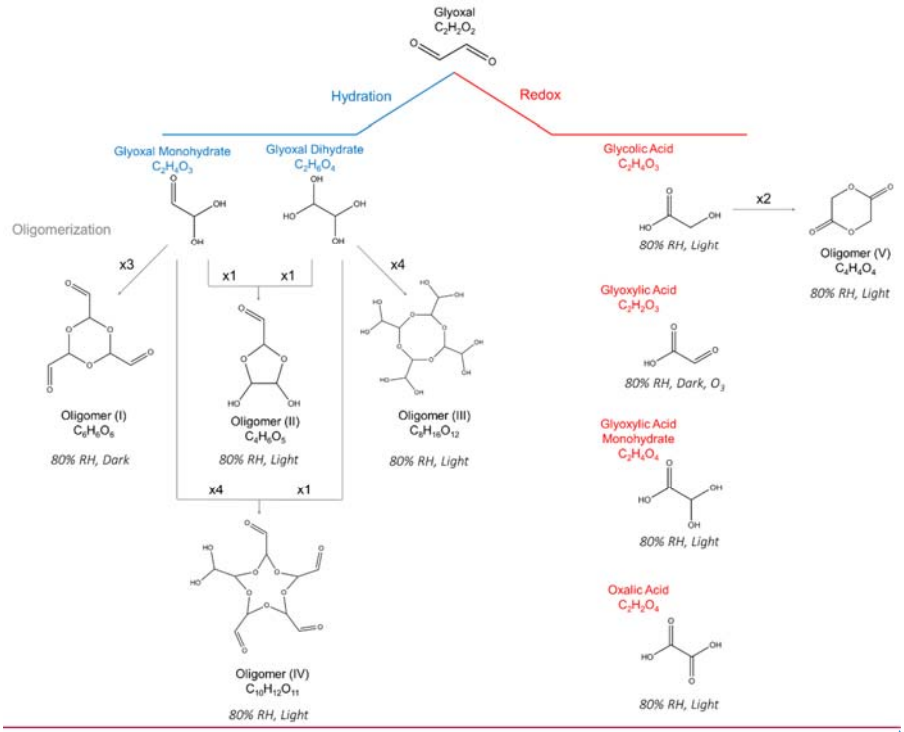

Figure 8. Proposed reaction scheme to explain the glyoxal-related molecular formulas detected through ESI-Orbitrap mass spectrometry and SFE/GC-MS.

The primary oligomers detected are attributed to the condensation of hydrated glyoxal forms specifically the mono- and di-hydrated glyoxal forms, through hydrolysis. The oligomer V is attributed to the condensation of two glycolic acid molecules.

Glyoxal-derived oligomers could significantly influence the optical properties of mineral dust aerosols. Spectroscopic analyses revealed broadened OH and C–O bands and enhanced Raman activity in these oligomers, indicative of their hydrated and cyclic

Mis en forme : Anglais (États-Unis)

Mis en forme : Police :12 pt

Mis en forme : Espace Avant : 6 pt, Après : 0 pt

Mis en forme : Police :12 pt, Anglais (États-Unis)

Mis en forme : Police :12 pt, Surlignage

~~structures (Avzianova & Brooks, 2013). Core-shell models showed that glyoxal uptake increased particle size and optical extinction cross sections, with refractive indices of n ≈ 1.68 + 0.01i at 50% RH and n ≈ 1.65 + 0.02i at 75% RH (Trainic et al., 2011).~~

~~These oligomers exhibited enhanced UV visible absorption, particularly between 300–600 nm, with characteristic shoulders at ~280 and 345 nm attributed to acetal and aldol condensation products (Schwier et al., 2010; Shapiro et al., 2009). High RH conditions (>80%) facilitated brown carbon formation, further evidenced by UV-visible absorbance peaks and Raman background signals (De Haan et al., 2020; Zhang et al., 2022).~~

~~3.3. Organic composition~~

~~This section discusses the chemical composition of the organic matter on mineral dust following the interaction with glyoxal. Details on the organic composition of the native dust are provided in Text S4 in the supplementary material.~~

~~*3.3.1. Measurements by the ACSM*~~

~~Figure 5 shows the time evolution of the intensity of the organic fragments detected by the ACSM at 80% RH (experiment D_{15}) before the injection of glyoxal (dust only), during the POM formation, after the maximum concentration, and at the end of the experiment, when it returned to its initial value.~~

Mis en forme : Espace Avant : 0 pt, Après : 8 pt

Commenté [PFO2]: Conclusion?

Mis en forme : Police :11 pt

Mis en forme : Anglais (États-Unis), Surlignage

Mis en forme : Surlignage

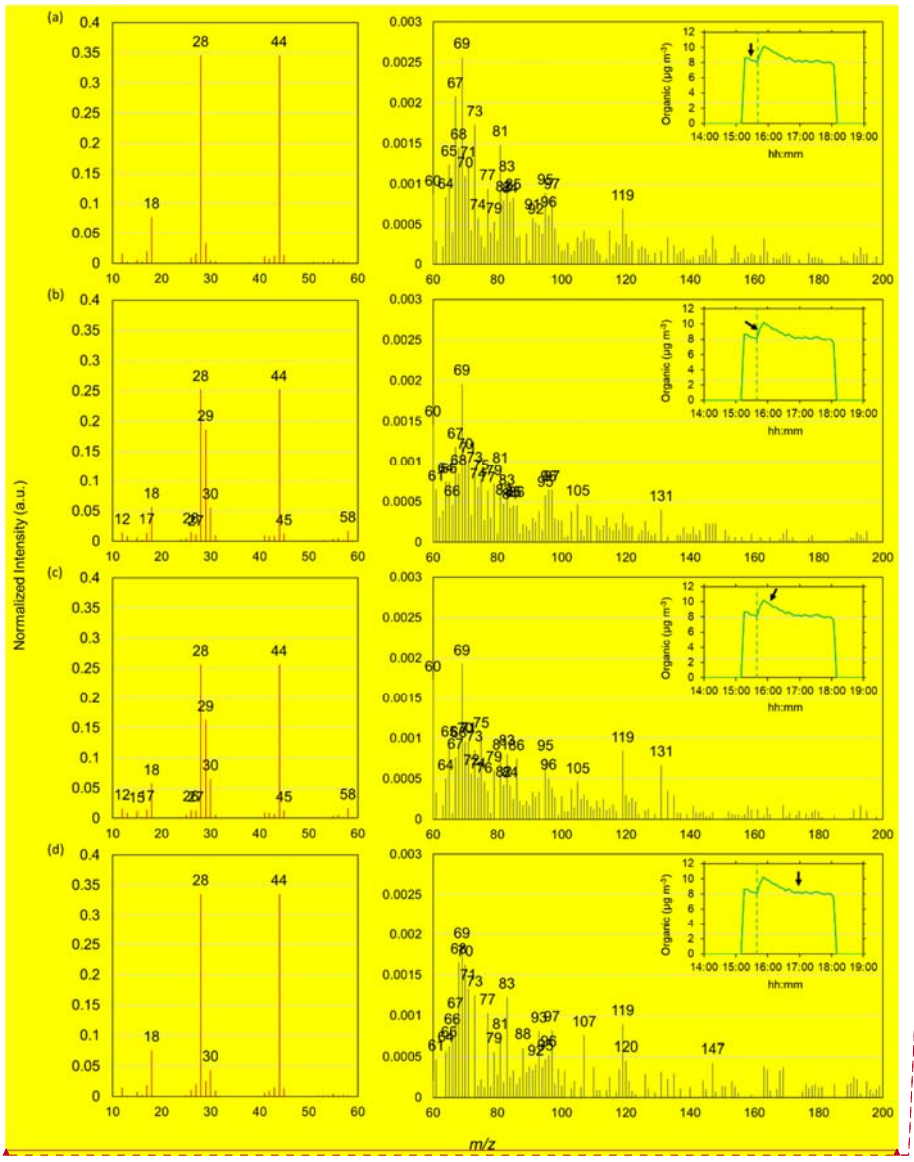

Figure 5. *ACSM organic mass spectra (intensities normalized to the total organic concentration) recorded during the experiment D15: (a) before glyoxal uptake (dust organic fraction composition), (b) during glyoxal uptake, (c) after reaching the maximum uptake on the particles and (d) 1h later under irradiation. Panels on the left show the mass spectra ranging from 10 to 60 m/z, while the panels on the right represent fragments from 60 to 200 m/z (their intensity is approximately one hundred times lower). The inserts display the time series of organic concentrations measured by the ACSM. A black arrow indicates the time corresponding to the mass spectrum shown. The yellow-highlighted shaded area indicates the interval where irradiation takes place, while the green vertical dashed lines indicate the moment of glyoxal injection in the chamber.*

Mis en forme : Surlignage

Mis en forme : Anglais (États-Unis), Surlignage

Mis en forme : Surlignage

Mis en forme : Surlignage

Mis en forme : Surlignage

~~Fragments at 28 m/z and 44 m/z, typical of oxidised compounds, are ubiquitous at all stages of the experiment. Their relative intensity follows the kinetic of the uptake, decreasing during the formation of organic aerosols and reverting to their initial value towards the end of the experiments. Fragment 69 m/z, attributed to $C_3HO_2^+$ and $C_4H_5O^+$, has the highest intensity among ions above m/z 60 in all four spectra, suggesting that it is not related to glyoxal reactivity. Galloway et al. (2009) observed this fragment and identified it as a nitrogen-containing organic molecule with a formula $C_3H_3NO^+$ from the reaction of glyoxal with ammonia during the uptake of glyoxal on ammonium sulphate. This fragment was also observed at significant intensities in organic aerosols originating from phenolic derivatives, such as guaiacol and syringic acid, metabolites of plants (Sun et al., 2010), and could be explained as soil residues from vegetation but also animals (Nieder et al., 2018).~~

~~The signal of fragments at 29 m/z (CHO^+), 30 m/z (CH_2O^+), and 58 m/z (molecular peak $C_2H_2O_2^+$), characteristics of glyoxal, appear during the uptake (second panel from the top in Figure 5) but their relative intensity decreases with time. Fragments m/z = 105 and m/z = 131 observed during both the uptake and the photolysis are specific markers of the interaction between dust and glyoxal (Liggio et al., 2005). The former is attributed to an oligomeric structure of glyoxal generated by the condensation of two molecules of glyoxal hydrate (see also Table 3 in Liggio et al. (2005)). The latter is not identified, yet it consistently accompanies the glyoxal's primary ions. In photo-oxidation experiments of glyoxal in the aqueous phase, Carlton et al. (2007) found that its abundance increased proportionally with the increase in glyoxal concentration. In our study, this fragment is detected in all conditions (with and without light or ozone).~~

~~Fragments at 119 and 120 m/z have been observed in organic aerosols derived from isoprene and attributed to an organic acid with the formula $C_3H_8O_4$ (m/z 120) and its deprotonated form (Safi Shalamzari et al., 2013). In our experiments, they consistently increase after glyoxal uptake, and in particular upon irradiation. Although it is not straightforward to assign these fragments to a unique glyoxal-derived formula, we hypothesise that they may arise from oxidised forms of oligomers.~~

~~Upon irradiation, m/z = 147 is accompanied by m/z = 165. These fragments have been observed in organic aerosols produced in experiments of aqueous-phase glyoxal oxidation via OH radicals (Lim et al., 2010). The fragment m/z 165 is attributed to the~~

condensation of one molecule of glyoxal di-hydrate with one molecule of oxalic acid or two molecules of glyoxylic acid hydrate. The fragment m/z 147 could result from the dehydration of the aforementioned products. These fragments are present with similar intensity in the spectrum of native dust, and their increase in intensity under irradiated conditions might therefore be due to the reversibility of the interaction rather than an oxidation process of glyoxal.

The occurrence of the fragment at 18 m/z is often resulting from the loss of a water molecule (H_2O) from hydrated organic compounds. The slight decrease of the intensity of this fragment during glyoxal uptake could therefore be explained by the presence of the oligomerization of hydrated glyoxal molecules. This process leads to the loss of two hydroxide groups for each added molecule in favour of the formation of acetal or hemiacetal bonds in the structure of the resulting newly formed secondary organic aerosol.

3.3.2. Molecular analysis

The list and conditions of the samples analysed by SFE/GC-MS and ESI-Orbitrap are reported in Table S2 in the Supplementary Material. The summary of the organic molecules detected by those analysis is presented in Table 3 and discussed in the next paragraphs.

Table 3. Summary of frequently observed compounds identified by SFE/GC-MS analysis and glyoxal-related formulas observed with ESI-Orbitrap, along with the suggested structures under the different experimental conditions tested.

Molecular formula	Name	Tentative Structure	Technique	Experimental conditions
$C_2H_2O_3$	Glyoxylic acid	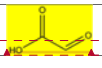	ESI-Orbitrap	Dust+Gly, 80%, Dark, O_3
$C_2H_4O_3$	Glycolic acid	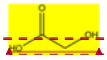	ESI-Orbitrap SFE/GC-MS	Dust+Gly, 30%, Dark Dust+Gly, 30%, Light Dust+Gly, 80%, Light Dust+Gly, 80%, Light, O_3
$C_2H_2O_4$	Oxalic acid	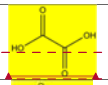	ESI-Orbitrap	Dust+Gly, 80%, Light
$C_2H_4O_4$	Glyoxylic acid monohydrate	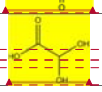	ESI-Orbitrap SFE/GC-MS	Dust+Gly, 80%, Light
$C_3H_6O_3$	Lactic acid	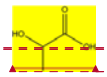	SFE/GC-MS	Dust, 80%, Light Dust+Gly, Dry, Dark Dust+Gly, 30%, Dark Dust+Gly, 30%, Light Dust+Gly, 80%, Light Dust+Gly, 80%, Dark, O_3 Dust+Gly, 80%, Light, O_3

Mis en forme : Surlignage
Mis en forme : Surlignage
Mis en forme : Surlignage
Mis en forme : Surlignage
Mis en forme : Surlignage
Mis en forme : Anglais (États-Unis), Surlignage
Mis en forme : Surlignage
Mis en forme : Surlignage
Mis en forme : Surlignage
Mis en forme : Surlignage
Mis en forme : Anglais (États-Unis), Surlignage
Mis en forme : Anglais (États-Unis), Surlignage
Mis en forme : Surlignage
Mis en forme : Anglais (États-Unis), Surlignage
Mis en forme : Surlignage
Mis en forme : Surlignage
Mis en forme : Surlignage
Mis en forme : Anglais (États-Unis), Surlignage
Mis en forme : Surlignage
Mis en forme : Anglais (États-Unis), Surlignage
Mis en forme : Surlignage
Mis en forme : Surlignage
Mis en forme : Anglais (États-Unis), Surlignage
Mis en forme : Anglais (États-Unis), Surlignage
Mis en forme : Anglais (États-Unis), Surlignage
Mis en forme : Surlignage
Mis en forme : Surlignage
Mis en forme : Surlignage
Mis en forme : Surlignage
Mis en forme : Anglais (États-Unis), Surlignage
Mis en forme : Surlignage
Mis en forme : Anglais (États-Unis), Surlignage
Mis en forme : Surlignage
Mis en forme : Anglais (États-Unis), Surlignage
Mis en forme : Surlignage
Mis en forme : Anglais (États-Unis), Surlignage

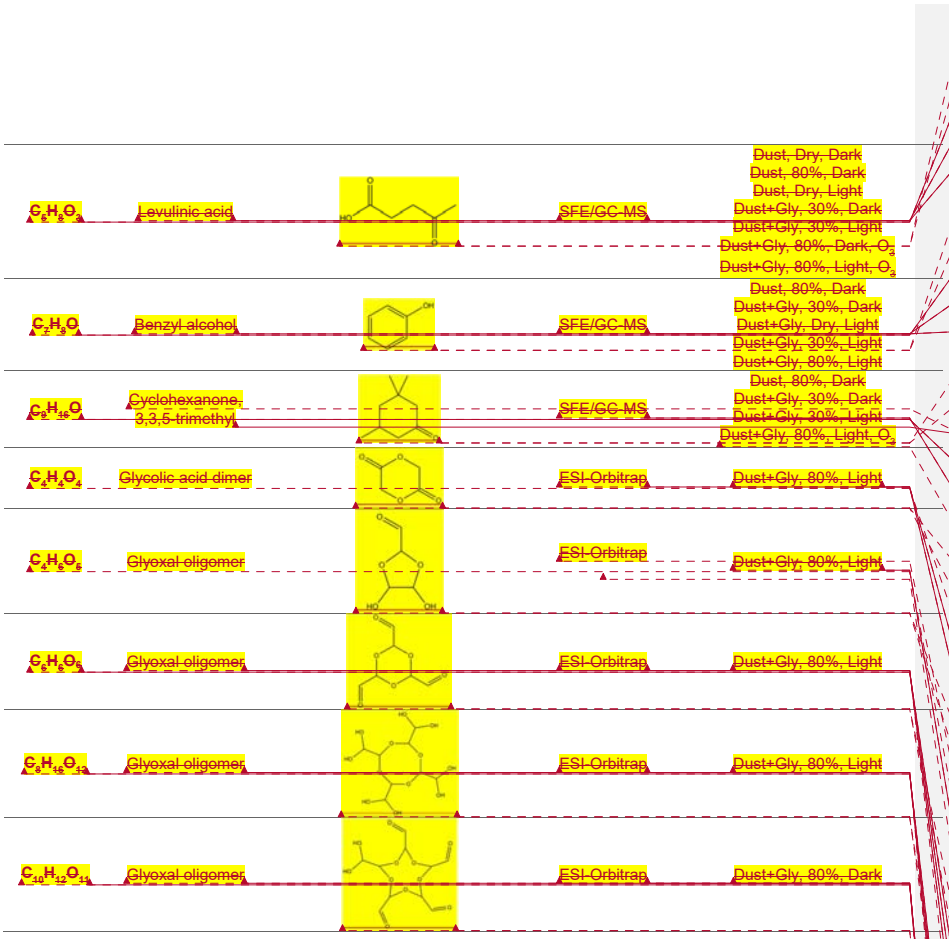

~~3.3.2.1. SFE/GC-MS analysis~~

~~Figure 6 shows the comparison of four gas chromatograms obtained for experiments D_2, D_{13}, D_{15} and D_{16} at 80% RH, with and without irradiation, with and without ozone (Table 1).~~

Mis en forme ... [3]
Mis en forme ... [4]
Mis en forme ... [1]
Mis en forme ... [2]
Mis en forme ... [5]
Mis en forme ... [8]
Mis en forme ... [9]
Mis en forme ... [6]
Mis en forme ... [7]
Mis en forme ... [10]
Mis en forme ... [13]
Mis en forme ... [14]
Mis en forme ... [12]
Mis en forme ... [11]
Mis en forme ... [15]
Mis en forme ... [16]
Mis en forme ... [18]
Mis en forme ... [19]
Mis en forme ... [17]
Mis en forme ... [20]
Mis en forme ... [21]
Mis en forme ... [23]
Mis en forme ... [24]
Mis en forme ... [25]
Mis en forme ... [22]
Mis en forme ... [27]
Mis en forme ... [26]
Mis en forme ... [30]
Mis en forme ... [31]
Mis en forme ... [28]
Mis en forme ... [29]
Mis en forme ... [32]
Mis en forme ... [33]
Mis en forme ... [36]
Mis en forme ... [37]
Mis en forme ... [34]
Mis en forme ... [35]
Mis en forme ... [38]
Mis en forme ... [39]
Mis en forme ... [42]
Mis en forme ... [43]
Mis en forme ... [40]
Mis en forme ... [41]
Mis en forme ... [44]
Mis en forme ... [45]
Mis en forme ... [46]

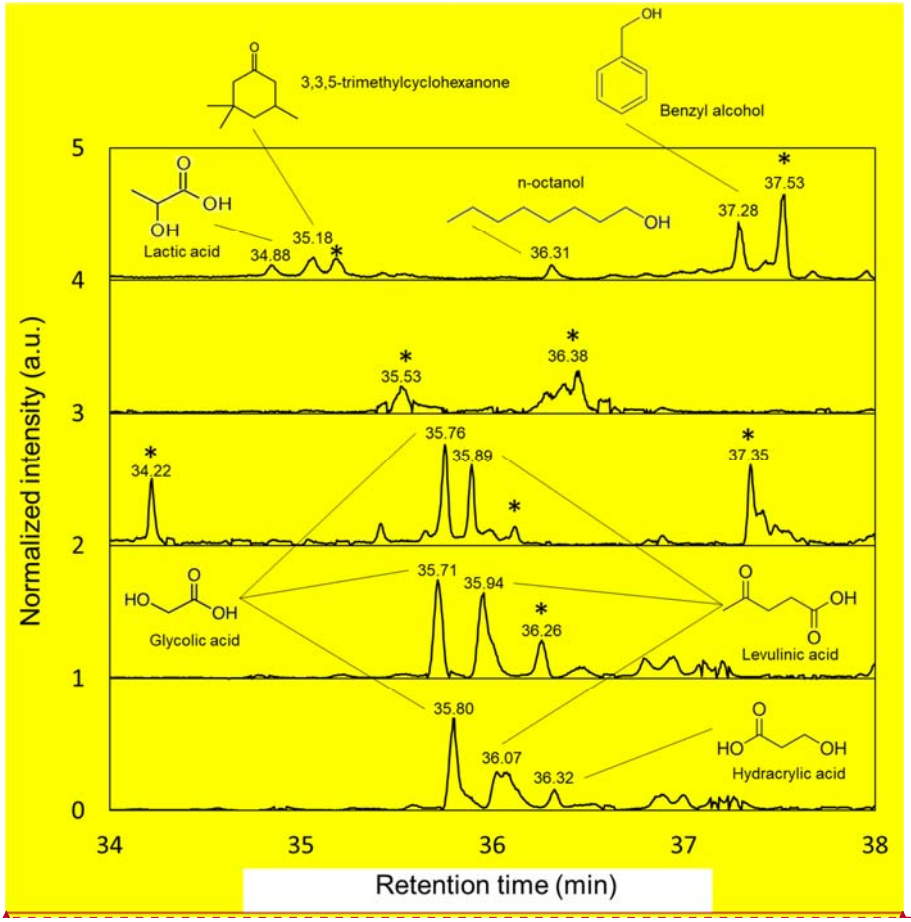

Figure 6. *SFE/GC-MS chromatograms recorded from filters collected during one dust control experiment and four glyoxal uptake experiments under four different conditions. From up to bottom: the first chromatogram is from Experiment D_2, dust control experiment under 80% RH and irradiation. The second is from Experiment D_{16} with dust and glyoxal at 80% RH under dark conditions. The third is from Experiment D_{15} with dust and glyoxal at 80% RH under irradiated conditions. The fourth and fifth chromatograms are from Experiment D_{13} with dust and glyoxal at 80% RH in the presence of ozone under dark and irradiated conditions, respectively. The two peaks of higher intensity appearing after 41 minutes are from the internal standards added to the solution: tridecane around 41 minutes and ortho-toluic acid at about 41.8 minutes. The intensity is normalized to peak of the internal standard ortho-toluic acid. The chromatograms start at 32 minutes as 15 minutes are required for the removal of CO_2 from the extraction fluid, and approximately another 15 minutes represent the delay required for the solvent to pass through the column and reach the electron ionization (EI) MS detection. For the second and third spectra, is noticeable that under irradiated conditions the number of peaks increases significantly compared to dark conditions, likely due to enhanced chemical reactions driven by light. This effect appears to be less pronounced in the presence of ozone.*

Mis en forme : Surlignage
Mis en forme : Surlignage
Mis en forme : Surlignage
Mis en forme : Surlignage

The chromatograms of samples collected in the presence of glyoxal generally exhibit a higher number of peaks compared to samples of dust only, indicating glyoxal oxidation and production of organic aerosols. A higher number of peaks are detected in samples after irradiation compared to dark conditions (see Figure 6). This suggests that the exposure to light influences the chemical composition of the samples by promoting pathways that alter the chromatogram profile, possibly through photochemical reactions, which could lead to glyoxal oxidation products. However, in the presence of ozone and glyoxal, the chromatogram profile recorded under dark conditions is comparable to that recorded in the presence of light, suggesting that ozone may play a significant role in the oxidation process, driving similar chemical reactions in both light and dark environments. This could imply that the oxidative capacity of ozone is sufficient to promote glyoxal oxidation and organic formation independently of photolytic processes, resulting in comparable chromatogram profiles regardless of the presence of light.

The compounds identified using SFE/GC-MS primarily consist of carboxylic acids and relatively light-weight carbonyl compounds (<150 Da). Lactic and levulinic acids are detected in 10 and 9 samples, respectively, regardless of the experimental conditions. Compounds detected less frequently include benzyl alcohol, 3,3,5-trimethylcyclohexanone, methylphosphonic acid (5 samples), decanal (4 samples), and various organic acids, including heptanoic, propanedioic, and hydroacrylic acid (3 samples), as well as benzoic acid and 1-octanol (2 samples).

Glycolic acid and is only detected during experiments with glyoxal. Light and the presence of ozone seem to favour its formation. Indeed, the fourth panel in Figure 6 suggests that ozone might substitute light in promoting the formation of glycolic acid from glyoxal at high RH, suggesting an alternative oxidative pathway. Glycolic acid is also detected at 30% RH (not showed), both with and without light, in agreement with the experiments on dust by Shen et al. (2016), but differently than reported by Galloway et al. (2009) on ammonium sulphate. Monohydrated glyoxylic acid is found in one sample at 80% RH under irradiated conditions, likely due to the known pattern of oxidation of glyoxal and glycolic acid with OH radicals (Buxton et al., 1997).

Twelve mass spectra have a profile unrecognised by the NIST library. An example is shown in Figure 7.

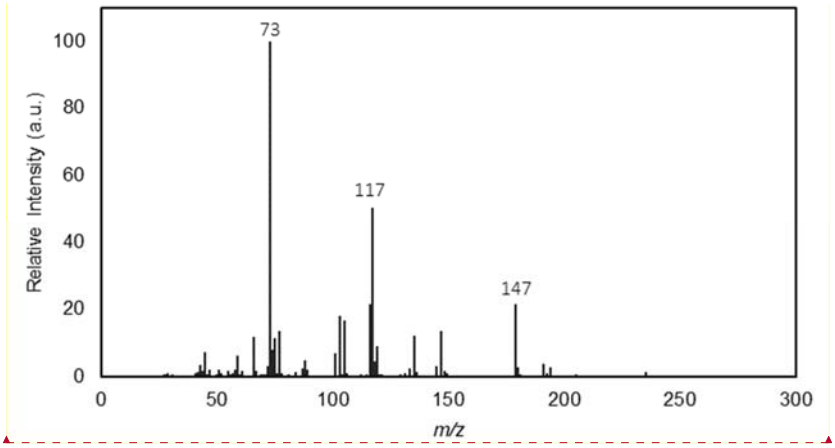

Figure 7. *SFE Electron ionization mass spectrum recorded from the filter collected during the experiment D_{13} (80% relative humidity in the presence of O_3), where the characteristic peaks of the TMS functionalization of two hydroxyl groups (74 and 147 m/z) and one carboxylic group (117 m/z) are observed. The retention time of the peak corresponding to this mass spectrum was 39.58 min.*

Notably, ten are collected under humid conditions (both 30% and 80% RH) and in the presence of light. Eleven are characterised by 73 m/z $[Si(CH_3)_3]^+$ for at least one functionalization, 147 m/z $[(CH_3)_2Si=OSi(CH_3)_3]^+$ for at least two, and their multiples for a greater number of hydroxyl functionalities (-OH). In addition, the fragment at 117 m/z $[COO=Si(CH_3)_3]^+$ is detected. These compounds are attributed to trimethylsilyl-multi-functionalised molecules from small oligomers of hydrated glyoxal (multiple functionalities) that have undergone partial oxidation, as indicated by the presence of carboxylic group peak in most of the spectra (117 m/z).

3.3.2.2. ESI-Orbitrap

On the 15 samples analysed by ESI-Orbitrap (Table S2 in the Supplementary Material), signals attributable to products of the oxidation, hydration, or oligomerization of glyoxal are found only for experiments at high relative humidity (80%), both in the dark but mostly in irradiated conditions. Figure 8 illustrates the mass spectrum and the assigned formula for experiment D_{10}.

Mis en forme : Surlignage
Mis en forme : Surlignage
Mis en forme : Surlignage
Mis en forme : Surlignage
Mis en forme : Surlignage

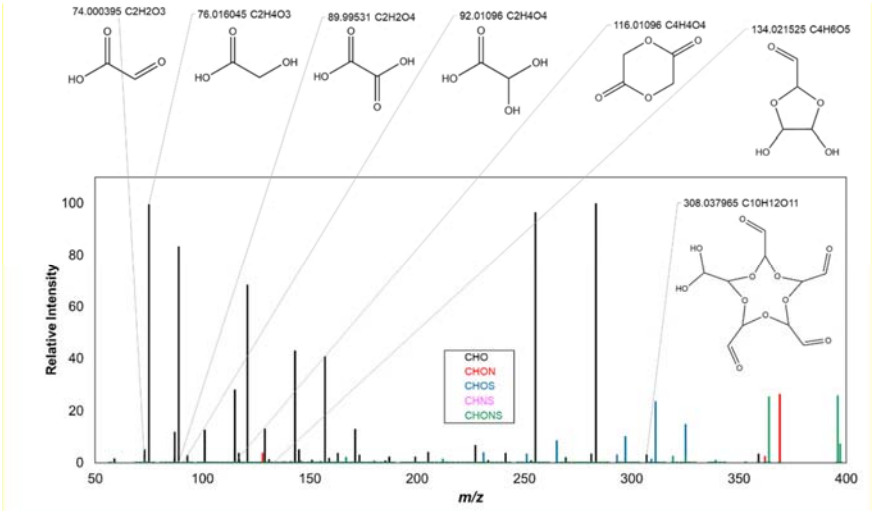

~~***Figure 8.*** *ESI Orbitrap MS from the filter D_{16}: uptake of glyoxal on mineral dust at 80% RH and under irradiation. In the mass spectra, the peaks referring to formulas for which is possible to suggest a structure from glyoxal reactivity are labelled.*~~

~~Molecules corresponding to oxidised compounds are predominantly observed on filters collected under irradiated conditions: $C_2H_4O_3$ (also detected by SFE/GC-MS) attributed to glycolic acid; $C_2H_2O_4$, attributed to oxalic acid, and $C_4H_4O_4$, attributed to a dimer of glycolic acid. Its monohydrated form, $C_2H_4O_4$ (also detected by SFE/GC-MS) is also observed in dark conditions. In the presence of ozone, glyoxylic acid is also observed in dark conditions. Particle phase formic acid, observed on both dust and ammonium sulphate by various authors (Galloway et al., 2009; Rubasinghege et al., 2013; Shen et al., 2016), is not detected in our study neither by molecular analysis nor the ACSM. Although the reasons remain unclear, Shen et al. (2016) suggested that, above approximately 50% RH, adsorbed water could compete for surface reactive sites resulting in suppressing the formation of organic acids onto the dust particles. In contrast, the formation of glycolic and glyoxylic acid appears to be less affected by the presence of adsorbed water, as they are detected solely in humid conditions. This is possibly due to differences in their chemical pathways or their interactions with the dust surface. These acids may form through mechanisms that are less competitive with water adsorption, or their precursors have a higher affinity for the reactive sites on dust~~

Mis en forme : Surlignage
Mis en forme : Surlignage
Mis en forme : Surlignage
Mis en forme : Surlignage

particles (possibly due to the presence of two carbonyl regions) allowing their formation to proceed even in the presence of high humidity.

Compounds from C_4 to C_{10}, oligomerization products of the glyoxal mono and di hydrate forms, are observed only at 80% RH. The following peaks are detected and attributed: $C_4H_6O_6$ (1 monohydrated glyoxal + 1 dehydrated glyoxal forming a 5-atom ring), $C_8H_{16}O_{12}$ (4 dehydrated glyoxal molecules forming an 8-membered ring), and $C_{10}H_{12}O_{11}$ (4 monohydrated glyoxal molecules + 1 dehydrated glyoxal molecule forming a ring structure). The oligomer $C_6H_6O_6$ (3 molecules of monohydrated glyoxal forming a 6-membered ring) is detected only under dark conditions. $C_8H_{16}O_6$ corresponds to an oligomer previously observed by Shen et al. (2016) on mineral dust.

Based on the observations above, Figure 9 shows the suggested chemical mechanism.

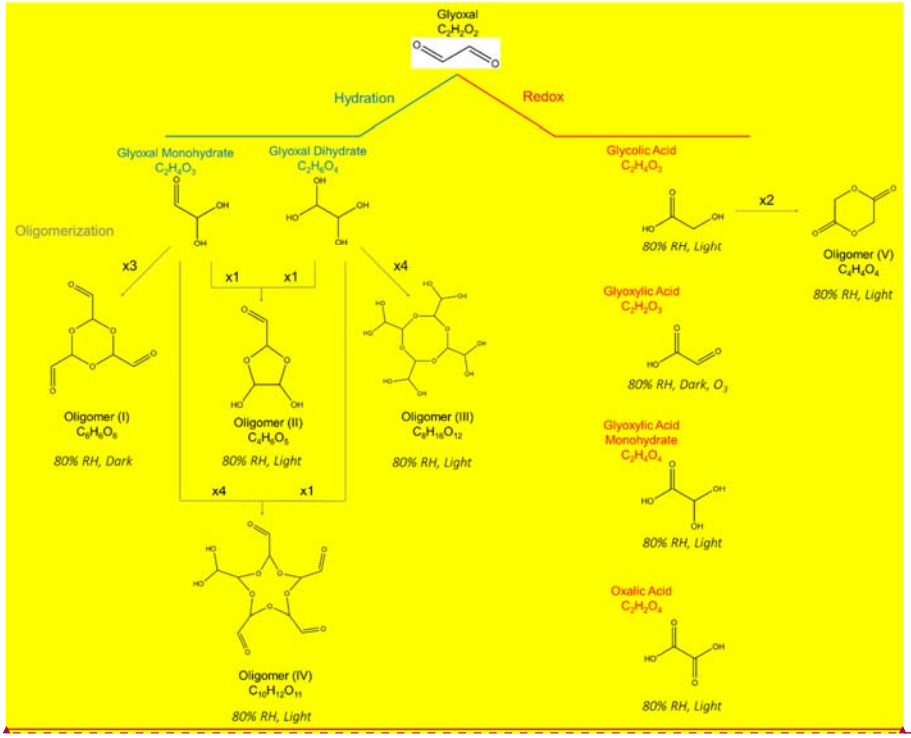

Figure 9. *Proposed reaction scheme to explain the glyoxal-related molecular formulas detected through ESI-Orbitrap mass spectrometry and SFE/GC-MS.*

Mis en forme : Surlignage
Mis en forme : Surlignage
Mis en forme : Surlignage
Mis en forme : Surlignage

The primary oligomers detected are attributed to the condensation of hydrated glyoxal forms specifically the mono- and di-hydrated glyoxal forms, through hydrolysis. The oligomer V is attributed to the condensation of two glycolic acid molecules.

3.4 Oxidation state and reversibility

The comparison of the results in Figures 10 and 11 suggests that while glyoxal and high volatility oxidation products evaporate, low volatility and heavy compounds such as oligomers, remains on the dust and modifies in an irreversible way its surface composition. This is in agreement with previous studies carried out on ammonium sulphate seeds (Kroll et al., 2005; Galloway et al., 2009; De Haan et al., 2020; Hu et al., 2022;).

The results on the oxidative properties of the aged dust are summarised in **Figure 9**10 showing the van Krevelen diagram obtained from the ESI-Orbitrap analysis of a sample collected during experiment D_2 (dust control experiments without glyoxal) and a sample collected during experiment D_{10} (dust and glyoxal), both in the dark and with irradiation and 80% RH.

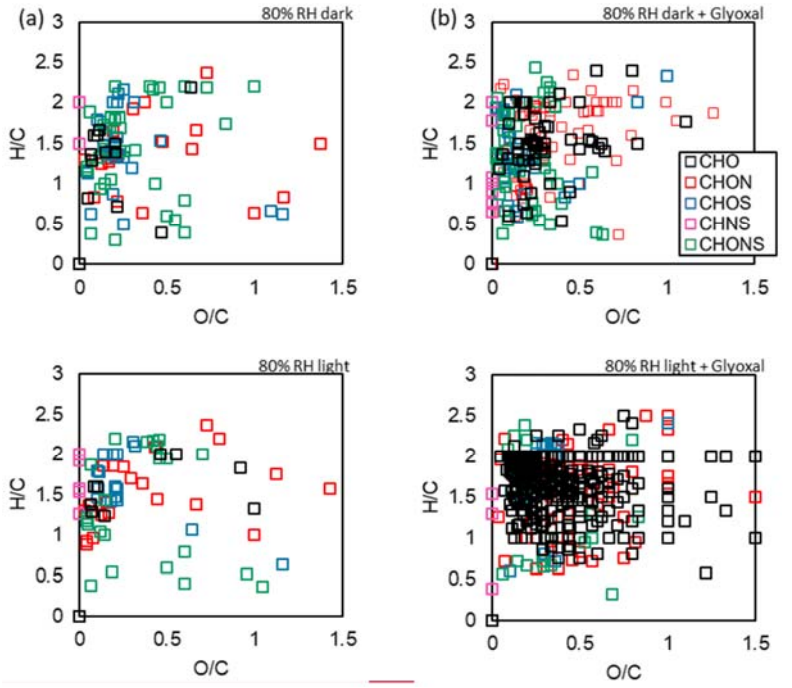

Figure 910. Van Krevelen diagrams recorded at 80% RH for: in the top line (a) experiments in the dark for mineral dust only (control experiment D_2, left) and one ageing experiment of dust with glyoxal (experiment D10); bottom line (b) same with irradiation.

Under the different conditions presented, the samples exhibited varying levels of particulate organic matter and number of ESI Orbitrap peaks detected.

In the absence of glyoxal, only a few signals are detected. In dark conditions, the particulate organic matter of filter is 0.9 µg with 102 peaks detected. In irradiated conditions, the particulate organic matter is 0.8 µg with 86 peaks detected. Peaks are mostly in the range of O/C < 1 and 0.5 < H/C < 2.5, both in the dark and with irradiation. The distribution of values of both ratios is rather similar, while the appearance of molecules for families CHON and CHONS is observed when the lights are on.

The number of detected signals increases significantly in the presence of glyoxal, (right column of **Figure 9**10), in particular in the presence of light. In dark conditions, the particulate organic matter on the filter is 1.7 µg, yielding 398 signals detected. In irradiated conditions, the particulate organic matter is 0.6 µg, resulting in 310 signals

detected. The predominant family in this case is that of CHO molecules. The appearance of signals with O/C ratio higher than 1 is attributed to photo-oxidation.

For comparison, the O/C ratio of the bulk aerosol measured at 80% RH by the ACSM and XPS is shown in **Figure 10**1 (results in dry and 30% RH conditions are shown in **Figure S6**4 in the Supplementary Material).

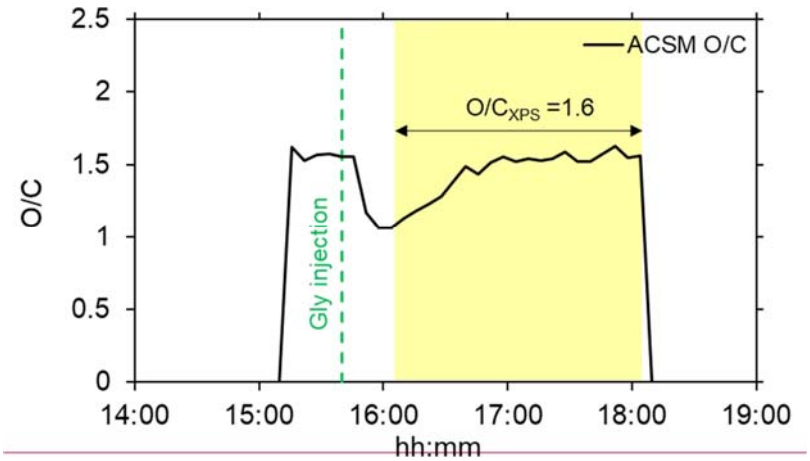

Figure 10. Time series of O/C ratio measured with the ACSM during ageing and 80% RH (experiment D_{15}). The black arrows show the duration of filter sampling and the corresponding O/C values obtained by XPS analysis. The yellow-highlighted portion of the graph indicates the interval where irradiation takes place, while the green vertical dashed lines indicate the moment of glyoxal injection in the chamber.

Figure 101 shows that the O/C ratio of the organic material in the native dust is around 1.5. During the uptake of glyoxal, the ratio decreases to 1 to finally revert to 1.5 within approximately one hour. The agreement between the measurements of the ACSM and the XPS analysis indicates that the ACSM probes the organic matter at the surface of the particles, which we expect to be involved in the reactivity towards glyoxal. The comparison of the results in Figures 10 and 11 suggests that while glyoxal and high volatility oxidation products evaporate, low volatility and heavy compounds such as oligomers, remains on the dust and modifies in an irreversible way its surface composition. This is in agreement with previous studies carried out on ammonium sulphate seeds (Kroll et al., 2005; Galloway et al., 2009; De Haan et al., 2020; Hu et al., 2022;).

Mis en forme : Surlignage

4. Discussion

4.1. Comparison of uptake coefficients

The uptake of glyoxal on the dust particles occurs in humid conditions exceeding 30% RH. These observations agree with the results of Liggio et al. (2005a; 2005b) on the uptake of glyoxal on ammonium sulphate aerosols, observing the formation of organic matter only when RH exceeded 50%. Trainic et al. (2011) ~~found~~ also observed that the uptake of glyoxal on glycine and ammonium sulphate particles occurred only when the relative humidity was above 35%. On the contrary, both Shen et al (2016) and Zogka et al. (2024) demonstrated that the uptake can occur in dry conditions too, which~~-~~ was not observed in this work~~we did not observe~~.

At 80% RH, the experimental-average of the~~At 80% RH, the~~ measured uptake coefficient of glyoxal on mineral dust is $\gamma = (9 \pm 5) \times 10^{-3}$~~.~~. Our values are approximately one order of magnitude higher than those obtained by Shen et al. (2016) who investigated the uptake of glyoxal on mineral proxies, i.e. SiO_2, and $CaCO_3$ and α-Al_2O_3 under various levels of RH~~relative humidity~~. These authors determined the uptake coefficients after a long exposition of the surface to glyoxal (steady state uptakes) and found that the uptake coefficients decrease with increasing the gas phase concentration of glyoxal. At 1 ppb concentration and~~ a relative humidity of~~ 60% RH, the uptake coefficient determined on suspended particles of calcite ($CaCO_3$) is ~~$\gamma =$~~ 1.4 ($\pm$ 0.1) $\times 10^{-4}$ and ~~$\gamma =$~~ 5.5 $\pm$ (0.1) $\times 10^{-5}$ on alumina (α-Al_2O_3~~AlO~~$_3$).

Zogka et al. (2024) used a Knudsen cell to evaluate the initial and steady state glyoxal uptake coefficient bulk soil samples of various origins. At low RH~~relative humidity~~, these authors found that for Gobi soil sieved to less than 63 µm in diameter, the initial uptake coefficient using the geometric surface area was 0.18 (corresponding to an upper limit of the uptake), independent of glyoxal concentration. However, the steady state uptake coefficients determined after a long processing of surface were found to decrease with increasing glyoxal concentration, due to aging of the surface.

Various reasons could induce those apparent differences. ~~First of all~~First, the differences in the experimental set up as in CESAM ~~we measure~~ the initial uptake coefficient was measured on~~f~~ dust aerosol particles in suspension in a large volume, compared to sieved soil (Zogka et al., 2024) and grinded mineral powders (Shen et al., 2016). The uptake coefficient is inversely proportional to the available particle surface.

Mis en forme : Paragraphes solidaires, Lignes solidaires

Mis en forme : Police :(Par défaut) Arial, 12 pt

Mis en forme : Police :12 pt

Mis en forme : Police :(Par défaut) Arial, 12 pt

Mis en forme : Normal

In our experiments, the dust available geometric surface density, calculated from the measured size distribution assuming spherical particles, is in the range 0.35-6.3 × 10^{-3} m^2 m^{-3} (**Table 2**). As the the CESAM chamber volume is equal to 4.2 m^3, the total dust surface area available for the reaction ranges from 2 to 2.6 × 10^{-3} m^2, several orders of magnitude lower than in the experiments designed by Shen et al. (2016) and Zogka et al. (2024). Shen et al. (2016) used model powders of various sizes between 35 nm and 5 µm, with BET (define BET) surface areas ranging between 1.4 and 440 m^2 g^{-1}. In the conservative assumption that only 5 mg of the model powder was used, the total reactive surface area was up to 2.2 m^2. Zogka et al. (2024) used the soil from Gobi sieved to 63 µm and a BET surface area of 10.5 ± 1.0 m^2 g^{-1}. Using even just 1 g would yield a surface area of the order of 10.5 m^2. Differences in the results could also arise by differences in the dust mineralogy, which are difficult to ascertain in the present study.

Our estimated uptake coefficient of glyoxal on mineral dust is also nearly ~~Because the uptake follows a first order kinetic, the measured uptake coefficient is independent on the glyoxal concentration and transferable to atmospheric conditions. The uptake coefficient on dust is nearly~~ two orders of magnitude higher than for ammonium sulphate ($\gamma_{gas\text{-}AS}$ = 1.1 (± 0.2) × 10^{-4}; ~~) at the same relative humidity~~ (our study as well as Curry et al., 2018; De Haan et al., 2020; Galloway et al., 2009; Liggio et al., 2005b, a; Trainic et al., 2011), ~~-~~but lower than $\gamma_{gas\text{-}AS}$ = 2.9 × 10^{-3} at a lower RH~~relative humidity~~ (Liggio et al., 2005).

The difference could be due to the higher hygroscopicity of ammonium sulphate, enhancinges water's competition with glyoxal for adsorption sites at 80% RH, when indeed ammonium sulphate is deliquescent. This suggest nonetheless that dust aerosols could play a very substantial role in the formation of organic aerosols at high RH~~relative humidity~~ compared to ammonium sulphate, which is often used as an aerosol proxy. ~~Additionally, we found that the uptake coefficient measured by the loss of gas phase glyoxal molecules agrees very well with the rate of formation of secondary organic mass on the particles. This suggests that the totality of the mass of reacting glyoxal is transformed in organic matter on the surface of the dust particles.~~

~~4.2. Mechanism of chemical transformation~~

Mis en forme : Anglais (États-Unis)
Mis en forme : Anglais (États-Unis)
Mis en forme : Police :Gras, Anglais (États-Unis)
Mis en forme : Anglais (États-Unis)
Mis en forme : Anglais (États-Unis)
Mis en forme : Anglais (États-Unis)
Mis en forme : Anglais (États-Unis)
Mis en forme : Anglais (États-Unis)
Mis en forme : Police :(Par défaut) Arial, 12 pt
Mis en forme : Police :(Par défaut) Arial, 12 pt
Mis en forme : Police :(Par défaut) Arial, 12 pt
Mis en forme : Police :(Par défaut) Arial, 12 pt
Mis en forme : Police :(Par défaut) Arial, 12 pt, Couleur de police : Automatique
Mis en forme : Police :(Par défaut) Arial, 12 pt
Mis en forme : Normal, Sans numérotation ni puces
Mis en forme : Police :(Par défaut) Arial, 12 pt
Mis en forme : Police :(Par défaut) Arial, 12 pt
Mis en forme : Normal, Justifié

Figure 8 illustrates the suggested chemical mechanism of the transformation of gas-phase glyoxal on the mineral dust particles.

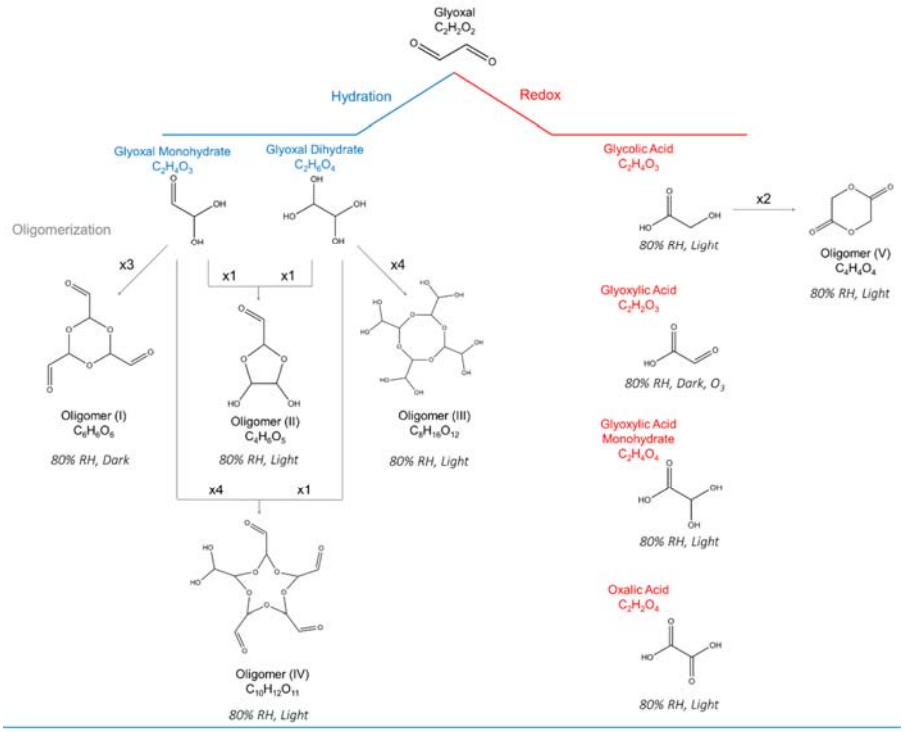

Figure 8. Proposed reaction scheme to explain the glyoxal-related molecular formulas detected through ESI-Orbitrap mass spectrometry and SFE/GC-MS.

The primary oligomers detected are hypothesized to result from the condensation through hydrolysis of hydrated glyoxal forms, specifically the mono- and di-hydrated glyoxal forms. For oligomer V, we suggest that it arises from the condensation of two glycolic acid molecules. Our findings support several key insights into the irreversible uptake of glyoxal on mineral particles, as discussed by Shen et al. (2016), that found that glyoxal oligomers exhibited a higher degree of oligomerization (≥ 4) than previously reported in the aqueous phase and on acidic seed particles (≤ 3; Liggio et al., 2005; Nozière et al., 2009) and that adsorbed water on particles favoured the formation of oligomers. Our findings support several key insights into the irreversible

Mis en forme : Justifié, Espace Avant : 6 pt, Après : 0 pt, Interligne : 1.5 ligne

Mis en forme : Espace Avant : 6 pt, Après : 0 pt

~~uptake of glyoxal on mineral particles, as discussed by Shen et al. (2016), that found that glyoxal oligomers exhibited a higher degree of oligomerization (≥ 4) than previously reported in the aqueous phase and on acidic seed particles (≤ 3; Liggio et al., 2005a; Nozière et al., 2009) and that adsorbed water on particles favoured the formation of oligomers. This is also in agreement with the field observations by consistent with the observations conducted by Wang et al. (2015).~~

~~Ortiz-Montalvo et al. (2014), even mildly acidic conditions significantly enhance glyoxal oligomerization and favoured the formation of low-volatility compounds, contributing to SOA mass through gas-particle partitioning.~~

Mis en forme : Normal, Justifié

4.2. Mechanism of chemical transformation

Figure 7 illustrates the suggested chemical mechanisms of the transformation of gas-phase glyoxal on the mineral dust particles.

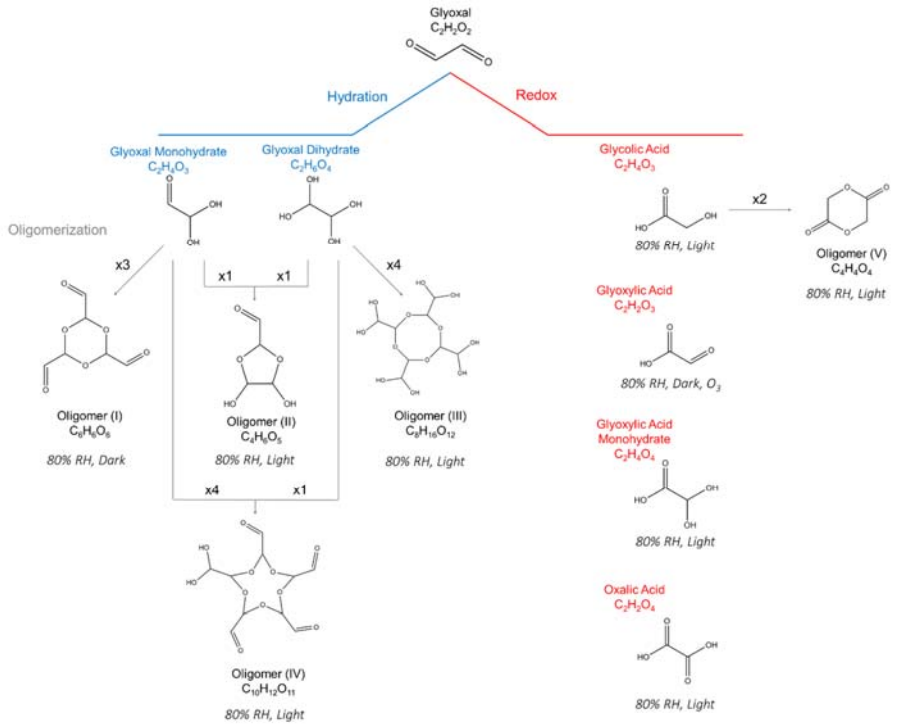

Figure 7. Proposed reaction scheme to explain the glyoxal-related molecular formulas detected through ESI-Orbitrap mass spectrometry and SFE/GC-MS.

~~The mechanistic scheme presented in **Figure 7** highlights t~~The ~~complex~~ multiphase chemistry of glyoxal on mineral dust particles, leading to the formation of low-volatility, particle-phase products, is complex, involving hydration, redox, and oligomerization pathways. ~~These processes collectively lead to the formation of low-volatility, particle-phase products that contribute significantly to organic aerosol mass.~~The

~~Our findings indicate that glyoxal undergoes significant~~ chemical transformation of glyoxal upon uptake by mineral dust particles~~,~~ primarily occurs through aqueous-phase reactions. The ~~transformation~~ mechanism is initiated by hydration of glyoxal's aldehyde groups, forming mono- and di-hydrated species. These hydrated intermediates undergo condensation reactions, which involve nucleophilic attack and lead to the formation of cyclic acetal structures, particularly from two to five-membered dioxolane rings. This mechanism is well supported by prior studies (Loeffler et al., 2006; Kua et al., 2008; Hastings et al., 2005), which have described similar pathways for glyoxal oligomerization in aqueous environments.

This ~~Importantly, our~~ study provides new insight into how this chemistry on mineral surfaces. While previous research has shown that glyoxal typically forms dimers and trimers in aqueous solution (Liggio et al., 2005; Nozière et al., 2009), our mass spectral data reveal the presence of oligomeric species containing up to 5 glyoxal units. This higher degree of oligomerization - ~~—~~also observed by Shen et al. (2016)~~ on mineral surfaces —~~ suggests that the particle-phase environment allows for extended oligomer growth. The likely contributing factors include reduced water activity, surface confinement, and enhanced proximity of reactants, all of which promote successive addition reactions that may be hindered in bulk solution (Gomez et al., 2015; Avzianova & Brooks, 2013).

Redox reactions derive into ~~yield~~ oxidized species such as glycolic, glyoxylic, and oxalic acids. These compounds not only represent aging products but also participate in further condensation reactions, expanding the chemical diversity of ~~secondary organic aerosols (~~SOA~~)SOA constituents~~. In particular, we detected the presence of oligomer V, which we propose results not from direct glyoxal self-reactions but rather from the condensation of two glycolic acid molecules. This suggests a broader heterogeneous transformation process~~es~~ occurring on the dust surface, possibly involving oxidative pathways. Such cross-reactions are consistent with mechanisms

proposed in glyoxal–methylglyoxal systems (Zhang et al., 2022), where mixed oligomers form through shared reaction intermediates.

A key aspect of our findings is the irreversibility of glyoxal uptake on mineral dust. In contrast to bulk aqueous systems, where glyoxal oligomerization can exist in equilibrium with monomeric species, our results suggest that oligomer formation on mineral particles is effectively irreversible. The persistence of high-molecular-weight products following drying and thermal analysis confirms that these species are chemically stable and remain in the condensed phase. This ~~behavior~~behaviour is consistent with previous observations (Hastings et al., 2005; Ortiz-Montalvo et al., 2014), and ~~further~~ highlights the significance of particle-phase reactions in the formation of ~~secondary organic aerosol (SOA) mass~~SOA.

The acidity of the particle surface could potentially play a role in ~~catalyzing~~catalysing glyoxal oligomerization. It is plausible that localized acidity arises or is enhanced by the accumulation of transformation products such as glycolic and oxalic acids, which were detected in ~~our analyses~~this study. This in-~~-~~situ acidification may facilitate acid-~~catalyzed~~catalysed reaction pathways even under ~~otherwise~~ neutral or weakly acidic conditions. The importance of acidity in glyoxal chemistry is supported by mechanistic proposals involving carbenium ion intermediates or hydrogen-bond-assisted nucleophilic mechanisms, which can operate effectively without requiring strongly acidic environments (Zhang et al., 2022; Gomez et al., 2015). These pathways are known to promote the formation of low-volatility oligomers, contributing to organic aerosol mass. Similarly, Ortiz-Montalvo et al. (2014) demonstrated that even mildly acidic aerosols significantly enhance glyoxal oligomerization and SOA~~secondary organic aerosol~~ formation.

Another critical factor is the presence of adsorbed water on mineral dust particles. Our findings demonstrate in fact that the availability of surface water facilitates organic aerosol formation from glyoxal. This agrees with chamber and field studies (Hastings et al., 2005; Shen et al., 2016) that identified a RH ~~relative humidity~~ threshold above which glyoxal uptake dramatically increases. The presence of a thin aqueous film on the particle surface creates a reactive medium where glyoxal can concentrate, hydrate, and polymerize efficiently. Even after evaporation, the products formed are retained in the particle phase, evidencing their low volatility and chemical resilience.

~~In summary, our results extend current understanding of glyoxal chemistry in atmospheric systems. We confirm that oligomerization occurs through well-established aqueous-phase pathways, but show that mineral dust particles uniquely facilitate higher-order oligomer formation, support irreversible uptake, and possibly promote alternative reaction channels such as glycolic acid condensation. These findings underscore the importance of mineral surfaces as active sites for multiphase OA formation, with implications for understanding aerosol growth, composition, and climate-relevant properties.~~

~~This is also in agreement with the field observations by consistent with the observations conducted by Wang et al. (2015).~~

4.3. Implications for the dust properties

The irreversible transformation of the chemical composition of mineral dust following the uptake of glyoxal could influence the physico-chemical ~~have important implications for the~~ properties of mineral dust particles. The formation of organic acids (glycolic, glyoxylic and oxalic acids) should change the dust pH, increasing its acidity and ability to dissolve transition metals like iron and copper. This could alter their speciation, ~~and~~ enhancing their bioavailability in aqueous aerosol environments and potentially impacting atmospheric chemistry and the reactivity of aerosol particles (Giorio et al., 2022). Changes in dust pH could also affect its hygroscopic properties, influencing their ability to adsorb water and grow in size. This is consistent with our observation regarding the volume increase of dust particles after the uptake and the subsequent growth that enhance particles interaction with light and cloud droplets formation~~that the volume of the dust particle increases during the uptake and that this growth is persistent, henceforth becoming more efficient in interacting with visible light and form cloud droplets~~. Collectively, these processes highlight how aerosol acidity modulates not only chemical transformations but also key physical properties and atmospheric lifetimes of dust-glyoxal systems.

The newly formed organic matter from glyoxal on dust particles could also alter the aerosol's optical properties, affecting its ability to absorb solar radiation, as recently observed in aqueous solution (De Haan et al., 2023) or on ammonium sulphate aerosols (De Haan et al. 2020; Trainic et al. 2011). The presence of hydrated glyoxal oligomeric structures has already been observed to have UV radiation absorption properties (Kalberer et al., 2004; Shapiro et al., 2009). Glyoxal-derived oligomers could

Mis en forme : Titre 3

Mis en forme : Police :(Par défaut) Arial, 12 pt

Mis en forme : Police :(Par défaut) Arial, 12 pt

Mis en forme : Normal, Sans numérotation ni puces

Mis en forme : Police :(Par défaut) Arial, 12 pt

Mis en forme : Police :(Par défaut) Arial, 12 pt

Mis en forme : Police :(Par défaut) Arial, 12 pt

Mis en forme : Police :(Par défaut) Arial, 12 pt

Mis en forme : Police :(Par défaut) Arial, 12 pt

Mis en forme : Police :(Par défaut) Arial, 12 pt

Mis en forme : Police :(Par défaut) Arial, 12 pt

Mis en forme : Police :(Par défaut) Arial, 12 pt

Mis en forme : Police :(Par défaut) Arial, 12 pt

Mis en forme : Police :(Par défaut) Arial, 12 pt

Mis en forme : Police :(Par défaut) Arial, 12 pt

Mis en forme : Normal, Justifié

Mis en forme : Police :(Par défaut) Arial, 12 pt

significantly influence the optical properties of mineral dust aerosols. Spectroscopic analyses revealed that these oligomers have broadened OH and C–O bands and enhanced Raman activity, indicative of their hydrated and cyclic structures (Avzianova and Brooks, 2013). They also have strong UV-visible absorption, particularly between 300–600 nm, with characteristic shoulders at ~280 and 345 nm attributed to acetal and aldol condensation products (Schwier et al., 2010; Shapiro et al., 2009). High RH conditions (> 80%) facilitate brown carbon formation, evidenced by the further appearance of UV-visible absorbance peaks and Raman background signals (De Haan et al., 2020; Zhang et al., 2022).

5. Conclusionve sremarks

In tThis phis paper presented a novel investigation of the , we investigated the uptake interaction between gas-phaseof glyoxal by and mineral dust. By taking advantage of the capabilities of the CESAM atmospheric simulation chamber to perform multiphase experiments on time scales relevant to atmospheric processes and dispersion, including aerosols,realistic submicron mineral dust aerosol particles from a natural soil (Gobi Desert) our experiments considered airborne submicron mineral dust particles generated from a natural soil (Gobi Desert) in realistic concentrations, composition and size distribution. While airborne, the dust aerosol was aged under variable conditions of RHrelative humidity, irradiation, and ozone concentrations. Thanks to the realism of the tools and the experimental conditions, our study investigates, for the first time, both the rate of uptake of glyoxal and the rate of formation of the organic aerosol from the gas-phase uptake. We provide, the chemical composition of the particle formed on the dust particles, and their implicationsfinally the consequences on the particle microphysics, in atmospheric-relevant conditions.

OurThis study used a single and instantaneous injection of glyoxal, and not a constant steady state flux. Above 30% RH,The uptake of glyoxal on the dust particles starts as soon as the glyoxal is injected in the chamber. In this study we used a single and instantaneous injection of glyoxal, and not a constant steady state flux. Furthermore, in humid conditions, upon injection, glyoxal is partitionedis partitioned almost instantaneouslyrapidly between the gas phase, the chamber walls and , the chamber walls. the dust particles. This is an advantage to scale our results to ambient conditions. Indeed, Volkamer et al. (2005) estimated that the daytime lifetime of glyoxal is around 1.3 hours. Alvarado et al. (2020) showed that the long-range transport of

Mis en forme : Police :Arial, Non Surlignage
Mis en forme : Normal, Sans numérotation ni puces
Mis en forme : Anglais (États-Unis)
Mis en forme : Anglais (États-Unis)
Mis en forme : Police :(Par défaut) Arial, 12 pt
Mis en forme : Police :(Par défaut) Arial, 12 pt
Mis en forme : Police :(Par défaut) Arial, 12 pt
Mis en forme : Police :(Par défaut) Arial, 12 pt
Mis en forme : Police :(Par défaut) Arial, 12 pt
Mis en forme : Police :(Par défaut) Arial, 12 pt
Mis en forme : Police :(Par défaut) Arial, 12 pt
Mis en forme : Police :(Par défaut) Arial, 12 pt
Mis en forme : Police :(Par défaut) Arial, 12 pt
Mis en forme : Police :(Par défaut) Arial, 12 pt

glyoxal produced from a point source (Canadian wildfires) may be possible only by invoking the progressive oxidation of its longer-lived precursors in the plume. In the scenario where dust aerosols interact with a glyoxal plume from a point source, one can expect an interaction time of a few minutes, compatible with that of this study. Furthermore, because the uptake follows a first order kinetic, the measured uptake coefficient ($\gamma = (9 \pm 5) \times 10^{-3}$ at 80% RH) is independent of the glyoxal concentration and transferable to atmospheric conditions.

~~Both facts are actually an advantage to scale our results to ambient conditions. Indeed, Volkamer et al. (2005) estimated that the lifetime of glyoxal in the daytime is of around 1.3 hours. Alvarado et al. (2020) showed that the long range transport of glyoxal produced from a point source (Canadian wildfires) may be possible only by invoking the progressive oxidation of its longer-lived precursors in the plume. In the scenario where dust aerosols interact with a glyoxal plume from a point source, one can expect an interaction time of a few minutes, compatible with that of this study.~~

~~Overall, although the experiments performed in literature with those of the current study were performed under different conditions, results indicate that natural Gobi dust is an effective sink of glyoxal, with initial uptake coefficient independent of glyoxal concentration, pointing to a first order removal process. However, the long term ageing of particles leads to lower uptake coefficients that strongly depend on glyoxal concentration due to the depletion of surface sites.~~

~~, airborne in a large simulation chamber, and aged under variable experimental conditions of relative humidity, irradiation, and ozone concentrations. Results can be summarised and commented as follows:~~

- ~~The uptake of glyoxal on the dust particles occurs in humid conditions exceeding 30% RH. These observations agree with the results of Liggio et al. (2005a; 2005b) on the uptake of glyoxal on ammonium sulphate aerosols, observing the formation of organic matter only when RH exceeded 50%. Trainic et al. (2011) found that the uptake of glyoxal on glycine and ammonium sulphate particles occurred only when the relative humidity was above 35%. On the contrary, both Shen et al (2016) and Zogka et al. (2024) demonstrated that the uptake can occur in dry conditions too, which we did not observe.~~

Mis en forme : Police :(Par défaut) Arial, 12 pt

Mis en forme : Normal, Sans numérotation ni puces

Mis en forme : Police :(Par défaut) Arial, 12 pt

Mis en forme : Normal, Sans numérotation ni puces

~~• The uptake of glyoxal on the dust particles starts as soon as the glyoxal is injected in the chamber. In this study we used a single and instantaneous injection of glyoxal, and not a constant steady state flux. Furthermore, in humid conditions, upon injection, glyoxal is partitioned rapidly between the gas phase and the chamber walls. Both facts are actually an advantage to scale our results to ambient conditions. Indeed, Volkamer et al. (2005) estimated that the lifetime of glyoxal in the daytime is of around 1.3 hours. Alvarado et al. (2020) showed that the long-range transport of glyoxal produced from a point source (Canadian wildfires) may be possible only by invoking the progressive oxidation of its longer-lived precursors in the plume. In the scenario where dust aerosols interact with a glyoxal plume from a point source, one can expect an interaction time of a few minutes, compatible with that of this study.~~

~~• At 80% RH, the measured uptake coefficient of glyoxal on mineral dust is $\gamma = (0 \pm 5) \times 10^{-3}$. Because the uptake follows a first order kinetic, the measured uptake coefficient is independent on the glyoxal concentration and transferable to atmospheric conditions. The uptake coefficient on dust is nearly two orders of magnitude higher than for ammonium sulphate ($\gamma_{gas\text{-}AS} = 1.1 (\pm 0.2) \times 10^{-4}$) at the same relative humidity (our study as well as Curry et al., 2018; De Haan et al., 2020; Galloway et al., 2009; Liggio et al., 2005b, a; Trainic et al., 2011) but lower than $\gamma_{gas\text{-}AS} = 2.9 \times 10^{-3}$ at a lower relative humidity (Liggio et al., 2005).~~

~~• The difference could be due to the higher hygroscopicity of ammonium sulphate, enhances water's competition with glyoxal for adsorption sites at 80% RH, when indeed ammonium sulphate is deliquescent. This suggest nonetheless that dust aerosols could play a very substantial role in the formation of organic aerosols at high relative humidity compared to ammonium sulphate, which is often used as an aerosol proxy. Additionally, we found that the uptake coefficient measured by the loss of gas-phase glyoxal molecules agrees very well with the rate of formation of secondary organic mass on the particles. This suggests that the totality of the mass of reacting glyoxal is transformed in organic matter on the surface of the dust particles.~~

The uptake of glyoxal and the formation of organic matter start as soon as the glyoxal is injected in the chamber and last approximately 20 minutes. The uptake coefficient measured by the loss of gas-phase glyoxal molecules agrees very well with the rate of formation of the particulate organic mass on the dust, suggesting that the totality of the mass of reacting glyoxal is condensed on the dust particles. While some of the organic

Mis en forme : Police :12 pt

Mis en forme : Police :(Par défaut) Arial, 12 pt

Mis en forme : Police :(Par défaut) Arial, 12 pt

matter is lost again from the dust particles due to ~~, after which evaporation occurs.~~ evaporation, oligomers and organic acids are detected on the dust even after the uptake has finished, indicating that ~~However, we demonstrate~~ the uptake of glyoxal modifies irreversibly both the composition and the physical properties of mineral dust. ~~Oligomers and organic acids are detected on the dust even after the uptake has finished.~~ ~~Our findings support several key insights into the irreversible uptake of glyoxal on mineral particles, as discussed by Shen et al. (2016), that found that glyoxal oligomers exhibited a higher degree of oligomerization (≥ 4) than previously reported in the aqueous phase and on acidic seed particles (≤ 3; Liggio et al., 2005a; Nozière et al., 2009) and that adsorbed water on particles favoured the formation of oligomers. This is also in agreement with the field observations by consistent with the observations conducted by Wang et al. (2015).~~

~~The presence of organic acids, such as glycolic and glyoxylic acids has implications for aerosol pH, as they can influence the acidity of aerosols and their ability to dissolve metals, potentially impacting atmospheric chemistry and the reactivity of aerosol particles (Giorio et al., 2022). Changes in aerosol pH can, in turn, affect the hygroscopic properties of aerosols, influencing their ability to adsorb water and grow in size. Indeed, we observe that the volume of the dust particle increases during the uptake and that this growth is persistent, henceforth becoming more efficient in interacting with visible light and form cloud droplets. The newly formed organic matter from glyoxal on dust particles could also alter the aerosol's optical properties, affecting its ability to absorb solar radiation, as recently observed in aqueous solution (De Haan et al., 2023) or on ammonium sulphate aerosols (De Haan et al. 2020; Trainic et al. 2011). For example, the presence of hydrated glyoxal oligomeric structures has already been observed to have UV radiation absorption properties (Kalberer et al., 2004; Shapiro et al., 2009). The observation of organic acid formation following glyoxal uptake could have important implications for aerosol properties. In the study from (Ortiz-Montalvo et al., 2014), even mildly acidic conditions significantly enhanced glyoxal oligomerization and favoured the formation of low volatility compounds, contributing to SOA mass through gas-particle partitioning. An organic acid produced from glyoxal oxidation, such as~~

Mis en forme : Police :(Par défaut) Arial, 12 pt

Mis en forme : Police :(Par défaut) Arial, 12 pt

Mis en forme : Paragraphe de liste, Avec puces + Niveau : 1 + Alignement : 0.63 cm + Retrait : 1.27 cm

~~oxalic acid, was observed to facilitate the dissolution of transition metals like iron and copper, thereby altering their speciation and enhancing their bioavailability in aqueous aerosol environments (Giorio et al., 2022).~~

~~Furthermore, the acidification of aerosols increased their hygroscopicity, especially under high RH conditions, affecting particle growth dynamics, phase behaviour, and cloud condensation nuclei (CCN) potential (Song and Osada, 2021). Collectively, these processes highlight how aerosol acidity modulates not only chemical transformations but also key physical properties and atmospheric lifetimes of dust-glyoxal systems.~~

~~Glyoxal-derived oligomers could significantly influence the optical properties of mineral dust aerosols. Spectroscopic analyses revealed broadened OH and C=O bands and enhanced Raman activity in these oligomers, indicative of their hydrated and cyclic structures (Avzianova & Brooks, 2013). Core-shell models showed that glyoxal uptake increased particle size and optical extinction cross-sections, with refractive indices of n ≈ 1.68 + 0.01i at 50% RH and n ≈ 1.65 + 0.02i at 75% RH (Trainic et al., 2011).~~

~~These oligomers exhibited enhanced UV-visible absorption, particularly between 300–600 nm, with characteristic shoulders at ~280 and 345 nm attributed to acetal and aldol condensation products (Schwier et al., 2010; Shapiro et al., 2009). High RH conditions (>80%) facilitated brown carbon formation, further evidenced by UV-visible absorbance peaks and Raman background signals (De Haan et al., 2020; Zhang et al., 2022).~~

~~In conclusion, our~~Our This study reveals a significant quantitative transfer of gas-phase glyoxal molecules to mineral dust aerosol surfaces, occurring within a timescale of a few minutes, underscoring the important role of dust-glyoxal interactions in the atmosphere. Our results extend the current understanding of glyoxal chemistry in atmospheric systems. While oligomerization occurs through well-established aqueous-phase pathways, we suggest that mineral dust particles facilitate in a unique way higher-order oligomer formation, support irreversible uptake, and possibly promote alternative reaction channels such as glycolic acid condensation. These findings underscore the importance of mineral dust surfaces as active sites for multiphase SOA formation, with implications for understanding aerosol growth, composition, and climate-relevant properties. This is also in agreement with the field observations conducted by Wang et al. (2015). Neglecting the uptake pathway on dust could result in an underestimation of glyoxal removal from the atmosphere, potentially leading to disparities between model predictions and observed gaseous concentrations of glyoxal (Kluge et al., 2023; Ling et al., 2020; Volkamer et al., 2007; Washenfelder et al., 2011). The ~~results~~ findings of this study ~~could~~ have also important implications for the aerosol

Mis en forme : Paragraphe de liste, Gauche, Espace Avant : 0 pt, Interligne : simple

Mis en forme : Paragraphe de liste, Gauche, Interligne : simple

Commenté [PFO3]: Conclusion?

Mis en forme : Police :(Par défaut) Arial, 12 pt

Mis en forme : Gauche, Retrait : Gauche : 1.27 cm, Espace Avant : 0 pt, Après : 8 pt, Ne pas ajouter d'espace entre les paragraphes du même style, Interligne : Multiple 1.08 li, Sans numérotation ni puces

Mis en forme : Police :(Par défaut) Arial, 12 pt

Mis en forme : Police :(Par défaut) Arial, 12 pt

Mis en forme : Police :(Par défaut) Arial, 12 pt

Mis en forme : Police :(Par défaut) Arial, 12 pt

Mis en forme : Police :(Par défaut) Arial, 12 pt

direct and indirect radiative effect and aerosol pH. The acidification and the oxidation of the dust aerosols by glyoxal should increase their hygroscopicity, especially under high RH conditions, affecting particle growth dynamics, phase behaviour, and cloud condensation nuclei (CCN) potential (Song and Osada, 2021). Further data analysis are ~~studies should investigate dust from diff~~ongoing to address ~~erent sources and mineralogy, poly-disperse size distribution including the coarse mode and lower glyoxal concentration~~these aspects.

Data availability. The simulation chamber experiments that support the findings of this study are available through the Database of Atmospheric Simulation Chamber Studies (DASCS) of the EUROCHAMP Data Centre (https:// data.eurochamp.org/ data- access/ chamber-experiments/).

Code availability. The routine used for fitting the size distribution is available at https://doi.org/10.5281/zenodo.8135133 (Baldo and Lu, 2023). Note that in this study we only used the size distribution measured by the OPC instrument, which was fitted with a lognormal function. The Tof-ACSM data processing (including mass calibration, peaks integration and air beam correction of ion intensities) was conducted with Tofware version 3_2_40209, the ACSM data analysis package for the software Igor Pro 7.08 (Wavemetrics, Inc., Portland, OR, USA). SFE-GC-MS data analysis was conducted using the proprietary software (TurboMass Version 6.1.0.1965 PerkinElmer®).

Author contributions. PF, JFD and FB conceptualized the study. PF and FB led the paper writing, with contributions from all the authors. JFD provided with expertise on multi-phase chemistry. CB analysed the aerosol size distribution data. VM supervised the analysis of PTR-MS data. FB, ~~and~~ CG and DLP performed the ESI-Orbitrap analysis of filter samples. FB and JFB performed the analysis of ACSM observations. FB, TB and AG performed the SFE/CG-MS analysis of filter samples. FB, GN and SC performed the thermo-optical analysis of filter samples. FB, MC, AB, EP, VM, BPV and PF conducted the chamber experiments. MR provided with the soil sample and expertise on heterogeneous chemistry. PF provided with funding.

Competing interests. The authors declare no competing interests.

Special issue statement. This article is not part of a special issue. It is not associated with a conference.

Acknowledgements. The AERIS data center (www.aeris–data.fr) is acknowledged for distributing and curing the data produced by the CESAM chamber through the hosting of the EUROCHAMP data center (https://data.eurochamp.org). The initial contribution of M. Giordano (Afri-SET) to the conceptualisation of the project is gratefully acknowledged. The authors wish to thank the two anonymous referees for helping ~~improving~~to improve the manuscript.

Financial support. This work has received funding from the French National Research Agency (ANR) though the research project CLIMDO under the grant number ANR-19-CE01-0008-02. It has received support from the European Union's Horizon 2020 research and innovation program through the EUROCHAMP-2020 Infrastructure Activity under grant agreement no. 730997. CNRS-INSU is gratefully acknowledged for supporting the CESAM chamber as a national facility as part of the French ACTRIS Research Infrastructure.

Mis en forme : Police :(Par défaut) Arial, 12 pt

Mis en forme : Police :(Par défaut) Arial, 12 pt

Mis en forme : Police :11 pt, Non Italique

Mis en forme : Police :11 pt

Mis en forme : Police :12 pt

Mis en forme : Police :(Par défaut) Arial

Mis en forme : Police :11 pt

References

Adebiyi, A., Kok, J. F., Murray, B. J., Ryder, C. L., Stuut, J.-B. W., Kahn, R. A., Knippertz, P., Formenti, P., Mahowald, N. M., Pérez García-Pando, C., Klose, M., Ansmann, A., Samset, B. H., Ito, A., Balkanski, Y., Di Biagio, C., Romanias, M. N., Huang, Y., and Meng, J.: A review of coarse mineral dust in the Earth system, Aeolian Research, 60, 100849, https://doi.org/10.1016/j.aeolia.2022.100849, 2023.

Aiken, A. C., DeCarlo, P. F., Kroll, J. H., Worsnop, D. R., Huffman, J. A., Docherty, K. S., Ulbrich, I. M., Mohr, C., Kimmel, J. R., Sueper, D., Sun, Y., Zhang, Q., Trimborn, A., Northway, M., Ziemann, P. J., Canagaratna, M. R., Onasch, T. B., Alfarra, M. R., Prevot, A. S. H., Dommen, J., Duplissy, J., Metzger, A., Baltensperger, U., and Jimenez, J. L.: O/C and OM/OC Ratios of Primary, Secondary, and Ambient Organic Aerosols with High-Resolution Time-of-Flight Aerosol Mass Spectrometry, Environ. Sci. Technol., 42, 4478–4485, https://doi.org/10.1021/es703009q, 2008.

Alvarado, L. M. A., Richter, A., Vrekoussis, M., Hilboll, A., Kalisz Hedegaard, A. B., Schneising, O., and Burrows, J. P.: Unexpected long-range transport of glyoxal and formaldehyde observed from the Copernicus Sentinel-5 Precursor satellite during the 2018 Canadian wildfires, Atmos. Chem. Phys., 20, 2057–2072, https://doi.org/10.5194/acp-20-2057-2020, 2020.

Atkinson, J. D., Murray, B. J., Woodhouse, M. T., Whale, T. F., Baustian, K. J., Carslaw, K. S., Dobbie, S., O'Sullivan, D., and Malkin, T. L.: The importance of feldspar for ice nucleation by mineral dust in mixed-phase clouds, Nature, 498, 355–358, https://doi.org/10.1038/nature12278, 2013.

Avzianova, E. and Brooks, S. D.: Raman spectroscopy of glyoxal oligomers in aqueous solutions, Spectrochimica Acta Part A: Molecular and Biomolecular Spectroscopy, 101, 40–48, https://doi.org/10.1016/j.saa.2012.09.050, 2013.

Baldo, C., Formenti, P., Di Biagio, C., Lu, G., Song, C., Cazaunau, M., Pangui, E., Doussin, J.-F., Dagsson-Waldhauserova, P., Arnalds, O., Beddows, D., MacKenzie, A. R., and Shi, Z.: Complex refractive index and single scattering albedo of Icelandic dust in the shortwave part of the spectrum, Atmos. Chem. Phys., 23, 7975–8000, https://doi.org/10.5194/acp-23-7975-2023, 2023.

Battaglia, F., Baldo, C., Cazaunau, M., Bergé, A., Pangui, E., Picquet-Varrault, B., Doussin, J.-F., and Formenti, P.: Protocol for generating realistic submicron mono-dispersed mineral dust particles in simulation chambers and laboratory experiments, Aerosol Science and Technology, 59, 357–369, https://doi.org/10.1080/02786826.2024.2442518, 2025.

Bauer, S. E., Mishchenko, M. I., Lacis, A. A., Zhang, S., Perlwitz, J., and Metzger, S. M.: Do sulfate and nitrate coatings on mineral dust have important effects on radiative properties and climate modeling?, J. Geophys. Res., 112, D06307, https://doi.org/10.1029/2005JD006977, 2007.

Brégonzio-Rozier, L., Giorio, C., Siekmann, F., Pangui, E., Morales, S. B., Temime-Roussel, B., Gratien, A., Michoud, V., Cazaunau, M., DeWitt, H. L., Tapparo, A., Monod, A., and Doussin, J.-F.: Secondary organic aerosol formation from isoprene photooxidation during cloud condensation–evaporation cycles, Atmos. Chem. Phys., 16, 1747–1760, https://doi.org/10.5194/acp-16-1747-2016, 2016.

Buxton, G. V., Malone, T. N., and Arthur Salmon, G.: Oxidation of glyoxal initiated by OH in oxygenated aqueous solution, Faraday Trans., 93, 2889–2891, https://doi.org/10.1039/a701468f, 1997.

Carlton, A. G., Turpin, B. J., Altieri, K. E., Seitzinger, S., Reff, A., Lim, H.-J., and Ervens, B.: Atmospheric oxalic acid and SOA production from glyoxal: Results of aqueous photooxidation experiments, Atmospheric Environment, 41, 7588–7602, https://doi.org/10.1016/j.atmosenv.2007.05.035, 2007.

Castellanos, P., Colarco, P., Espinosa, W. R., Guzewich, S. D., Levy, R. C., Miller, R. L., Chin, M., Kahn, R. A., Kemppinen, O., Moosmüller, H., Nowottnick, E. P., Rocha-Lima, A., Smith, M. D., Yorks, J. E., and Yu, H.: Mineral dust optical properties for remote sensing and global modeling: A review, Remote Sensing of Environment, 303, 113982, https://doi.org/10.1016/j.rse.2023.113982, 2024.

Chan, C., Jacob, D. J., Marais, E. A., Yu, K., Travis, K. R., Kim, P. S., Fisher, J. A., Zhu, L., Wolfe, G. M., Hanisco, T. F., Keutsch, F. N., Kaiser, J., Min, K.-E., Brown, S. S., Washenfelder, R. A.,

Mis en forme : Anglais (Royaume-Uni)

Mis en forme : Anglais (États-Unis)

González Abad, G., and Chance, K.: Glyoxal yield from isoprene oxidation and relation to formaldehyde: chemical mechanism, constraints from SENEX aircraft observations, and interpretation of OMI satellite data, Atmos. Chem. Phys., 17, 8725–8738, https://doi.org/10.5194/acp-17-8725-2017, 2017.

Chen, S., Chen, J., Zhang, Y., Lin, J., Bi, H., Song, H., Chen, Y., Lian, L., Liu, C., and Zhang, R.: Anthropogenic dust: sources, characteristics and emissions, Environ. Res. Lett., 18, 103002, https://doi.org/10.1088/1748-9326/acf479, 2023.

Chirizzi, D.: Influence of Saharan dust outbreaks and carbon content on oxidative potential of water-soluble fractions of PM2.5 and PM10, Atmospheric Environment, 2017.

Crowley, J. N., Ammann, M., Cox, R. A., Hynes, R. G., Jenkin, M. E., Mellouki, A., Rossi, M. J., Troe, J., and Wallington, T. J.: Evaluated kinetic and photochemical data for atmospheric chemistry: Volume V – heterogeneous reactions on solid substrates, Atmos. Chem. Phys., 10, 9059–9223, https://doi.org/10.5194/acp-10-9059-2010, 2010.

De Haan, D. O., Hawkins, L. N., Jansen, K., Welsh, H. G., Pednekar, R., De Loera, A., Jimenez, N. G., Tolbert, M. A., Cazaunau, M., Gratien, A., Bergé, A., Pangui, E., Formenti, P., and Doussin, J.-F.: Glyoxal's impact on dry ammonium salts: fast and reversible surface aerosol browning, Atmos. Chem. Phys., 20, 9581–9590, https://doi.org/10.5194/acp-20-9581-2020, 2020.

De Haan, D. O., Hawkins, L. N., Wickremasinghe, P. D., Andretta, A. D., Dignum, J. R., De Haan, A. C., Welsh, H. G., Pennington, E. A., Cui, T., Surratt, J. D., Cazaunau, M., Pangui, E., and Doussin, J.-F.: Brown Carbon from Photo-Oxidation of Glyoxal and SO 2 in Aqueous Aerosol, ACS Earth Space Chem., 7, 1131–1140, https://doi.org/10.1021/acsearthspacechem.3c00035, 2023.

Denjean, C., Formenti, P., Picquet-Varrault, B., Katrib, Y., Pangui, E., Zapf, P., and Doussin, J. F.: A new experimental approach to study the hygroscopic and optical properties of aerosols: application to ammonium sulfate particles, Atmos. Meas. Tech., 7, 183–197, https://doi.org/10.5194/amt-7-183-2014, 2014.

Di Biagio, C., Formenti, P., Balkanski, Y., Caponi, L., Cazaunau, M., Pangui, E., Journet, E., Nowak, S., Caquineau, S., Andreae, M. O., Kandler, K., Saeed, T., Piketh, S., Seibert, D., Williams, E., and Doussin, J.-F.: Global scale variability of the mineral dust long-wave refractive index: a new dataset of in situ measurements for climate modeling and remote sensing, Atmos. Chem. Phys., 17, 1901–1929, https://doi.org/10.5194/acp-17-1901-2017, 2017.

Di Biagio, C., Formenti, P., Balkanski, Y., Caponi, L., Cazaunau, M., Pangui, E., Journet, E., Nowak, S., Andreae, M. O., Kandler, K., Saeed, T., Piketh, S., Seibert, D., Williams, E., and Doussin, J.-F.: Complex refractive indices and single-scattering albedo of global dust aerosols in the shortwave spectrum and relationship to size and iron content, Atmos. Chem. Phys., 19, 15503–15531, https://doi.org/10.5194/acp-19-15503-2019, 2019.

Dupart, Y., King, S. M., Nekat, B., Nowak, A., Wiedensohler, A., Herrmann, H., David, G., Thomas, B., Miffre, A., Rairoux, P., D'Anna, B., and George, C.: Mineral dust photochemistry induces nucleation events in the presence of SO 2, Proc. Natl. Acad. Sci. U.S.A., 109, 20842–20847, https://doi.org/10.1073/pnas.1212297109, 2012.

Ervens, B. and Volkamer, R.: Glyoxal processing by aerosol multiphase chemistry: towards a kinetic modeling framework of secondary organic aerosol formation in aqueous particles, Atmos. Chem. Phys., 10, 8219–8244, https://doi.org/10.5194/acp-10-8219-2010, 2010.

Fröhlich, R., Cubison, M. J., Slowik, J. G., Bukowiecki, N., Prévôt, A. S. H., Baltensperger, U., Schneider, J., Kimmel, J. R., Gonin, M., Rohner, U., Worsnop, D. R., and Jayne, J. T.: The ToF-ACSM: a portable aerosol chemical speciation monitor with TOFMS detection, Atmos. Meas. Tech., 6, 3225–3241, https://doi.org/10.5194/amt-6-3225-2013, 2013.

Fu, T.-M., Jacob, D. J., Wittrock, F., Burrows, J. P., Vrekoussis, M., and Henze, D. K.: Global budgets of atmospheric glyoxal and methylglyoxal, and implications for formation of secondary organic aerosols, J. Geophys. Res., 113, D15303, https://doi.org/10.1029/2007JD009505, 2008.

Mis en forme : Retrait : Gauche : 0 cm, Suspendu : 1 cm, Interligne : simple

Mis en forme : Anglais (États-Unis)

Galloway, M. M., Chhabra, P. S., Chan, A. W. H., Surratt, J. D., Flagan, R. C., Seinfeld, J. H., and Keutsch, F. N.: Glyoxal uptake on ammonium sulphate seed aerosol: reaction products and reversibility of uptake under dark and irradiated conditions, Atmos. Chem. Phys., 2009.

Giorio, C., Monod, A., Brégonzio-Rozier, L., DeWitt, H. L., Cazaunau, M., Temime-Roussel, B., Gratien, A., Michoud, V., Pangui, E., Ravier, S., Zielinski, A. T., Tapparo, A., Vermeylen, R., Claeys, M., Voisin, D., Kalberer, M., and Doussin, J.-F.: Cloud Processing of Secondary Organic Aerosol from Isoprene and Methacrolein Photooxidation, J. Phys. Chem. A, 121, 7641–7654, https://doi.org/10.1021/acs.jpca.7b05933, 2017.

Giorio, C., D'Aronco, S., Di Marco, V., Badocco, D., Battaglia, F., Soldà, L., Pastore, P., and Tapparo, A.: Emerging investigator series: aqueous-phase processing of atmospheric aerosol influences dissolution kinetics of metal ions in an urban background site in the Po Valley, Environ. Sci.: Processes Impacts, 24, 884–897, https://doi.org/10.1039/D2EM00023G, 2022.

Gomez, M. E., Lin, Y., Guo, S., & Zhang, R. (2015). Heterogeneous Chemistry of Glyoxal on Acidic Solutions. An Oligomerization Pathway for Secondary Organic Aerosol Formation. The Journal of Physical Chemistry A, 119(19), 4457–4463. https://doi.org/10.1021/jp509916r

Goodman, A. L., Underwood, G. M., and Grassian, V. H.: Heterogeneous Reaction of NO 2 : Characterization of Gas-Phase and Adsorbed Products from the Reaction, 2NO 2 (g) + H 2 O(a) → HONO(g) + HNO 3 (a) on Hydrated Silica Particles, J. Phys. Chem. A, 103, 7217–7223, https://doi.org/10.1021/jp9910688, 1999.

Guo, Y., Wang, S., Zhu, J., Zhang, R., Gao, S., Saiz-Lopez, A., and Zhou, B.: Atmospheric formaldehyde, glyoxal and their relations to ozone pollution under low- and high-NOx regimes in summertime Shanghai, China, Atmospheric Research, 258, 105635, https://doi.org/10.1016/j.atmosres.2021.105635, 2021.

Harrison, S. P., Kohfeld, K. E., Roelandt, C., and Claquin, T.: The role of dust in climate changes today, at the last glacial maximum and in the future, Earth-Science Reviews, 54, 43–80, https://doi.org/10.1016/S0012-8252(01)00041-1, 2001.

Hastings, W. P., Koehler, C. A., Bailey, E. L., & De Haan, D. O. (2005). Secondary Organic Aerosol Formation by Glyoxal Hydration and Oligomer Formation: Humidity Effects and Equilibrium Shifts during Analysis. Environmental Science & Technology, 39(22), 8728–8735. https://doi.org/10.1021/es050446l

Hettiarachchi, E. and Grassian, V. H.: Heterogeneous Reactions of Phenol on Different Components of Mineral Dust Aerosol: Formation of Oxidized Organic and Nitro-Phenolic Compounds, ACS EST Air, 1, 259–272, https://doi.org/10.1021/acsestair.3c00042, 2024.

Horowitz, A., Meller, R., and Moortgat, G. K.: The UV–VIS absorption cross sections of the , -dicarbonyl compounds: pyruvic acid, biacetyl and glyoxal, 2001.

Hu, J., Chen, Z., Qin, X., and Dong, P.: Reversible and irreversible gas–particle partitioning of dicarbonyl compounds observed in the real atmosphere, Atmos. Chem. Phys., 22, 6971–6987, https://doi.org/10.5194/acp-22-6971-2022, 2022.

Joshi, N., Romanias, M. N., Riffault, V., and Thevenet, F.: Investigating water adsorption onto natural mineral dust particles: Linking DRIFTS experiments and BET theory, Aeolian Research, 27, 35–45, https://doi.org/10.1016/j.aeolia.2017.06.001, 2017.

Lai, A. C. and Nazaroff, W. W.: MODELING INDOOR PARTICLE DEPOSITION FROM TURBULENT FLOW ONTO SMOOTH SURFACES, Journal of Aerosol Science, 31, 463–476, https://doi.org/10.1016/S0021-8502(99)00536-4, 2000.

Kalberer, M., Paulsen, D., Sax, M., Steinbacher, M., Dommen, J., Prevot, A. S. H., Fisseha, R., Weingartner, E., Frankevich, V., Zenobi, R., and Baltensperger, U.: Identification of Polymers as Major Components of Atmospheric Organic Aerosols, Science, 303, 1659–1662, https://doi.org/10.1126/science.1092185, 2004.

Kluge, F., Hüneke, T., Lerot, C., Rosanka, S., Rotermund, M. K., Taraborrelli, D., Weyland, B., and Pfeilsticker, K.: Airborne glyoxal measurements in the marine and continental atmosphere:

Mis en forme : Anglais (États-Unis)

Mis en forme : Police :10 pt

Mis en forme : Police :10 pt, Non Italique

Mis en forme : Police :10 pt

Mis en forme : Police :10 pt, Non Italique

Mis en forme : Police :10 pt

Mis en forme : Anglais (États-Unis)

comparison with TROPOMI observations and EMAC simulations, Atmos. Chem. Phys., 23, 1369–1401, https://doi.org/10.5194/acp-23-1369-2023, 2023.

Knippertz, P. and Stuut, J.-B. W. (Eds.): Mineral Dust: A Key Player in the Earth System, Springer Netherlands, Dordrecht, https://doi.org/10.1007/978-94-017-8978-3, 2014.

Knote, C., Hodzic, A., Jimenez, J. L., Volkamer, R., Orlando, J. J., Baidar, S., Brioude, J., Fast, J., Gentner, D. R., Goldstein, A. H., Hayes, P. L., Knighton, W. B., Oetjen, H., Setyan, A., Stark, H., Thalman, R., Tyndall, G., Washenfelder, R., Waxman, E., and Zhang, Q.: Simulation of semi-explicit mechanisms of SOA formation from glyoxal in aerosol in a 3-D model, Atmos. Chem. Phys., 14, 6213–6239, https://doi.org/10.5194/acp-14-6213-2014, 2014.

Kok, J. F., Adebiyi, A. A., Albani, S., Balkanski, Y., Checa-Garcia, R., Chin, M., Colarco, P. R., Hamilton, D. S., Huang, Y., Ito, A., Klose, M., Li, L., Mahowald, N. M., Miller, R. L., Obiso, V., Pérez García-Pando, C., Rocha-Lima, A., and Wan, J. S.: Contribution of the world's main dust source regions to the global cycle of desert dust, Aerosols/Atmospheric Modelling/Troposphere/Physics (physical properties and processes), https://doi.org/10.5194/acp-2021-4, 2021.

Kok, J. F., Storelvmo, T., Karydis, V. A., Adebiyi, A. A., Mahowald, N. M., Evan, A. T., He, C., and Leung, D. M.: Mineral dust aerosol impacts on global climate and climate change, Nat Rev Earth Environ, 4, 71–86, https://doi.org/10.1038/s43017-022-00379-5, 2023.

Kourtchev, I., Doussin, J.-F., Giorio, C., Mahon, B., Wilson, E. M., Maurin, N., Pangui, E., Venables, D. S., Wenger, J. C., and Kalberer, M.: Molecular composition of fresh and aged secondary organic aerosol from a mixture of biogenic volatile compounds: a high-resolution mass spectrometry study, Atmos. Chem. Phys., 15, 5683–5695, https://doi.org/10.5194/acp-15-5683-2015, 2015.

Kroll, J. H., Ng, N. L., Murphy, S. M., Varutbangkul, V., Flagan, R. C., and Seinfeld, J. H.: Chamber studies of secondary organic aerosol growth by reactive uptake of simple carbonyl compounds, J. Geophys. Res., 110, 2005JD006004, https://doi.org/10.1029/2005JD006004, 2005.

Kua, J., Hanley, S. W., & De Haan, D. O. (2008). Thermodynamics and Kinetics of Glyoxal Dimer Formation: A Computational Study. The Journal of Physical Chemistry A, 112(1), 66–72. https://doi.org/10.1021/jp076573q

Lewis, A. C., Hopkins, J. R., Carslaw, D. C., Hamilton, J. F., Nelson, B. S., Stewart, G., Dernie, J., Passant, N., and Murrells, T.: An increasing role for solvent emissions and implications for future measurements of volatile organic compounds, Phil. Trans. R. Soc. A., 378, 20190328, https://doi.org/10.1098/rsta.2019.0328, 2020.

Li, G., Cheng, Y., Kuhn, U., Xu, R., Yang, Y., Meusel, H., Wang, Z., Ma, N., Wu, Y., Li, M., Williams, J., Hoffmann, T., Ammann, M., Pöschl, U., Shao, M., and Su, H.: Physicochemical uptake and release of volatile organic compounds by soil in coated-wall flow tube experiments with ambient air, Atmos. Chem. Phys., 19, 2209–2232, https://doi.org/10.5194/acp-19-2209-2019, 2019.

Li, L., Mahowald, N. M., Miller, R. L., Pérez García-Pando, C., Klose, M., Hamilton, D. S., Gonçalves Ageitos, M., Ginoux, P., Balkanski, Y., Green, R. O., Kalashnikova, O., Kok, J. F., Obiso, V., Paynter, D., and Thompson, D. R.: Quantifying the range of the dust direct radiative effect due to source mineralogy uncertainty, Atmos. Chem. Phys., 21, 3973–4005, https://doi.org/10.5194/acp-21-3973-2021, 2021.

Li, Q., Gong, D., Wang, H., Wang, Y., Han, S., Wu, G., Deng, S., Yu, P., Wang, W., and Wang, B.: Rapid increase in atmospheric glyoxal and methylglyoxal concentrations in Lhasa, Tibetan Plateau: Potential sources and implications, Science of The Total Environment, 824, 153782, https://doi.org/10.1016/j.scitotenv.2022.153782, 2022.

Liggio, J.: Reactive uptake of glyoxal by particulate matter, J. Geophys. Res., 110, D10304, https://doi.org/10.1029/2004JD005113, 2005a.

Liggio, J., Li, S.-M., and McLaren, R.: Heterogeneous Reactions of Glyoxal on Particulate Matter: Identification of Acetals and Sulfate Esters, Environ. Sci. Technol., 39, 1532–1541, https://doi.org/10.1021/es048375y, 2005b.

Mis en forme : Néerlandais (Pays-Bas)

Mis en forme : Police :10 pt, Néerlandais (Pays-Bas)

Mis en forme : Police :10 pt

Mis en forme : Police :10 pt, Non Italique

Mis en forme : Police :10 pt

Mis en forme : Police :10 pt, Non Italique

Mis en forme : Police :10 pt

Mis en forme : Anglais (États-Unis)

Lim, Y. B., Tan, Y., Perri, M. J., Seitzinger, S. P., and Turpin, B. J.: Aqueous chemistry and its role in secondary organic aerosol (SOA) formation, Atmos. Chem. Phys., 10, 10521–10539, https://doi.org/10.5194/acp-10-10521-2010, 2010.

Ling, Z., Xie, Q., Shao, M., Wang, Z., Wang, T., Guo, H., and Wang, X.: Formation and sink of glyoxal and methylglyoxal in a polluted subtropical environment: observation-based photochemical analysis and impact evaluation, Atmos. Chem. Phys., 20, 11451–11467, https://doi.org/10.5194/acp-20-11451-2020, 2020.

Liu, C., Chu, B., Liu, Y., Ma, Q., Ma, J., He, H., Li, J., and Hao, J.: Effect of mineral dust on secondary organic aerosol yield and aerosol size in α-pinene/NOx photo-oxidation, Atmospheric Environment, 77, 781–789, https://doi.org/10.1016/j.atmosenv.2013.05.064, 2013.

Loeffler, K. W., Koehler, C. A., Paul, N. M., & De Haan, D. O. (2006). Oligomer Formation in Evaporating Aqueous Glyoxal and Methyl Glyoxal Solutions. Environmental Science & Technology, 40(20), 6318–6323. https://doi.org/10.1021/es060810w

Mahowald, N., Albani, S., Kok, J. F., Engelstaeder, S., Scanza, R., Ward, D. S., and Flanner, M. G.: The size distribution of desert dust aerosols and its impact on the Earth system, Aeolian Research, 15, 53–71, https://doi.org/10.1016/j.aeolia.2013.09.002, 2014.

Ng, N. L., Canagaratna, M. R., Jimenez, J. L., Chhabra, P. S., Seinfeld, J. H., and Worsnop, D. R.: Changes in organic aerosol composition with aging inferred from aerosol mass spectra, Atmos. Chem. Phys., 11, 6465–6474, https://doi.org/10.5194/acp-11-6465-2011, 2011.

Nie, W., Ding, A., Wang, T., Kerminen, V.-M., George, C., Xue, L., Wang, W., Zhang, Q., Petäjä, T., Qi, X., Gao, X., Wang, X., Yang, X., Fu, C., and Kulmala, M.: Polluted dust promotes new particle formation and growth, Sci Rep, 4, 6634, https://doi.org/10.1038/srep06634, 2014.

Nieder, R., Benbi, D. K., and Reichl, F. X.: Soil-Borne Particles and Their Impact on Environment and Human Health, in: Soil Components and Human Health, Springer Netherlands, Dordrecht, 99–177, https://doi.org/10.1007/978-94-024-1222-2_3, 2018.

Nozière, B., Dziedzic, P., and Córdova, A.: Products and Kinetics of the Liquid-Phase Reaction of Glyoxal Catalyzed by Ammonium Ions (NH 4 +), J. Phys. Chem. A, 113, 231–237, https://doi.org/10.1021/jp8078293, 2009.

Ooki, A. and Uematsu, M.: Chemical interactions between mineral dust particles and acid gases during Asian dust events, J. Geophys. Res., 110, 2004JD004737, https://doi.org/10.1029/2004JD004737, 2005.

Ortiz-Montalvo, D. L., Häkkinen, S. A. K., Schwier, A. N., Lim, Y. B., McNeill, V. F., and Turpin, B. J.: Ammonium Addition (and Aerosol pH) Has a Dramatic Impact on the Volatility and Yield of Glyoxal Secondary Organic Aerosol, Environ. Sci. Technol., 48, 255–262, https://doi.org/10.1021/es4035667, 2014.

Ponczek, M., Hayeck, N., Emmelin, C., and George, C.: Heterogeneous photochemistry of dicarboxylic acids on mineral dust, Atmospheric Environment, 212, 262–271, https://doi.org/10.1016/j.atmosenv.2019.05.032, 2019.

Romanias, M. N., El Zein, A., and Bedjanian, Y.: Heterogeneous Interaction of H 2 O 2 with TiO 2 Surface under Dark and UV Light Irradiation Conditions, J. Phys. Chem. A, 116, 8191–8200, https://doi.org/10.1021/jp305366v, 2012.

Romanías, Manolis N., Habib Ourrad, Frédéric Thévenet, and Véronique Riffault. 2016. "Investigating the Heterogeneous Interaction of VOCs with Natural Atmospheric Particles: Adsorption of Limonene and Toluene on Saharan Mineral Dusts." The Journal of Physical Chemistry A 120(8):1197–1212. doi: 10.1021/acs.jpca.5b10323.

Rossignol, S., Aregahegn, K. Z., Tinel, L., Fine, L., Nozière, B., and George, C.: Glyoxal Induced Atmospheric Photosensitized Chemistry Leading to Organic Aerosol Growth, Environ. Sci. Technol., 48, 3218–3227, https://doi.org/10.1021/es405581g, 2014.

Rubasinghege, G., Ogden, S., Baltrusaitis, J., and Grassian, V. H.: Heterogeneous Uptake and Adsorption of Gas-Phase Formic Acid on Oxide and Clay Particle Surfaces: The Roles of Surface

Mis en forme : Anglais (États-Unis)

Mis en forme : Police :10 pt

Mis en forme : Police :10 pt, Non Italique

Mis en forme : Police :10 pt

Mis en forme : Police :10 pt, Non Italique

Mis en forme : Police :10 pt

Mis en forme : Anglais (États-Unis)

Mis en forme : Français (France)

Mis en forme : Anglais (États-Unis)

Hydroxyl Groups and Adsorbed Water in Formic Acid Adsorption and the Impact of Formic Acid Adsorption on Water Uptake, J. Phys. Chem. A, 117, 11316–11327, https://doi.org/10.1021/jp408169w, 2013.

Safi Shalamzari, M., Ryabtsova, O., Kahnt, A., Vermeylen, R., Hérent, M., Quetin-Leclercq, J., Van Der Veken, P., Maenhaut, W., and Claeys, M.: Mass spectrometric characterization of organosulfates related to secondary organic aerosol from isoprene, Rapid Comm Mass Spectrometry, 27, 784–794, https://doi.org/10.1002/rcm.6511, 2013.

Schwier, A. N., Sareen, N., Mitroo, D., Shapiro, E. L., and McNeill, V. F.: Glyoxal-Methylglyoxal Cross-Reactions in Secondary Organic Aerosol Formation, Environ. Sci. Technol., 44, 6174–6182, https://doi.org/10.1021/es101225q, 2010.

Seisel, S., Lian, Y., Keil, T., Trukhin, M. E., and Zellner, R.: Kinetics of the interaction of water vapour with mineral dust and soot surfaces at T = 298 K, Phys. Chem. Chem. Phys., 6, 1926–1932, https://doi.org/10.1039/B314568A, 2004.

Shapiro, E. L., Szprengiel, J., Sareen, N., Jen, C. N., Giordano, M. R., and McNeill, V. F.: Light-absorbing secondary organic material formed by glyoxal in aqueous aerosol mimics, Atmos. Chem. Phys., 2009.

Shen, X., Wu, H., Zhao, Y., Huang, D., Huang, L., and Chen, Z.: Heterogeneous reactions of glyoxal on mineral particles: A new avenue for oligomers and organosulfate formation, Atmospheric Environment, 131, 133–140, https://doi.org/10.1016/j.atmosenv.2016.01.048, 2016.

Shrivastava, M., Cappa, C. D., Fan, J., Goldstein, A. H., Guenther, A. B., Jimenez, J. L., Kuang, C., Laskin, A., Martin, S. T., Ng, N. L., Petaja, T., Pierce, J. R., Rasch, P. J., Roldin, P., Seinfeld, J. H., Shilling, J., Smith, J. N., Thornton, J. A., Volkamer, R., Wang, J., Worsnop, D. R., Zaveri, R. A., Zelenyuk, A., and Zhang, Q.: Recent advances in understanding secondary organic aerosol: Implications for global climate forcing, Reviews of Geophysics, 55, 509–559, https://doi.org/10.1002/2016RG000540, 2017.

Song, Q. and Osada, K.: Direct measurement of aerosol acidity using pH testing paper and hygroscopic equilibrium under high relative humidity, Atmospheric Environment, 261, 118605, https://doi.org/10.1016/j.atmosenv.2021.118605, 2021.

Steinke, I., Funk, R., Busse, J., Iturri, A., Kirchen, S., Leue, M., Möhler, O., Schwartz, T., Schnaiter, M., Sierau, B., Toprak, E., Ullrich, R., Ulrich, A., Hoose, C., and Leisner, T.: Ice nucleation activity of agricultural soil dust aerosols from Mongolia, Argentina, and Germany, JGR Atmospheres, 121, https://doi.org/10.1002/2016JD025160, 2016.

Sun, Y. L., Zhang, Q., Anastasio, C., and Sun, J.: Insights into secondary organic aerosol formed via aqueous-phase reactions of phenolic compounds based on high resolution mass spectrometry, Atmos. Chem. Phys., 10, 4809–4822, https://doi.org/10.5194/acp-10-4809-2010, 2010.

Tang, M., Huang, X., Lu, K., Ge, M., Li, Y., Cheng, P., Zhu, T., Ding, A., Zhang, Y., Gligorovski, S., Song, W., Ding, X., Bi, X., and Wang, X.: Heterogeneous reactions of mineral dust aerosol: implications for tropospheric oxidation capacity, Atmos. Chem. Phys., 17, 11727–11777, https://doi.org/10.5194/acp-17-11727-2017, 2017.

Tegen, I. and Fung, I.: Contribution to the atmospheric mineral aerosol load from land surface modification, J. Geophys. Res., 100, 18707, https://doi.org/10.1029/95JD02051, 1995.

Trainic, M., Abo Riziq, A., Lavi, A., Flores, J. M., and Rudich, Y.: The optical, physical and chemical properties of the products of glyoxal uptake on ammonium sulfate seed aerosols, Atmos. Chem. Phys., 11, 9697–9707, https://doi.org/10.5194/acp-11-9697-2011, 2011.

Turpin, B. J. and Huntzicker, J. J.: Identification of secondary organic aerosol episodes and quantitation of primary and secondary organic aerosol concentrations during SCAQS, Atmospheric Environment, 29, 3527–3544, https://doi.org/10.1016/1352-2310(94)00276-Q, 1995.

Usher, C. R., Michel, A. E., and Grassian, V. H.: Reactions on Mineral Dust, Chem. Rev., 103, 4883–4940, https://doi.org/10.1021/cr020657y, 2003.

Volkamer, R., Platt, U., and Wirtz, K.: Primary and Secondary Glyoxal Formation from Aromatics: Experimental Evidence for the Bicycloalkyl−Radical Pathway from Benzene, Toluene, and p -Xylene, J. Phys. Chem. A, 105, 7865–7874, https://doi.org/10.1021/jp010152w, 2001.

Volkamer, R., Spietz, P., Burrows, J., and Platt, U.: High-resolution absorption cross-section of glyoxal in the UV–vis and IR spectral ranges, Journal of Photochemistry and Photobiology A: Chemistry, 172, 35–46, https://doi.org/10.1016/j.jphotochem.2004.11.011, 2005.

Volkamer, R., San Martini, F., Molina, L. T., Salcedo, D., Jimenez, J. L., and Molina, M. J.: A missing sink for gas-phase glyoxal in Mexico City: Formation of secondary organic aerosol, Geophysical Research Letters, 34, 2007GL030752, https://doi.org/10.1029/2007GL030752, 2007.

Vrekoussis, M., Wittrock, F., Richter, A., Burrows, J. P., and Cho, C.: Temporal and spatial variability of glyoxal as observed from space, Atmos. Chem. Phys., 2009.

Wagner, C., Hanisch, F., Holmes, N., de Coninck, H., Schuster, G., and Crowley, J. N.: The interaction of N2O5 with mineral dust: aerosol flow tube and Knudsen reactor studies, Atmos. Chem. Phys., 2008.

Walker, H., Stone, D., Ingham, T., Hackenberg, S., Cryer, D., Punjabi, S., Read, K., Lee, J., Whalley, L., Spracklen, D. V., Carpenter, L. J., Arnold, S. R., and Heard, D. E.: Observations and modelling of glyoxal in the tropical Atlantic marine boundary layer, Atmos. Chem. Phys., 22, 5535–5557, https://doi.org/10.5194/acp-22-5535-2022, 2022.

Wang, G., Cheng, C., Meng, J., Huang, Y., Li, J., and Ren, Y.: Field observation on secondary organic aerosols during Asian dust storm periods: Formation mechanism of oxalic acid and related compounds on dust surface, Atmospheric Environment, 113, 169–176, https://doi.org/10.1016/j.atmosenv.2015.05.013, 2015.

Wang, J., Doussin, J. F., Perrier, S., Perraudin, E., Katrib, Y., Pangui, E., and Picquet-Varrault, B.: Design of a new multi-phase experimental simulation chamber for atmospheric photosmog, aerosol and cloud chemistry research, Atmos. Meas. Tech., 4, 2465–2494, https://doi.org/10.5194/amt-4-2465-2011, 2011.

Washenfelder, R. A., Young, C. J., Brown, S. S., Angevine, W. M., Atlas, E. L., Blake, D. R., Bon, D. M., Cubison, M. J., De Gouw, J. A., Dusanter, S., Flynn, J., Gilman, J. B., Graus, M., Griffith, S., Grossberg, N., Hayes, P. L., Jimenez, J. L., Kuster, W. C., Lefer, B. L., Pollack, I. B., Ryerson, T. B., Stark, H., Stevens, P. S., and Trainer, M. K.: The glyoxal budget and its contribution to organic aerosol for Los Angeles, California, during CalNex 2010: GLYOXAL BUDGET FOR LOS ANGELES, J. Geophys. Res., 116, https://doi.org/10.1029/2011JD016314, 2011.

Webb, N. P. and Pierre, C.: Quantifying Anthropogenic Dust Emissions, Earth's Future, 6, 286–295, https://doi.org/10.1002/2017EF000766, 2018.

Xu, K., Liu, Y., Li, C., Zhang, C., Liu, X., Li, Q., Xiong, M., Zhang, Y., Yin, S., and Ding, Y.: Enhanced secondary organic aerosol formation during dust episodes by photochemical reactions in the winter in Wuhan, Journal of Environmental Sciences, 133, 70–82, https://doi.org/10.1016/j.jes.2022.04.018, 2023.

Zeineddine, M. N., Romanias, M. N., Gaudion, V., Riffault, V., and Thévenet, F.: Heterogeneous Interaction of Isoprene with Natural Gobi Dust, ACS Earth Space Chem., 1, 236–243, https://doi.org/10.1021/acsearthspacechem.7b00050, 2017.

Zeineddine, M. N., Urupina, D., Romanias, M. N., Riffault, V., and Thevenet, F.: Uptake and reactivity of acetic acid on Gobi dust and mineral surrogates: A source of oxygenated volatile organic compounds in the atmosphere?, Atmospheric Environment, 294, 119509, https://doi.org/10.1016/j.atmosenv.2022.119509, 2023.

Zhang, X., He, A., Guo, R., Zhao, Y., Yang, L., Morita, S., Xu, Y., Noda, I., and Ozaki, Y.: A new approach to removing interference of moisture from FTIR spectrum, Spectrochimica Acta Part A: Molecular and Biomolecular Spectroscopy, 265, 120373, https://doi.org/10.1016/j.saa.2021.120373, 2022.

Zhang, Y., He, L., Sun, X., Ventura, O. N., & Herrmann, H. (2022). Theoretical Investigation on the Oligomerization of Methylglyoxal and Glyoxal in Aqueous Atmospheric Aerosol Particles. ACS

Mis en forme : Anglais (États-Unis)

Mis en forme : Police :10 pt

Earth and Space Chemistry, 6(4), 1031–1043. https://doi.org/10.1021/acsearthspacechem.1c00422.

Zielinski, A. T., Kourtchev, I., Bortolini, C., Fuller, S. J., Giorio, C., Popoola, O. A. M., Bogialli, S., Tapparo, A., Jones, R. L., and Kalberer, M.: A new processing scheme for ultra-high resolution direct infusion mass spectrometry data, Atmospheric Environment, 178, 129–139, https://doi.org/10.1016/j.atmosenv.2018.01.034, 2018.

Adebiyi, A., Kok, J. F., Murray, B. J., Ryder, C. L., Stuut, J.-B. W., Kahn, R. A., Knippertz, P., Formenti, P., Mahowald, N. M., Pérez García-Pando, C., Klose, M., Ansmann, A., Samset, B. H., Ito, A., Balkanski, Y., Di Biagio, C., Romanias, M. N., Huang, Y., and Meng, J.: A review of coarse mineral dust in the Earth system, Aeol. Res., 60, 100849, https://doi.org/10.1016/j.aeolia.2022.100849, 2023.

Aiken, A. C., DeCarlo, P. F., Kroll, J. H., Worsnop, D. R., Huffman, J. A., Docherty, K. S., Ulbrich, I. M., Mohr, C., Kimmel, J. R., Sueper, D., Sun, Y., Zhang, Q., Trimborn, A., Northway, M., Ziemann, P. J., Canagaratna, M. R., Onasch, T. B., Alfarra, M. R., Prevot, A. S. H., Dommen, J., Duplissy, J., Metzger, A., Baltensperger, U., and Jimenez, J. L.: O/C and OM/OC Ratios of Primary, Secondary, and Ambient Organic Aerosols with High-Resolution Time-of-Flight Aerosol Mass Spectrometry, Environ. Sci. Technol., 42, 4478–4485, https://doi.org/10.1021/es703009q, 2008.

Baldo, C., Formenti, P., Di Biagio, C., Lu, G., Song, C., Cazaunau, M., Pangui, E., Doussin, J.-F., Dagsson-Waldhauserova, P., Arnalds, O., Beddows, D., MacKenzie, A. R., and Shi, Z.: Complex refractive index and single scattering albedo of Icelandic dust in the shortwave part of the spectrum, Atmos. Chem. Phys., 23, 7975–8000, https://doi.org/10.5194/acp-23-7975-2023, 2023.

Baldo, C. and G. Lu. (2023). Research code supporting "Complex refractive index and single scattering albedo of Icelandic dust in the shortwave spectrum" (v1.0.0). Zenodo. https://doi.org/10.5281/zenodo.8135133

Bauer, S. E., Mishchenko, M. I., Lacis, A. A., Zhang, S., Perlwitz, J., and Metzger, S. M.: Do sulfate and nitrate coatings on mineral dust have important effects on radiative properties and climate modeling?, J. Geophys. Res., 112, D06307, https://doi.org/10.1029/2005JD006977, 2007.

Brégonzio-Rozier, L., Giorio, C., Siekmann, F., Pangui, E., Morales, S. B., Temime-Roussel, B., Gratien, A., Michoud, V., Cazaunau, M., DeWitt, H. L., Tapparo, A., Monod, A., and Doussin, J.-F.: Secondary organic aerosol formation from isoprene photooxidation during cloud condensation–evaporation cycles, Atmos. Chem. Phys., 16, 1747–1760, https://doi.org/10.5194/acp-16-1747-2016, 2016.

Buxton, G. V., Malone, T. N., and Arthur Salmon, G.: Oxidation of glyoxal initiated by OH in oxygenated aqueous solution, Faraday Trans., 93, 2889–2891, https://doi.org/10.1039/a701468f, 1997.

Carlton, A. G., Turpin, B. J., Altieri, K. E., Seitzinger, S., Reff, A., Lim, H.-J., and Ervens, B.: Atmospheric oxalic acid and OA production from glyoxal: Results of aqueous photooxidation experiments, Atmos. Environ., 41, 7588–7602, https://doi.org/10.1016/j.atmosenv.2007.05.035, 2007.

Castellanos, P., Colarco, P., Espinosa, W. R., Guzewich, S. D., Levy, R. C., Miller, R. L., Chin, M., Kahn, R. A., Kemppinen, O., Moosmüller, H., Nowottnick, E. P., Rocha-Lima, A., Smith, M. D., Yorks, J. E., and Yu, H.: Mineral dust optical properties for remote sensing and global modeling: A review, Remote Sensing of Environment, 303, 113982, https://doi.org/10.1016/j.rse.2023.113982, 2024.

Chan Miller, C., Jacob, D. J., Marais, E. A., Yu, K., Travis, K. R., Kim, P. S., Fisher, J. A., Zhu, L., Wolfe, G. M., Hanisco, T. F., Keutsch, F. N., Kaiser, J., Min, K.-E., Brown, S. S., Washenfelder, R. A., González Abad, G., and Chance, K.: Glyoxal yield from isoprene oxidation and relation to formaldehyde: chemical mechanism, constraints from SENEX aircraft observations, and interpretation of OMI satellite data, Atmos. Chem. Phys., 17, 8725–8738, https://doi.org/10.5194/acp-17-8725-2017, 2017.

Mis en forme : Police :10 pt, Non Italique, Anglais (États-Unis)

Mis en forme : Police :10 pt, Anglais (États-Unis)

Mis en forme : Police :10 pt, Non Italique, Anglais (États-Unis)

Mis en forme : Police :10 pt, Anglais (États-Unis)

Mis en forme : Anglais (États-Unis)

Chen, S., Chen, J., Zhang, Y., Lin, J., Bi, H., Song, H., Chen, Y., Lian, L., Liu, C., and Zhang, R.: Anthropogenic dust: sources, characteristics and emissions, Environ. Res. Lett., 18, 103002, https://doi.org/10.1088/1748-9326/acf479, 2023.

Chiappini, L., Perraudin, E., Durand-Jolibois, R., and Doussin, J. F.: Development of a supercritical fluid extraction–gas chromatography–mass spectrometry method for the identification of highly polar compounds in secondary organic aerosols formed from biogenic hydrocarbons in smog chamber experiments, Anal. Bioanal. Chem., 386, 1749–1759, https://doi.org/10.1007/s00216-006-0744-3, 2006.

Chirizzi, D., Cesari, D., Guascito, M. R., Dinoi, A., Giotta, L., Donateo, A., and Contini, D., Influence of Saharan dust outbreaks and carbon content on oxidative potential of water-soluble fractions of PM2. 5 and PM10. Atmos. Environ., 163, 1-8, 2017

Crowley, J. N., Ammann, M., Cox, R. A., Hynes, R. G., Jenkin, M. E., Mellouki, A., Rossi, M. J., Troe, J., and Wallington, T. J.: Evaluated kinetic and photochemical data for atmospheric chemistry: Volume V – heterogeneous reactions on solid substrates, Atmos. Chem. Phys., 10, 9059–9223, https://doi.org/10.5194/acp-10-9059-2010, 2010.

Curry, L. A., Tsui, W. G., and McNeill, V. F.: Technical note: Updated parameterization of the reactive uptake of glyoxal and methylglyoxal by atmospheric aerosols and cloud droplets, Atmos. Chem. Phys., 18, 9823–9830, https://doi.org/10.5194/acp-18-9823-2018, 2018.

De Haan, D. O., Hawkins, L. N., Jansen, K., Welsh, H. G., Pednekar, R., De Loera, A., Jimenez, N. G., Tolbert, M. A., Cazaunau, M., Gratien, A., Bergé, A., Pangui, E., Formenti, P., and Doussin, J.-F.: Glyoxal's impact on dry ammonium salts: fast and reversible surface aerosol browning, Atmos. Chem. Phys., 20, 9581–9590, https://doi.org/10.5194/acp-20-9581-2020, 2020.

De Haan, D. O., Hawkins, L. N., Wickremasinghe, P. D., Andretta, A. D., Dignum, J. R., De Haan, A. C., Welsh, H. G., Pennington, E. A., Cui, T., Surratt, J. D., Cazaunau, M., Pangui, E., and Doussin, J.-F.: Brown Carbon from Photo-Oxidation of Glyoxal and SO_2 in Aqueous Aerosol, ACS Earth Space Chem., 7, 1131–1140, https://doi.org/10.1021/acsearthspacechem.3c00035, 2023.

Denjean, C., Formenti, P., Picquet-Varrault, B., Katrib, Y., Pangui, E., Zapf, P., and Doussin, J. F.: A new experimental approach to study the hygroscopic and optical properties of aerosols: application to ammonium sulfate particles, Atmos. Meas. Tech., 7, 183–197, https://doi.org/10.5194/amt-7-183-2014, 2014.

Di Biagio, C., Formenti, P., Balkanski, Y., Caponi, L., Cazaunau, M., Pangui, E., Journet, E., Nowak, S., Caquineau, S., Andreae, M. O., Kandler, K., Saeed, T., Piketh, S., Seibert, D., Williams, E., and Doussin, J.-F.: Global scale variability of the mineral dust long-wave refractive index: a new dataset of in situ measurements for climate modeling and remote sensing, Atmos. Chem. Phys., 17, 1901–1929, https://doi.org/10.5194/acp-17-1901-2017, 2017.

Di Biagio, C., Formenti, P., Balkanski, Y., Caponi, L., Cazaunau, M., Pangui, E., Journet, E., Nowak, S., Andreae, M. O., Kandler, K., Saeed, T., Piketh, S., Seibert, D., Williams, E., and Doussin, J.-F.: Complex refractive indices and single-scattering albedo of global dust aerosols in the shortwave spectrum and relationship to size and iron content, Atmos. Chem. Phys., 19, 15503–15531, https://doi.org/10.5194/acp-19-15503-2019, 2019.

Dupart, Y., King, S. M., Nekat, B., Nowak, A., Wiedensohler, A., Herrmann, H., David, G., Thomas, B., Miffre, A., Rairoux, P., D'Anna, B., and George, C.: Mineral dust photochemistry induces nucleation events in the presence of SO_2, Proc. Natl. Acad. Sci. U.S.A., 109, 20842–20847, https://doi.org/10.1073/pnas.1212297109, 2012.

Ervens, B. and Volkamer, R.: Glyoxal processing by aerosol multiphase chemistry: towards a kinetic modeling framework of secondary organic aerosol formation in aqueous particles, Atmos. Chem. Phys., 10, 8219–8244, https://doi.org/10.5194/acp-10-8219-2010, 2010.

Fu, T.-M., Jacob, D. J., Wittrock, F., Burrows, J. P., Vrekoussis, M., and Henze, D. K.: Global budgets of atmospheric glyoxal and methylglyoxal, and implications for formation of secondary organic aerosols, J. Geophys. Res., 113, D15303, https://doi.org/10.1029/2007JD009505, 2008.

Galloway, M. M., Chhabra, P. S., Chan, A. W. H., Surratt, J. D., Flagan, R. C., Seinfeld, J. H., and Keutsch, F. N.: Glyoxal uptake on ammonium sulphate seed aerosol: reaction products and reversibility of uptake under dark and irradiated conditions, Atmos. Chem. Phys., 2009.

Giorio, C., Monod, A., Brégonzio-Rozier, L., DeWitt, H. L., Cazaunau, M., Temime-Roussel, B., Gratien, A., Michoud, V., Pangui, E., Ravier, S., Zielinski, A. T., Tapparo, A., Vermeylen, R., Claeys, M., Voisin, D., Kalberer, M., and Doussin, J.-F.: Cloud Processing of Secondary Organic Aerosol from Isoprene and Methacrolein Photooxidation, J. Phys. Chem. A, 121, 7641–7654, https://doi.org/10.1021/acs.jpca.7b05933, 2017.

Giorio, C., D'Aronco, S., Di Marco, V., Badocco, D., Battaglia, F., Soldà, L., Pastore, P., and Tapparo, A.: Emerging investigator series: aqueous-phase processing of atmospheric aerosol influences dissolution kinetics of metal ions in an urban background site in the Po Valley, Environ. Sci.: Processes Impacts, 24, 884–897, https://doi.org/10.1039/D2EM00023G, 2022.

Goodman, A. L., Underwood, G. M., and Grassian, V. H.: Heterogeneous Reaction of NO2 : Characterization of Gas-Phase and Adsorbed Products from the Reaction, 2NO2(g) + H2O(a) → HONO(g) + HNO3(a) on Hydrated Silica Particles, J. Phys. Chem. A, 103, 7217–7223, https://doi.org/10.1021/jp9910688, 1999.

Guo, Y., Wang, S., Zhu, J., Zhang, R., Gao, S., Saiz-Lopez, A., and Zhou, B.: Atmospheric formaldehyde, glyoxal and their relations to ozone pollution under low- and high-NOx regimes in summertime Shanghai, China, Atmos. Res., 258, 105635, https://doi.org/10.1016/j.atmosres.2021.105635, 2021.

Hettiarachchi, E. and Grassian, V. H.: Heterogeneous Reactions of Phenol on Different Components of Mineral Dust Aerosol: Formation of Oxidized Organic and Nitro-Phenolic Compounds, ACS EST Air, 1, 259–272, https://doi.org/10.1021/acsestair.3c00042, 2024.

Horowitz, A., Meller, R., & Moortgat, G. K. (2001). The UV–VIS absorption cross sections of the α-dicarbonyl compounds: pyruvic acid, biacetyl and glyoxal. J. Photochem. Photobiol., A, 146(1-2), 19-27.

Hu, J., Chen, Z., Qin, X., and Dong, P.: Reversible and irreversible gas–particle partitioning of dicarbonyl compounds observed in the real atmosphere, Atmos. Chem. Phys., 22, 6971–6987, https://doi.org/10.5194/acp-22-6971-2022, 2022.

Joshi, N., Romanias, M. N., Riffault, V., and Thevenet, F.: Investigating water adsorption onto natural mineral dust particles: Linking DRIFTS experiments and BET theory, Aeolian Res, 27, 35–45, https://doi.org/10.1016/j.aeolia.2017.06.001, 2017.

Lai, A. C., Nazaroff, W. W., Modeling indoor particle deposition from turbulent flow onto smooth surfaces. J. Aerosol Sci., 31, 463-476, 2000.

Kalberer, M., Paulsen, D., Sax, M., Steinbacher, M., Dommen, J., Prevot, A. S. H., Fisseha, R., Weingartner, E., Frankevich, V., Zenobi, R., and Baltensperger, U.: Identification of Polymers as Major Components of Atmospheric Organic Aerosols, Science, 303, 1659–1662, https://doi.org/10.1126/science.1092185, 2004.

Kluge, F., Hüneke, T., Lerot, C., Rosanka, S., Rotermund, M. K., Taraborrelli, D., Weyland, B., and Pfeilsticker, K.: Airborne glyoxal measurements in the marine and continental atmosphere: comparison with TROPOMI observations and EMAC simulations, Atmos. Chem. Phys., 23, 1369–1401, https://doi.org/10.5194/acp-23-1369-2023, 2023.

Knippertz, P. and Stuut, J.-B. W. (Eds.): Mineral Dust: A Key Player in the Earth System, Springer Netherlands, Dordrecht, https://doi.org/10.1007/978-94-017-8978-3, 2014.

Knote, C., Hodzic, A., Jimenez, J. L., Volkamer, R., Orlando, J. J., Baidar, S., Brioude, J., Fast, J., Gentner, D. R., Goldstein, A. H., Hayes, P. L., Knighton, W. B., Oetjen, H., Setyan, A., Stark, H., Thalman, R., Tyndall, G., Washenfelder, R., Waxman, E., and Zhang, Q.: Simulation of semi-explicit mechanisms of OA formation from glyoxal in aerosol in a 3-D model, Atmos. Chem. Phys., 14, 6213–6239, https://doi.org/10.5194/acp-14-6213-2014, 2014.

Kok, J. F., Adebiyi, A. A., Albani, S., Balkanski, Y., Checa-Garcia, R., Chin, M., Colarco, P. R., Hamilton, D. S., Huang, Y., Ito, A., Klose, M., Li, L., Mahowald, N. M., Miller, R. L., Obiso, V., Pérez García-

Pando, C., Rocha-Lima, A., and Wan, J. S.: Contribution of the world's main dust source regions to the global cycle of desert dust, Aerosols/Atmospheric Modelling/Troposphere/Physics (physical properties and processes), https://doi.org/10.5194/acp-2021-4, 2021.

Kok, J. F., Storelvmo, T., Karydis, V. A., Adebiyi, A. A., Mahowald, N. M., Evan, A. T., He, C., and Leung, D. M.: Mineral dust aerosol impacts on global climate and climate change, Nat Rev Earth Environ, 4, 71–86, https://doi.org/10.1038/s43017-022-00379-5, 2023.

Kourtchev, I., Doussin, J.-F., Giorio, C., Mahon, B., Wilson, E. M., Maurin, N., Pangui, E., Venables, D. S., Wenger, J. C., and Kalberer, M.: Molecular composition of fresh and aged secondary organic aerosol from a mixture of biogenic volatile compounds: a high-resolution mass spectrometry study, Atmos. Chem. Phys., 15, 5683–5695, https://doi.org/10.5194/acp-15-5683-2015, 2015.

Kroll, J. H., Ng, N. L., Murphy, S. M., Varutbangkul, V., Flagan, R. C., and Seinfeld, J. H.: Chamber studies of secondary organic aerosol growth by reactive uptake of simple carbonyl compounds, J. Geophys. Res., 110, 2005JD006004, https://doi.org/10.1029/2005JD006004, 2005.

Lewis, A. C., Hopkins, J. R., Carslaw, D. C., Hamilton, J. F., Nelson, B. S., Stewart, G., Dernie, J., Passant, N., and Murrells, T.: An increasing role for solvent emissions and implications for future measurements of volatile organic compounds, Phil. Trans. R. Soc. A., 378, 20190328, https://doi.org/10.1098/rsta.2019.0328, 2020.

Li, L., Mahowald, N. M., Miller, R. L., Pérez García-Pando, C., Klose, M., Hamilton, D. S., Gonçalves Ageitos, M., Ginoux, P., Balkanski, Y., Green, R. O., Kalashnikova, O., Kok, J. F., Obiso, V., Paynter, D., and Thompson, D. R.: Quantifying the range of the dust direct radiative effect due to source mineralogy uncertainty, Atmos. Chem. Phys., 21, 3973–4005, https://doi.org/10.5194/acp-21-3973-2021, 2021.

Li, Q., Gong, D., Wang, H., Wang, Y., Han, S., Wu, G., Deng, S., Yu, P., Wang, W., and Wang, B.: Rapid increase in atmospheric glyoxal and methylglyoxal concentrations in Lhasa, Tibetan Plateau: Potential sources and implications, Sci. Total Environ., 824, 153782, https://doi.org/10.1016/j.scitotenv.2022.153782, 2022.

Liggio, J., Li, S.-M., and McLaren, R.: Heterogeneous Reactions of Glyoxal on Particulate Matter: Identification of Acetals and Sulfate Esters, Environ. Sci. Technol., 39, 1532–1541, https://doi.org/10.1021/es048375y, 2005a.

Liggio, J., Li, S., and McLaren, R.: Reactive uptake of glyoxal by particulate matter, J. Geophys. Res., 110, 2004JD005113, https://doi.org/10.1029/2004JD005113, 2005b.

Lim, Y. B., Tan, Y., Perri, M. J., Seitzinger, S. P., and Turpin, B. J.: Aqueous chemistry and its role in secondary organic aerosol (OA) formation, Atmos. Chem. Phys., 10, 10521–10539, https://doi.org/10.5194/acp-10-10521-2010, 2010.

Ling, Z., Xie, Q., Shao, M., Wang, Z., Wang, T., Guo, H., and Wang, X.: Formation and sink of glyoxal and methylglyoxal in a polluted subtropical environment: observation-based photochemical analysis and impact evaluation, Atmos. Chem. Phys., 20, 11451–11467, https://doi.org/10.5194/acp-20-11451-2020, 2020.

Liu, C., Chu, B., Liu, Y., Ma, Q., Ma, J., He, H., Li, J., and Hao, J.: Effect of mineral dust on secondary organic aerosol yield and aerosol size in α-pinene/NOx photo-oxidation, Atmos. Environ., 77, 781–789, https://doi.org/10.1016/j.atmosenv.2013.05.064, 2013.

Mahowald, N., Albani, S., Kok, J. F., Engelstaeder, S., Scanza, R., Ward, D. S., and Flanner, M. G.: The size distribution of desert dust aerosols and its impact on the Earth system, Aeolian Research, 15, 53–71, https://doi.org/10.1016/j.aeolia.2013.09.002, 2014.

Nault, B. A., Croteau, P., Jayne, J., Williams, A., Williams, L., Worsnop, D., Katz, E. F., DeCarlo, P. F., and Canagaratna, M.: Laboratory evaluation of organic aerosol relative ionization efficiencies in the aerodyne aerosol mass spectrometer and aerosol chemical speciation monitor, Aerosol Science and Technology, 57, 981–997, https://doi.org/10.1080/02786826.2023.2223249, 2023.

Ng, N. L., Canagaratna, M. R., Jimenez, J. L., Chhabra, P. S., Seinfeld, J. H., and Worsnop, D. R.: Changes in organic aerosol composition with aging inferred from aerosol mass spectra, Atmos. Chem. Phys., 11, 6465–6474, https://doi.org/10.5194/acp-11-6465-2011, 2011.

Nie, W., Ding, A., Wang, T., Kerminen, V.-M., George, C., Xue, L., Wang, W., Zhang, Q., Petäjä, T., Qi, X., Gao, X., Wang, X., Yang, X., Fu, C., and Kulmala, M.: Polluted dust promotes new particle formation and growth, Sci Rep, 4, 6634, https://doi.org/10.1038/srep06634, 2014.

Nieder, R., Benbi, D. K., and Reichl, F. X.: Soil-Borne Particles and Their Impact on Environment and Human Health, in: Soil Components and Human Health, Springer Netherlands, Dordrecht, 99–177, https://doi.org/10.1007/978-94-024-1222-2_3, 2018.

Nozière, B., Dziedzic, P., and Córdova, A.: Products and Kinetics of the Liquid-Phase Reaction of Glyoxal Catalyzed by Ammonium Ions (NH4+), J. Phys. Chem. A, 113, 231–237, https://doi.org/10.1021/jp8078293, 2009.

Ooki, A. and Uematsu, M.: Chemical interactions between mineral dust particles and acid gases during Asian dust events, J. Geophys. Res., 110, 2004JD004737, https://doi.org/10.1029/2004JD004737, 2005.

Patriarca, C., Bergquist, J., Sjöberg, P. J. R., Tranvik, L., and Hawkes, J. A.: Online HPLC-ESI-HRMS Method for the Analysis and Comparison of Different Dissolved Organic Matter Samples, Environ. Sci. Technol., 52, 2091–2099, https://doi.org/10.1021/acs.est.7b04508, 2018.

Ponczek, M., Hayeck, N., Emmelin, C., and George, C.: Heterogeneous photochemistry of dicarboxylic acids on mineral dust, Atmos. Environ., 212, 262–271, https://doi.org/10.1016/j.atmosenv.2019.05.032, 2019.

Romanias, M. N., El Zein, A., and Bedjanian, Y.: Heterogeneous Interaction of H_2O_2 with TiO_2 Surface under Dark and UV Light Irradiation Conditions, J. Phys. Chem. A, 116, 8191–8200, https://doi.org/10.1021/jp305366v, 2012.

Rossignol, S., Aregahegn, K. Z., Tinel, L., Fine, L., Nozière, B., and George, C.: Glyoxal Induced Atmospheric Photosensitized Chemistry Leading to Organic Aerosol Growth, Environ. Sci. Technol., 48, 3218–3227, https://doi.org/10.1021/es405581g, 2014.

Rubasinghege, G., Ogden, S., Baltrusaitis, J., and Grassian, V. H.: Heterogeneous Uptake and Adsorption of Gas-Phase Formic Acid on Oxide and Clay Particle Surfaces: The Roles of Surface Hydroxyl Groups and Adsorbed Water in Formic Acid Adsorption and the Impact of Formic Acid Adsorption on Water Uptake, J. Phys. Chem. A, 117, 11316–11327, https://doi.org/10.1021/jp408169w, 2013.

Safi Shalamzari, M., Ryabtsova, O., Kahnt, A., Vermeylen, R., Hérent, M., Quetin-Leclercq, J., Van Der Veken, P., Maenhaut, W., and Claeys, M.: Mass spectrometric characterization of organosulfates related to secondary organic aerosol from isoprene, Rapid Comm Mass Spectrometry, 27, 784–794, https://doi.org/10.1002/rcm.6511, 2013.

Seisel, S., Lian, Y., Keil, T., Trukhin, M. E., and Zellner, R.: Kinetics of the interaction of water vapour with mineral dust and soot surfaces at T = 298 K, Phys. Chem. Chem. Phys., 6, 1926–1932, https://doi.org/10.1039/B314568A, 2004.

Shapiro, E. L., Szprengiel, J., Sareen, N., Jen, C. N., Giordano, M. R., and McNeill, V. F.: Light-absorbing secondary organic material formed by glyoxal in aqueous aerosol mimics, Atmos. Chem. Phys., 9, 2289–2300, https://doi.org/10.5194/acp-9-2289-2009, 2009.

Shen, X., Wu, H., Zhao, Y., Huang, D., Huang, L., and Chen, Z.: Heterogeneous reactions of glyoxal on mineral particles: A new avenue for oligomers and organosulfate formation, Atmos. Environ., 131, 133–140, https://doi.org/10.1016/j.atmosenv.2016.01.048, 2016.

Shrivastava, M., Cappa, C. D., Fan, J., Goldstein, A. H., Guenther, A. B., Jimenez, J. L., Kuang, C., Laskin, A., Martin, S. T., Ng, N. L., Petaja, T., Pierce, J. R., Rasch, P. J., Roldin, P., Seinfeld, J. H., Shilling, J., Smith, J. N., Thornton, J. A., Volkamer, R., Wang, J., Worsnop, D. R., Zaveri, R. A., Zelenyuk, A., and Zhang, Q.: Recent advances in understanding secondary organic aerosol: Implications for global climate forcing, Rev. Geophys., 55, 509–559, https://doi.org/10.1002/2016RG000540, 2017.

Sun, Y. L., Zhang, Q., Anastasio, C., and Sun, J.: Insights into secondary organic aerosol formed via aqueous-phase reactions of phenolic compounds based on high resolution mass spectrometry, Atmos. Chem. Phys., 10, 4809–4822, https://doi.org/10.5194/acp-10-4809-2010, 2010.

Tang, M., Huang, X., Lu, K., Ge, M., Li, Y., Cheng, P., Zhu, T., Ding, A., Zhang, Y., Gligorovski, S., Song, W., Ding, X., Bi, X., and Wang, X.: Heterogeneous reactions of mineral dust aerosol: implications for tropospheric oxidation capacity, Atmos. Chem. Phys., 17, 11727–11777, https://doi.org/10.5194/acp-17-11727-2017, 2017.

Tegen, I. and Fung, I.: Contribution to the atmospheric mineral aerosol load from land surface modification, J. Geophys. Res., 100, 18707, https://doi.org/10.1029/95JD02051, 1995.

Trainic, M., Abo Riziq, A., Lavi, A., Flores, J. M., and Rudich, Y.: The optical, physical and chemical properties of the products of glyoxal uptake on ammonium sulfate seed aerosols, Atmos. Chem. Phys., 11, 9697–9707, https://doi.org/10.5194/acp-11-9697-2011, 2011.

Turpin, B. J. and Huntzicker, J. J.: Identification of secondary organic aerosol episodes and quantitation of primary and secondary organic aerosol concentrations during SCAQS, Atmos. Environ., 29, 3527–3544, https://doi.org/10.1016/1352-2310(94)00276-Q, 1995.

Usher, C. R., Michel, A. E., and Grassian, V. H.: Reactions on Mineral Dust, Chem. Rev., 103, 4883–4940, https://doi.org/10.1021/cr020657y, 2003.

Volkamer, R., Platt, U., and Wirtz, K.: Primary and Secondary Glyoxal Formation from Aromatics: Experimental Evidence for the Bicycloalkyl–Radical Pathway from Benzene, Toluene, and p -Xylene, J. Phys. Chem. A, 105, 7865–7874, https://doi.org/10.1021/jp010152w, 2001.

Volkamer, R., San Martini, F., Molina, L. T., Salcedo, D., Jimenez, J. L., and Molina, M. J.: A missing sink for gas-phase glyoxal in Mexico City: Formation of secondary organic aerosol, Geophysical Research Letters, 34, 2007GL030752, https://doi.org/10.1029/2007GL030752, 2007.

Vrekoussis, M., Wittrock, F., Richter, A., Burrows, J. P., and Cho, C.: Temporal and spatial variability of glyoxal as observed from space, Atmos. Chem. Phys., 2009.

Wagner, C., Hanisch, F., Holmes, N., de Coninck, H., Schuster, G., and Crowley, J. N.: The interaction of N_2O_5 with mineral dust: aerosol flow tube and Knudsen reactor studies, Atmos. Chem. Phys., 2008.

Walker, H., Stone, D., Ingham, T., Hackenberg, S., Cryer, D., Punjabi, S., Read, K., Lee, J., Whalley, L., Spracklen, D. V., Carpenter, L. J., Arnold, S. R., and Heard, D. E.: Observations and modelling of glyoxal in the tropical Atlantic marine boundary layer, Atmos. Chem. Phys., 22, 5535–5557, https://doi.org/10.5194/acp-22-5535-2022, 2022.

Wang, G., Cheng, C., Meng, J., Huang, Y., Li, J., and Ren, Y.: Field observation on secondary organic aerosols during Asian dust storm periods: Formation mechanism of oxalic acid and related compounds on dust surface, Atmos. Environ., 113, 169–176, https://doi.org/10.1016/j.atmosenv.2015.05.013, 2015.

Washenfelder, R. A., Young, C. J., Brown, S. S., Angevine, W. M., Atlas, E. L., Blake, D. R., Bon, D. M., Cubison, M. J., De Gouw, J. A., Dusanter, S., Flynn, J., Gilman, J. B., Graus, M., Griffith, S., Grossberg, N., Hayes, P. L., Jimenez, J. L., Kuster, W. C., Lefer, B. L., Pollack, I. B., Ryerson, T. B., Stark, H., Stevens, P. S., and Trainer, M. K.: The glyoxal budget and its contribution to organic aerosol for Los Angeles, California, during CalNex 2010: Glyoxal Budget for Los Angeles, J. Geophys. Res., 116, https://doi.org/10.1029/2011JD016314, 2011.

Webb, N. P. and Pierre, C.: Quantifying Anthropogenic Dust Emissions, Earth's Future, 6, 286–295, https://doi.org/10.1002/2017EF000766, 2018.

Zeineddine, M. N., Romanias, M. N., Gaudion, V., Riffault, V., and Thévenet, F.: Heterogeneous Interaction of Isoprene with Natural Gobi Dust, ACS Earth Space Chem., 1, 236–243, https://doi.org/10.1021/acsearthspacechem.7b00050, 2017.

Zielinski, A. T., Kourtchev, I., Bortolini, C., Fuller, S. J., Giorio, C., Popoola, O. A. M., Bogialli, S., Tapparo, A., Jones, R. L., and Kalberer, M.: A new processing scheme for ultra-high resolution direct infusion mass spectrometry data, Atmos. Environ., 178, 129–139, https://doi.org/10.1016/j.atmosenv.2018.01.034, 2018.

Zogka, A. G., Lostier, A., Papadimitriou, V. C., Thevenet, F., Formenti, P., Rossi, M. J., Chen, H., and Romanias, M. N.: Unraveling the Uptake of Glyoxal on a Diversity of Natural Dusts and

Surrogates: Linking Dust Composition to Glyoxal Uptake and Estimation of Atmospheric Lifetimes, ACS Earth Space Chem., 8, 1165–1178, https://doi.org/10.1021/acsearthspacechem.3c00359, 2024.

Page 44 : [1] Mis en forme **Paola FORMENTI** **02/06/2025 10:24:00**

Anglais (États-Unis), Surlignage

Page 44 : [1] Mis en forme **Paola FORMENTI** **02/06/2025 10:24:00**

Anglais (États-Unis), Surlignage

Page 44 : [2] Mis en forme **Paola FORMENTI** **02/06/2025 10:24:00**

Anglais (États-Unis), Surlignage

Page 44 : [2] Mis en forme **Paola FORMENTI** **02/06/2025 10:24:00**

Anglais (États-Unis), Surlignage

Page 44 : [3] Mis en forme **Paola FORMENTI** **02/06/2025 10:24:00**

Surlignage

Page 44 : [4] Mis en forme **Paola FORMENTI** **02/06/2025 10:24:00**

Surlignage

Page 44 : [5] Mis en forme **Paola FORMENTI** **02/06/2025 10:24:00**

Anglais (États-Unis), Surlignage

Page 44 : [5] Mis en forme **Paola FORMENTI** **02/06/2025 10:24:00**

Anglais (États-Unis), Surlignage

Page 44 : [6] Mis en forme **Paola FORMENTI** **02/06/2025 10:24:00**

Anglais (États-Unis), Surlignage

Page 44 : [6] Mis en forme **Paola FORMENTI** **02/06/2025 10:24:00**

Anglais (États-Unis), Surlignage

Page 44 : [7] Mis en forme **Paola FORMENTI** **02/06/2025 10:24:00**

Anglais (États-Unis), Surlignage

Page 44 : [7] Mis en forme **Paola FORMENTI** **02/06/2025 10:24:00**

Anglais (États-Unis), Surlignage

Page 44 : [8] Mis en forme **Paola FORMENTI** **02/06/2025 10:24:00**

Surlignage

Page 44 : [9] Mis en forme **Paola FORMENTI** **02/06/2025 10:24:00**

Surlignage

Page 44 : [10] Mis en forme **Paola FORMENTI** **02/06/2025 10:24:00**

Anglais (États-Unis), Surlignage

Page 44 : [10] Mis en forme **Paola FORMENTI** **02/06/2025 10:24:00**

Anglais (États-Unis), Surlignage

Page 44 : [11] Mis en forme **Paola FORMENTI** **02/06/2025 10:24:00**

Anglais (États-Unis), Surlignage

Page 44 : [11] Mis en forme **Paola FORMENTI** **02/06/2025 10:24:00**

Anglais (États-Unis), Surlignage

Page 44 : [12] Mis en forme **Paola FORMENTI** **02/06/2025 10:24:00**

Anglais (États-Unis), Surlignage

Page 44 : [12] Mis en forme **Paola FORMENTI** **02/06/2025 10:24:00**

Anglais (États-Unis), Surlignage

Page 44 : [13] Mis en forme **Paola FORMENTI** **02/06/2025 10:24:00**

Surlignage

Page 44 : [14] Mis en forme **Paola FORMENTI** **02/06/2025 10:24:00**

Surlignage

Page 44 : [15] Mis en forme **Paola FORMENTI** **02/06/2025 10:24:00**

Anglais (États-Unis), Surlignage

Page 44 : [15] Mis en forme **Paola FORMENTI** **02/06/2025 10:24:00**

Anglais (États-Unis), Surlignage

Page 44 : [16] Mis en forme **Paola FORMENTI** **02/06/2025 10:24:00**

Anglais (États-Unis), Surlignage

Page 44 : [17] Mis en forme **Paola FORMENTI** **02/06/2025 10:24:00**

Anglais (États-Unis), Surlignage

Page 44 : [18] Mis en forme **Paola FORMENTI** **02/06/2025 10:24:00**

Surlignage

Page 44 : [19] Mis en forme **Paola FORMENTI** **02/06/2025 10:24:00**

Surlignage

Page 44 : [20] Mis en forme **Paola FORMENTI** **02/06/2025 10:24:00**

Anglais (États-Unis), Surlignage

Page 44 : [20] Mis en forme **Paola FORMENTI** **02/06/2025 10:24:00**

Anglais (États-Unis), Surlignage

Page 44 : [21] Mis en forme **Paola FORMENTI** **02/06/2025 10:24:00**

Anglais (États-Unis), Surlignage

Page 44 : [21] Mis en forme	Paola FORMENTI	02/06/2025 10:24:00

Anglais (États-Unis), Surlignage

Page 44 : [22] Mis en forme	Paola FORMENTI	02/06/2025 10:24:00

Anglais (États-Unis), Surlignage

Page 44 : [23] Mis en forme	Paola FORMENTI	02/06/2025 10:24:00

Surlignage

Page 44 : [24] Mis en forme	Paola FORMENTI	02/06/2025 10:24:00

Surlignage

Page 44 : [25] Mis en forme	Paola FORMENTI	02/06/2025 10:24:00

Anglais (États-Unis), Surlignage

Page 44 : [26] Mis en forme	Paola FORMENTI	02/06/2025 10:24:00

Surlignage

Page 44 : [27] Mis en forme	Paola FORMENTI	02/06/2025 10:24:00

Anglais (États-Unis), Surlignage

Page 44 : [27] Mis en forme	Paola FORMENTI	02/06/2025 10:24:00

Anglais (États-Unis), Surlignage

Page 44 : [28] Mis en forme	Paola FORMENTI	02/06/2025 10:24:00

Anglais (États-Unis), Surlignage

Page 44 : [28] Mis en forme	Paola FORMENTI	02/06/2025 10:24:00

Anglais (États-Unis), Surlignage

Page 44 : [29] Mis en forme	Paola FORMENTI	02/06/2025 10:24:00

Anglais (États-Unis), Surlignage

Page 44 : [29] Mis en forme	Paola FORMENTI	02/06/2025 10:24:00

Anglais (États-Unis), Surlignage

Page 44 : [30] Mis en forme	Paola FORMENTI	02/06/2025 10:24:00

Surlignage

Page 44 : [31] Mis en forme	Paola FORMENTI	02/06/2025 10:24:00

Surlignage

Page 44 : [32] Mis en forme	Paola FORMENTI	02/06/2025 10:24:00

Anglais (États-Unis), Surlignage

Page 44 : [32] Mis en forme **Paola FORMENTI** **02/06/2025 10:24:00**

Anglais (États-Unis), Surlignage

Page 44 : [33] Mis en forme **Paola FORMENTI** **02/06/2025 10:24:00**

Anglais (États-Unis), Surlignage

Page 44 : [34] Mis en forme **Paola FORMENTI** **02/06/2025 10:24:00**

Anglais (États-Unis), Surlignage

Page 44 : [34] Mis en forme **Paola FORMENTI** **02/06/2025 10:24:00**

Anglais (États-Unis), Surlignage

Page 44 : [35] Mis en forme **Paola FORMENTI** **02/06/2025 10:24:00**

Anglais (États-Unis), Surlignage

Page 44 : [35] Mis en forme **Paola FORMENTI** **02/06/2025 10:24:00**

Anglais (États-Unis), Surlignage

Page 44 : [36] Mis en forme **Paola FORMENTI** **02/06/2025 10:24:00**

Surlignage

Page 44 : [37] Mis en forme **Paola FORMENTI** **02/06/2025 10:24:00**

Surlignage

Page 44 : [38] Mis en forme **Paola FORMENTI** **02/06/2025 10:24:00**

Anglais (États-Unis), Surlignage

Page 44 : [38] Mis en forme **Paola FORMENTI** **02/06/2025 10:24:00**

Anglais (États-Unis), Surlignage

Page 44 : [39] Mis en forme **Paola FORMENTI** **02/06/2025 10:24:00**

Anglais (États-Unis), Surlignage

Page 44 : [40] Mis en forme **Paola FORMENTI** **02/06/2025 10:24:00**

Anglais (États-Unis), Surlignage

Page 44 : [40] Mis en forme **Paola FORMENTI** **02/06/2025 10:24:00**

Anglais (États-Unis), Surlignage

Page 44 : [41] Mis en forme **Paola FORMENTI** **02/06/2025 10:24:00**

Anglais (États-Unis), Surlignage

Page 44 : [41] Mis en forme **Paola FORMENTI** **02/06/2025 10:24:00**

Anglais (États-Unis), Surlignage

Page 44 : [42] Mis en forme **Paola FORMENTI** **02/06/2025 10:24:00**

Surlignage

Page 44 : [43] Mis en forme	**Paola FORMENTI**	**02/06/2025 10:24:00**

Surlignage

Page 44 : [44] Mis en forme	**Paola FORMENTI**	**02/06/2025 10:24:00**

Anglais (États-Unis), Surlignage

Page 44 : [44] Mis en forme	**Paola FORMENTI**	**02/06/2025 10:24:00**

Anglais (États-Unis), Surlignage

Page 44 : [45] Mis en forme	**Paola FORMENTI**	**02/06/2025 10:24:00**

Anglais (États-Unis), Surlignage

Page 44 : [46] Mis en forme	**Paola FORMENTI**	**02/06/2025 10:24:00**

Surlignage